University of Alberta

Improved Gecko Inspired Dry Adhesives Applied to the Packaging of MEMS

by

Brendan James Ferguson

A thesis submitted to the Faculty of Graduate Studies and Research
in partial fulfillment of the requirements for the degree of

Master of Science

Department of Mechanical Engineering

©Brendan James Ferguson
Spring 2013
Edmonton, Alberta

Abstract

An alternative method of manipulating fragile MEMS devices during fabrication has been developed. A specialized manual or robotic end effector utilizing a gecko inspired adhesive can replace the slow and costly manual tweezers used by the MEMS foundry Micralyne Inc. Improving the adhesive fabrication techniques greatly increased adhesion strength, which was tested with a custom programmed apparatus. An antistatic, nanoparticle-polymer composite was developed for the adhesive material to prevent static discharge.

The improved adhesive was then used with a specially designed end effector that contacts only the bonding pads or perimeter of the MEMS device, preventing damage to sensitive central structures. Using special techniques that only rely on shearing motions, the adhesive is engaged and disengaged to move the MEMS device between common carriers such as tacky Gel-Paks. This is the first part of a project to implement such adhesives into commercial manufacturing of MEMS or other sensitive electronic devices.

Acknowledgement

Table of Contents

List of Tables

List of Figures

List of Symbols, Nomenclature, Abbreviations

a	Contact area between two spheres
A	Hamaker constant
D	Separation distance between macroscopic bodies
ε	Interatomic spacing
E	Young's modulus
E^*	Equivalent Young's modulus
F	Van der Waals force per unit area
F_{max}	Maximum tensile load during adhesion testing
k	Sphere elastic constant
P	Load
P_c	Pull off force
R	Sphere Radius
Rs	Hemispherical indenter radius
μ	Tabor parameter
υ	Poisson number
γ	Surface energy
γ_{xy}	Interfacial energy of materials x and y
ω	Work of adhesion
W_{ad}	Effective work of adhesion
AR	Aspect Ratio

CNT	Carbon NanoTubes
DUV	Deep UltraBiolet
FEM	Finite Element Model
IC	Integrated Circuits
IPA	IsoPropyl Alcohol
JKR	Johnson-Kendall-Roberts
LDP	Load-Drag-Pull
MEMS	MicroElectroMechanical Systems
PDMS	PolyDiMethylSiloxane
PMMA	PolyMethylMethAcrylate
SEM	Scanning Electron Microscope
UV	UltraViolet

1   INTRODUCTION

Researchers have often turned to nature for inspiring the next generation of technology. From clingy plant seeds leading to Velcro, to the Lotus leaf inspiring superhydrophobic surfaces, nature has already solved many of the problems we have today. Geckos are one of the latest animals to be investigated, due to their peculiar ability to cling to walls without using hooks or claws. They do this with the help of nano-scale hairs on their feet that make intimate contact with other surfaces. Many synthetic versions of gecko feet are the product of a decade of research, but, for now, there are very few commercial applications of this technology.

There is one industry in particular that could greatly benefit from an alternative adhesion system. In the field of manufacturing, products need to be safely handled many times during their fabrication. In the electronics industry this is especially important, as small, electronic devices can be very fragile. This issue has largely been solved for the large corporations that make computer chips, but a subset of microelectronic devices known as microelecromechanical systems (MEMS) have an added set of fabrication challenges. There are a wide variety of commercial MEMS products including accelerometers, pressure sensors, micro-mirrors, and gyroscopes. Unlike traditional computer devices, where the entire device is passivated for protection, MEMS devices often require that their sensitive instruments are exposed to the environment for sensing purposes. This makes handling these devices risky, as these sensitive instruments are easily damaged, and the current methods of moving them are less than ideal.

1.1   Background

Located in Edmonton, Alberta, Micralyne Inc. is one such MEMS foundry that has issues moving these fragile MEMS devices. During manufacturing, multiple MEMS devices are fabricated on a single silicon wafer. To separate the devices, the wafer is placed on an adhesive tape and diced with a diamond saw. The individual devices, known as dies, are then moved from the tape into their final packaging, or to another location using a Gel-Pak for further testing or other purposes. For Integrated Circuit (IC) fabrication, and MEMS devices where the working apparatus has undergone passivation, the die is most often moved using a rubber vacuum tip, which is controlled with a basic robotic system. The rubber tip contacts the die, and vacuum suction provides the adhesion to remove the die from tape drum; the suction is later deactivated to release the die in the desired location. This method works well for IC, but contact from a rubber end effector and suction force would destroy most MEMS devices. To avoid this problem, Micralyne Inc. will normally have an operator remove the die from the tape drum manually using a pair of specialized tweezers. Unfortunately this method is highly dependent on operator skill level and much slower than an optimized robotic system. It risks damaging the device, resulting in a loss of time and money. A large portion of the final device cost is often a result of the packaging step, which is why manufacturers need to find the best solution for die manipulation.

It is desirable to have an alternative method of adhesion to replace the vacuum tips and manual tweezers that can effectively adhere to a MEMS device without damaging the working structures. The alternative adhesive should be strong enough to remove the die from the strongest tape decks and Gel-Paks while still having a simple method of releasing it. It is critical that the new tool is safe, and does not damage the working

2

structures of the die. Therefore, the tool will need to be applied to a safe contact location on the die.

1.1.1 *Current Die Sorting Methods*

Die sorting for both MEMS and Integrated Circuits has significant challenges in order to safely and accurately move die. The die can be very thin, small, and fragile, requiring delicate handling to prevent damage or contamination. Micralyne Inc. has dies as small as 1 mm x 0.7 mm, and as large as 14 mm x 8 mm. From fully automated to manual, there are a number of options available, and the option is selected to best meet the needs of the process.

For IC, the top surface of the device is often sealed or passivated to protect the internal working devices. The best option for manipulating this type of device is a suction based system that contacts the passivized surface with a conductive rubber or metallic suction tip. This method can be integrated with a robotic system that easily and quickly controls the suction based adhesion. These systems have been used extensively and are available commercially from companies such as Muehlabuer [1]. There are also handheld versions available that consist of a pen sized suction device for moving small quantities of die [2] as seen in Figure 1.

Figure 1: Vacuum pen for manual die manipulation. A lever on the side depresses a spring, and when the spring regains its shape air is pulled in through a hole in the rubber tip, creating a negative vacuum.

Some MEMS devices do not have this passivized surface since they need to interact with the environment or have freely moving parts, like mirrors, actuators and springs that vulnerable to damage if directly contacted. This creates a significant problem during packaging because the device would be damaged by contact with a vacuum tip. The simplest solution is to use a set of tweezers operated manually to move each device individually, taking care to only contact the sides of the die. Manual manipulation is highly dependent on operator skill, and devices can often be damaged during handling. Compared with robotics, this method is much slower, less accurate, and more expensive. There are robotic options available; Royce Instruments has a non-contact die sorter that helps to prevent damage to the surface of the device [3]. Their system involves pushing the die from below with ejection needles to raise the edges from the adhesive tape. A gripper mechanism then grasps the edges of the die, retracts from the tape, and moves the die to the desired location. This option is viable for large scale production of a specific product line, but for small scale prototyping with many different products this becomes too expensive. This option also relies on the ejection pins pushing the die up from below when removing it from adhesive tape. For many of the small scale transportation vessels, such as Gel-Paks [4], this is not a viable option.

1.1.2   *Tape Drums and Gel-Pak Challenges*

One surface that die are frequently in contact with prior to packaging are tape drums. Wafers are adhered to this tape to hold them in place during the dicing process, and then the tape is moved to a drum where die can more easily be transported to the next stage in manufacturing [5]. Tape drums consist of a thin, sticky membrane pulled taut within a metal ring. This tape can have variable tackiness controlled by heat or ultraviolet (UV) exposure, but often needs some mechanical assistance to remove die after cutting

4

operations are complete. The tape is flexible, and thus the die can be pushed up from below and grabbed from above simultaneously for subsequent placement in temporary holding packages such as Gel-Paks, or permanent plastic or ceramic packages. This is a very common solution for moving die in today's fabrication facilities [6] and an example can be seen in Figure 2.

Standard Gel-Paks consist of a rigid container with a tacky gel enclosed within [4]. They are designed for handling small quantities of die which are loaded or unloaded manually, either by hand or with tweezers. They come in different levels of adhesion based on the customer's needs (determined by the durometer of the gel). The hinged plastic box is designed for safe transportation as the box can be shaken or dropped without the devices coming loose from the gel and sustaining damage. The rigid container means that pushing up from below to assist die removal is not an option and robotic vacuum actuation is rarely, if ever used. A safe alternative to tweezers is desirable to reduce the likelyhood of damaged die from this manual manipulation process. A commonly used Gel-Pak can be seen in Figure 2.

Figure 2: A typical tape drum and Gel-Pak used by Micralyne Inc. The tape drum consists of a sticky tape held within a metallic ring. A diced wafer can be seen in its center with the devices scattered. The Gel-Pak contains a sticky, transparent gel to hold die stationary and it measures approximately 5 x 5 x 1 cm.

More advanced Gel-Paks are able to control the adhesion using a vacuum release system. The gel sits atop a loosely spaced frame and, when vacuum is applied, the gel is pulled into the openings of the framework, causing a rippled surface on the gel which greatly decreases the contact area with the die, and subsequently reduces adhesion strength as seen in Figure 3. These Gel-Paks are an excellent option for fragile die, but still require tweezers to remove the die in addition to a vacuum source.

6
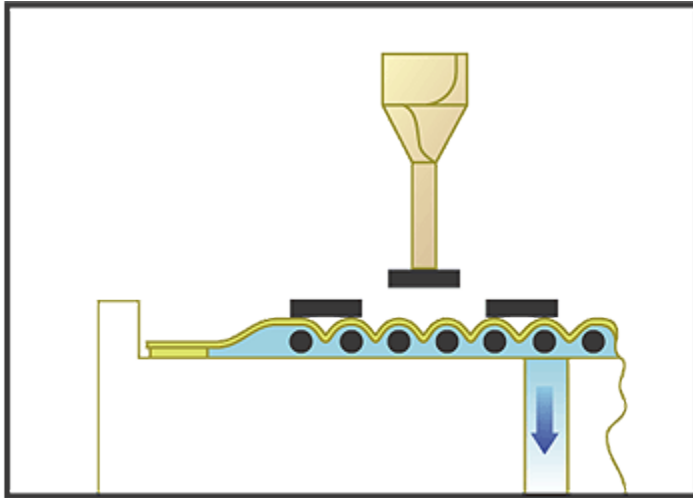
Figure 3: Demonstration of the working apparatus for vacuum Gel-Paks. A vacuum is applied from below, which creates a rippled surface on the gel and greatly reduces adhesion. Image reproduced from [4] **with permission.**

1.2 Gecko Adhesion

The primary reason that regular tacky adhesives have not been used in the manipulation of MEMS die is that they can contaminate or destroy MEMS devices with their high adhesion. Additionally, traditionally tacky materials will lose their adhesion over time as the tape dries out or gets contaminated, and the adhesion forces are not controllable or switchable. The relatively young field of gecko-inspired adhesives however has promised the potential to avoid many of these pitfalls. Unlike regular pressure sensitive adhesives like scotch tape, gecko-inspired adhesives may be reusable for thousands of cycles, readily cleaned, non-contaminating, and have directional or switchable adhesion properties. The gecko inspired adhesive system has had a number of successes relevant to pick and place manipulation of individual MEMS devices. It was demonstrated that a microstructured adhesive is able to accurately manipulate silicon platelets [7-9,9,10,10]. By controlling the contact area, a polydimethylsiloxane (PDMS) surface can pick up and release silicon platelets onto nearly any surface. These studies demonstrate the feasibility

7

of gecko-inspired adhesives in a silicon environment, although have so far been used mainly to manipulate individual devices on a chip, rather than moving whole chips from commercial packaging technologies. Because the manipulation of full die may be a more commercially important task, we are aiming to demonstrate the basic system of using gecko-inspired manipulation to pick and place MEMS die from existing commercial packaging technologies.

1.2.1   *Advantages of Gecko Adhesion*

Using gecko adhesives to replace current die sorting methods will have a number of distinct advantages. When comparing to suction, a gecko adhesive will likely be simpler, not requiring complex vacuum actuation and controls. The robotic system could be programmed to control the adhesive through its movements, especially for anisotropic adhesives where the shearing direction will affect the normal adhesion strength. This can potentially reduce the cost of manufacturing including maintenance costs as no complex vacuum system will be necessary. Gecko adhesion has potential to be much stronger than vacuum adhesion, since a circular vacuum tip can only create suction on a small location on the die, whereas the gecko adhesive can adhere to all available area. Many vacuum actuators require assistance to remove the die from the tape drum as well. This is most often done by partially lifting the die off the tape drum by pushing up from below. If theoretical upper adhesion limits for gecko adhesives are achieved, the normal adhesive strength should be enough to remove a die from any tape drum or Gel-Pak. In addition, the stiff backing of the Gel-Pak case will prevent the assisted release needed for vacuum actuation, while a gecko adhesive will not need such assistance. The adhesion limits are more likely to be based on the forces the die can safely withstand. Gecko adhesives can also function in a vacuum, with suction accounting for no more than 10% of adhesive

strength at high withdraw speeds [11]. This could one day be used in a vacuum manufacturing setting as a way of eliminating the risk of contamination.

The gecko adhesive actuation system should be far superior to manual tweezers. An operator with tweezers is very susceptible to dropping or damaging the device since, as it is moved, its safety is dependent on the grip strength of the operator. Sometimes slight changes can be enough to damage the die, or have it come loose and drop. If proper adhesion engagement and disengagement techniques are used with a gecko adhesive, the likelihood of accidental loss of adhesion should be very low.

A flexible solution incorporating gecko adhesives can provide a customizable pick and place system. It can be usable both by robotic and manual pick and place as an inexpensive alternative to the options listed previously. The remainder of this thesis will detail the methods used to manufacture a synthetic dry adhesive strong enough to pick up silicon die with minimal contact area, and integrate them with a simple robotic pick and place system to pick and place these die from commercial Gel-Paks. This task is the first stage in the creation of a truly microfabrication compatible dry adhesive pick and place system.

1.3   Literature Review

1.3.1   *Introduction*

In the early 21st century it was discovered that geckos, along with some insects and spiders, adhere to surfaces using van der Waals forces [12-14]. These forces are generated by secondary intermolecular bonds that are weak compared to covalent, ionic, and metallic bonds. Van der Waals forces include dipole-dipole interactions or Keesom force, induced dipole interactions or Debye force, and instantaneous polarization or

London dispersion forces [15]. These three forces are highly dependent on the separation distance of the two surfaces and increase with surface polarizability. The strongest force, London dispersion, is a quantum phenomenon where the instantaneous dipole of neutral atoms will polarize nearby neutral atoms resulting in a net attractive force. These interactions can occur in all polarizable atoms and molecules, allowing these animals to adhere to nearly any material.

The attachment structures on the animals have specialized geometry that take advantage of these van der Waals forces to provide significant adhesion for animal locomotion. Often resembling a spatula or mushroom, the animals have these structures on their feet often as a replacement or supplement for hooks or claws. The size of these structures is often inversely proportional to the size of the animal, with heavier animals requiring smaller structures [16]. The largest animal to use this attachment mechanism is the gecko, and as a result it has been the main focus of research in the field of bioinspired adhesion.

Geckos have a hierarchical hair structure that consists of millions of setae, each of which split into thousands of spatula-shaped structures known as spatulae [17] as seen in Figure 4. The 200-500 nm wide spatulae are the structures that make contact with the opposing surface and engage van der Waals forces [18]. According to the Johnson-Kendall-Roberts (JKR) model of contact mechanics [19][20], this splitting of a single contact point into multiple contact points results in greatly increased adhesion. This explains why the heavier gecko has a hierarchal structure and higher hair density than lighter insects [19]. The small size of these structures and the increased compliance from the hierarchical structure allows the gecko to stick to a wide range of surfaces including those with high surface roughness [21-23].
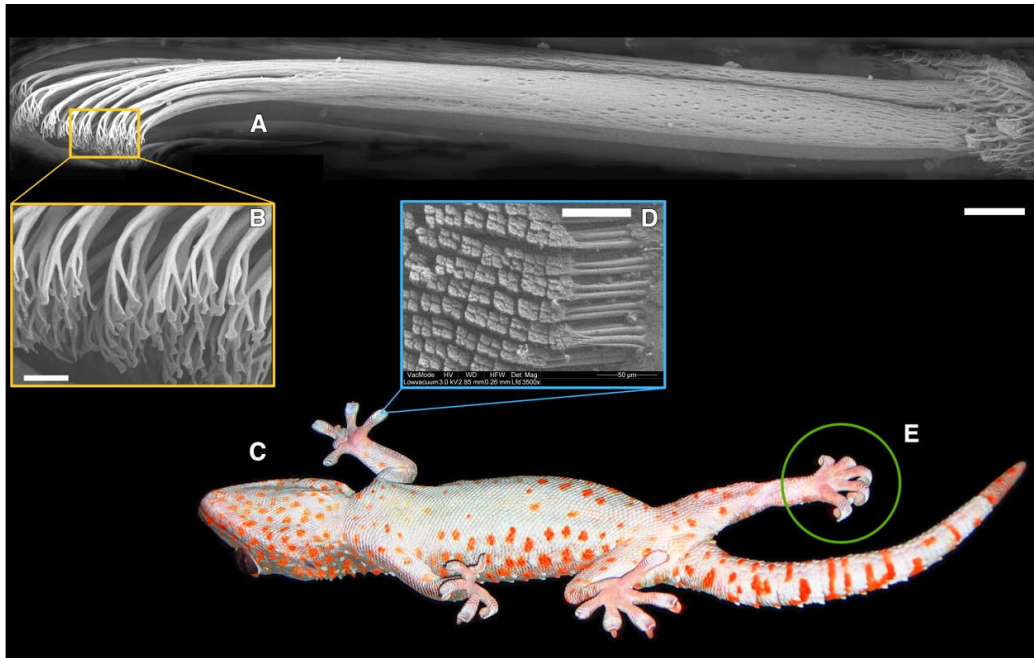
Figure 4: SEM images of the Tokay gecko's hierarchical setae and spatulae. A single complete setae (A) and groups of setae arranged in a grid-like pattern (D). The terminal spatulae of a single setae (B). The peeling motion of the gecko's toes during detachment is clear (E). Scale bars are 50 µm (D), 5 µm (A), 1 µm (B). Printed from [24] **with permission**

Gecko adhesion is often referred to as being "dry" since the gecko does not have any secretions on its feet that aid with adhesion. There are minor secretions in the form of phospholipids left behind in their footprints [25], but this is significantly less than what is constantly secreted by tree frogs or slugs [26,27]. In addition to being a dry adhesive, the gecko's foot pads are self-cleaning [28], meaning a dirty gecko's foot will slowly recover adhesive strength as the gecko walks on a clean surface. Very rarely will the gecko encounter a smooth clean surface in nature, but the increased compliance from the hierarchical foot hairs compensates for this [22], allowing the gecko to continue using their adhesive throughout its lifetime without loss of adhesion [29].

For effective locomotion, the gecko's foot needs not only strong adhesion, but fast and easy detachment. The gecko uses a few key techniques to accomplish this. First, it was

11

found that the orientation of the gecko's setae is important, with an angle between the setal shaft and adhering surface of greater than 30° causing detachment [14]. Second, geckos peel the tips of their toes away from the surface as they move [30] as seen in Figure 4, this is similar to how a piece of standard adhesive tape would be removed suggesting that this peeling motion reduces the force required for the gecko to detach an adhered foot [13,24,31]. However, the more widely accepted model is that adhesion is a function of shear force between the gecko's feet and the surface [24], and geckos control their adhesion via the shearing force rather than peeling [32]. Additionally, gecko adhesion is preload dependent [13,33], providing another way for geckos to control their adhesion. Geckos can move very quickly using these techniques with detachment times as low as 15 ms [24].

It was not long after the discovery of van der Waals adhesion mechanisms in geckos that researchers began attempts to mimic the gecko's foot to make a synthetic adhesive. Many of the natural features of the gecko's foot are desirable characteristics in a synthetic adhesive. As discussed in detail by Autumn [34], these characteristics include:

- Strong adhesion to a variety of surfaces
- Non-tacky
- Fast, easy detachment
- Durable, self-cleaning
- Directional

There are a wide variety of different manufacturing methods for these adhesives, but they can be categorized into two main groups [35], gaseous growth/etching and micro/nano scale casting. The first group, bottom up patterning, is less common, and often involves

carbon nanotubes as the adhesive. The second group is the most prominent fabrication type, and often involves casting a polymer based adhesive.

1.3.2   *Gaseous Growth and Etching*

Within this group, there are two sub-categories [36], bottom up patterning and top down patterning. The first group involves adding material to grow the adhesive on a substrate. It most often involves the growth of carbon nanotubes. The second category involves etching material, often a polymer, to produce the structured adhesive. Both categories do not make use of templates for the adhesive.

1.3.3   *Bottom Up Techniques*

The first growth attempts were done by chemical vapor deposition on a silicon wafer to make carbon nanotubes (CNT) [37,38]. These preliminary versions showed great promise, with nanoscale adhesion strengths of up to 200 times greater than the real gecko [37]. However, this number does not correspond to macroscale adhesion strength and thus represents an upper adhesion limit for these types of adhesives [39]. In addition to this high strength, CNT are more suited towards high temperature applications [40] when compared to polymer adhesives which will often melt at temperatures above 200°C. Nitto Denko, a Japanese materials manufacturing company, is the first to have a commercial CNT based adhesive tape available for use in fixing analytical devices such as atomic force microscopes and scanning electron microscopes [41]. These Nitto Denko tapes takes advantage of the CNT's high temperature stability and non-contaminating characteristics when compared to traditional electrical tapes or metal pastes. CNT also are electrically conducting [42,43], which can lead to applications such as electroswitching [44]. Research has progressed with CNT based adhesives [45-47] and a number of key observations have been made.

13

CNT based adhesives are limited in their commercial applications due to the high cost of fabrication [35]. Additionally, CNT adhesives are normally only tested on very small areas (1 x 1 cm^2) [48], and the resulting adhesion may not be relevant when used over larger areas. Despite this, CNT adhesives have been able to closely mimic the real gecko in terms of adhesion strength and behavior. They have excellent shear adhesion that often needs to be engaged by applying a normal or shear preload [46,49-52]. The normal adhesion strength is a function of the preload [53] and the adhesives can be made anisotropic [51,54]. After loading, most CNT are permanently deformed [48], making subsequent loading cycles difficult to predict and possibly reducing the potential for a long lasting, repeatable adhesive.

In summary, these CNT adhesives could be suitable for high temperature MEMS fabrication, but are not economically feasible for the fast, inexpensive pick and place operations that are needed for this project.

1.3.4   *Top Down Techniques*

The earliest instances of patterning adhesives using a top down approach were simply cutting a polymer film using a razor blade [55-57]. These crude films demonstrated that fracture energy, and thus adhesion, could be increased significantly (x10-20) with a patterned fibrillar surface. The resolution using a razor blade is on the order of millimeters, and researchers were attempting to mimic the gecko's foot which is on the order of nanometers, and thus research followed to create nanoscale structures. A combination of electron beam lithography and dry etching was used to create an array of micropillars with a minimum diameter of 0.2 µm [58] as seen in Figure 5. These adhesives showed promise, with an adhesive pressure of 3 N cm^{-2}, which is comparable to the real gecko (10 N cm^{-2}), but were only able to go through a few attachment and

14

detachment cycles before degradation through the fibers bunching or other issues. Furthermore, electron beam lithography is very slow and expensive, and can only pattern a very small area (<1 cm^2).
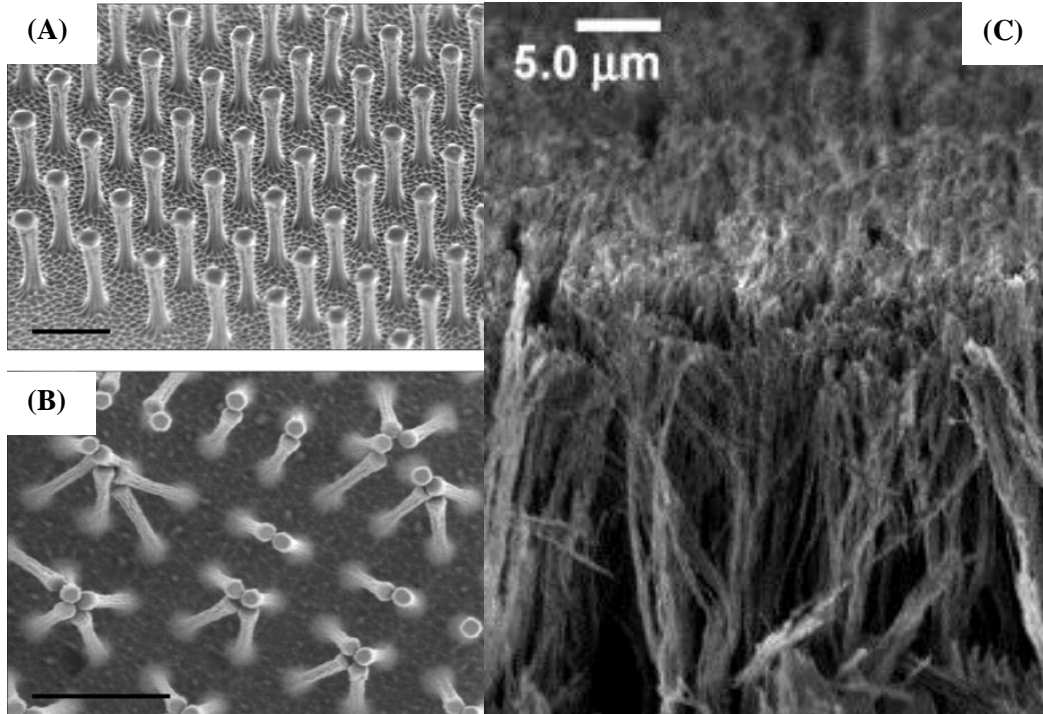
Figure 5: Nanoscale polyimide hairs fabricated with electron beam lithography (A). Clumping is found to be a significant source of adhesion reduction after multiple attachment and detachment cycles (B). Cross section of micromask generated grass landscape (C). Scale bars represent 2 μm (A,B). (A,B) reprinted by permission from Macmillan Publishers Ltd: Nature Materials [58], copyright 2003. (C) reprinted from [59] with permission from Elsevier.

Reactive ion etching has also been used to pattern polymer surfaces using a micromasking technique [59,60] as seen in Figure 5. The result is a grass-like forest of fibers on the surface which can enhance the compliance of microstructured fibers or a flat surface [60].Very high (AR) (80:1) fibers can be produced using these methods and they have been applied to the adhesives on the feet of a climbing robot [61], but the normal

strength and survivability is lacking for such applications. This is also a costly process for a one time adhesive, and thus, to achieve costs low enough for commercialization, other fabrication methods need to be considered.

1.3.5   *Replica Molding*

Currently one of the best options to reduce cost and increase fabrication time is to use a template or mold and fabricate the final working adhesives from a master copy [62]. The first groups to use molds simply indented a wax surface to create a negative array of cones [63] or by the ablation of stainless steel to create a negative array of cylinders [64]. This mold making technology eventually lead to one of the most common methods of using photolithography to pattern a surface for use as a template [10,39,65-74,74-90]. Casting from a template puts the bulk of manufacturing costs into fabricating the original master, allowing many copies to be made and reducing the price of the final adhesive. A commercial gecko adhesive will almost certainly be made with a mold.

Molded fibers can be enhanced with a dipping technique to create overhanging caps [70,91-93], a complete film covering the fiber tops [88,94-96], or a second layer of fibers resulting in a hierarchical design [97,98]. A hierarchical adhesive can also be made using multi-step fabrication processes [76,78,97,99]. Hierarchical adhesives have the advantage of increasing compliance to a surface, allowing the adhesive to attach to rougher surfaces depending on the fiber size; however, adhesion strength is often reduced due to manufacturing defects that arise from the more complicated fabrication process.
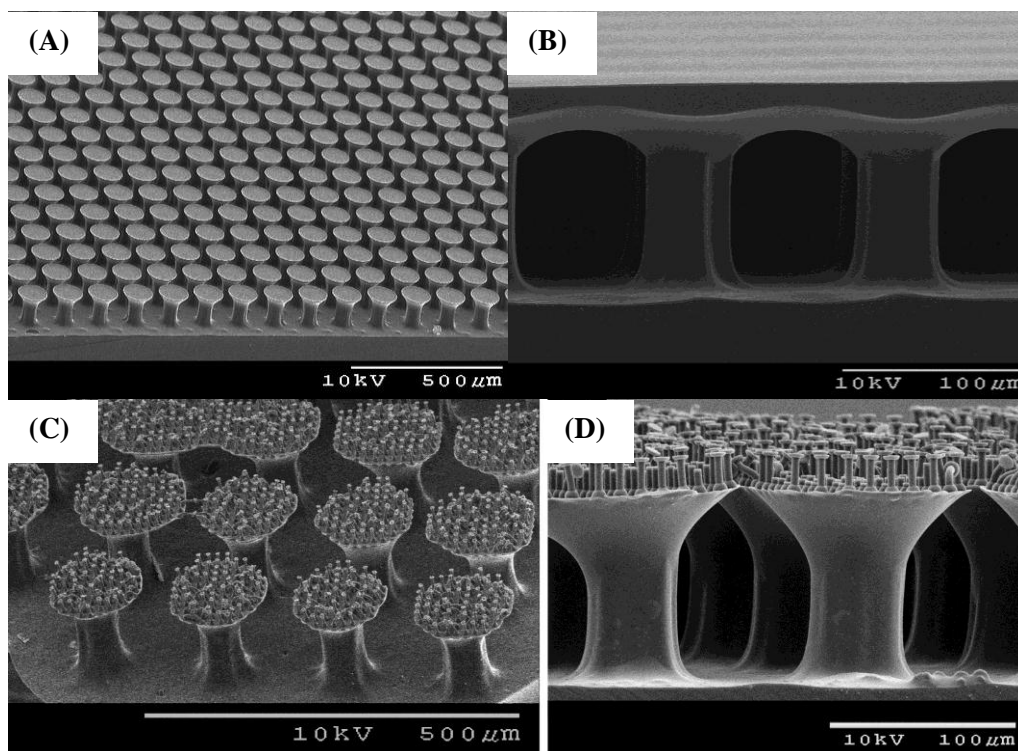
Figure 6: Examples of various polymer adhesive structures created using a dipping technique. Examples include mushroom-like fibers (A), a complete film (B), and hierarchical fibers (C,D). The hierarchical fibers can be seen to contain many defects which will reduce their adhesive strength. Reprinted with permission from (A) [70]**, (B)** [88]**, (C, D)** [97]**. Copyright 2009 American Chemical Society.**

Anisotropic adhesives can be created using casting techniques such as molding with an offset cap [100], anisotropic cap geometry [101], or angled fibers [102,103]. These adhesives often have reduced normal adhesion compared to isotropic versions, and the manufacturing processes are slightly more complex and thus more susceptible to defects, but they show promise in a reliable method of controllable adhesion.

Replica molding can have some limitations for material choice. Stiffness is the first material property that should be considered when designing a replica molding process. The mold and/or the sample material must be flexible enough to allow demolding to occur. In the case of interlocked structures such as a fiber with an overhanging cap, the

17

materials must have the ability to deform around the structures to release the sample. If the material stiffness is too high, there is a risk of the structures fracturing within the mold or plastically deforming. Too soft and the finished structures can collapse, limiting the AR of fibers and their ability to adhere to rough surfaces [65].

The mold and sample material must be considered together, as the interaction between each other can be a source of catastrophic failure for replica molding. Curable polymers must be chosen such that they are not inhibited during fabrication; inhibition will prevent certain polymers from curing into a solid material from a liquid prepolymer. The mold should wet the prepolymer well, preventing any repulsion that could hinder the filling of the microstructures. Poor control over fiber geometry will result from non-wetting behavior. After curing is complete, the structural polymer should not strongly adhere or bond to the mold. High adhesive forces during demolding can damage the sample or the mold. One way to avoid this is to apply a surface treatment to the mold before casting [104-107]. This treatment must occasionally be repeated on a regular basis if it degrades with repeated molding cycles.

One of the most commonly used polymer that meets these requirements for a gecko-inspired adhesive is ST-1060 from BJB Enterprises [68,70,79,88,93,97,108,109]. ST-1060 has a Young's modulus of 2-3 MPa and Shore A 60 hardness [110], making it much softer than the gecko's stiff keratin hairs. This makes the adhesive better able to conform smoothly to a surface, and also easily demold from a stiff mold, but it limits the maximum AR as the softer fibers will more easily collapse. The ultimate strength of the adhesive is limited by the strength of the material and fiber geometry, but ST-1060 can be strengthened with the use of composites to enhance adhesion [111].

Polymer fibers are also frequently made from a common PDMS called Sylgard 184 from Dow Corning [73,87,112]. Sylgard 184 can easily demold from a rigid or soft template with a Shore A 44 hardness. The failure of Sylgard 184 is in its peel strength, as a minor tear will quickly and easily propagate through the adhesive, often destroying it. For a high strength adhesive this is a fatal flaw and one reason why ST-1060 is the more commonly used material.

Polymer molds are often fabricated from silicone rubbers cast from a master copy [68,113]. One silicone rubber used in our group is TC-5045 from BJB Enterprises [109]. TC-5045 is a durable silicone rubber with high peel strength and fast curing time. TC-5045 also inhibits few curable materials, allowing a wide range of possible adhesive materials [114].

1.3.6 *Contact Mechanics*

Van der Waals force per unit area, *F*, between macroscopic bodies can be calculated as a function of separation distance, *D*, as follows [115]:

$$F = \frac{A}{6\pi D^3}$$

Where A is the Hamaker constant, which is a function of material properties and normally is in the range of 10^{-19} to 10^{-20} [15].

It is clear that separation distance has a large influence on the strength of van der Waals forces and thus a gecko inspired adhesive should be designed to take advantage of this. The separation distance is often an unknown when dealing with van der Waals based adhesives, and thus the equation is not useful for predicting adhesive forces.

The most widely cited theory in predicting adhesion forces between surfaces is the JKR theory [20]. The theory builds off of the Hertz theory [116] which first investigated the contact between two elastic bodies. The Hertz theory found that the zone of contact between the two spheres was dependent on their elastic deformation. The contact area a can be found for two spheres of radius R_1 and R_2 that are being pressed together with a force P:

$$a^3 = \frac{3}{4}\pi(k_1 + k_2)\frac{R_1 R_2}{R_1 + R_2}P$$

k_1 and k_2 represent the elastic constants of the spheres:

$$k_1 = \frac{1-v_1^2}{\pi E_1} \text{ and } k_2 = \frac{1-v_2^2}{\pi E_2}$$

Where E represents the Young's Modulus and ν represents Poisson's ratio of the spheres.

The main issues with applying Hertz theory to adhesion problems is that it assumes a frictionless, adhesionless interaction between the spheres. Obviously this renders the theory unusable for adhesion prediction so an amendment to the theory was needed.

In the late 1960s, Kendall and Roberts noted that two soft elastic contacts would show a contact area without the preload force P required in the Hertz theory [117,118]. In addition, the contact area a was actually larger than predicted by Hertz for finite preloads and the two contacts required an external force to remove them despite the lack of a preload. These observations lead to their collaborative work in establishing the JKR theory. The theory adds the effect of surface energy γ when predicting the contact radius between two spheres:

$$a^3 = \frac{R}{K}(P + 3\omega\pi R + \sqrt{6\omega\pi RP + (3\omega\pi R)^2})$$

Where $R = \frac{R_1 R_2}{(R_1 + R_2)}$, $K = \frac{4}{3}\pi(k_1 + k_2)$, the work of adhesion $\omega = \gamma_1 + \gamma_2 - \gamma_{12}$, γ_1 and

γ_2 are the surface energies of the two surfaces, and γ_{12} is the interfacial surface energy.

When two surfaces are in intimate contact, mechanical work must be done to separate the

surfaces and overcome the adhesive forces. This work is expended in creating a "new"

surface similar to the fracture mechanics model of fatigue crack propagation [119].

According to JKR theory, the resulting separation of the two spheres will occur when the

pull-off force P_c is

$$P_c \geq \frac{3}{2}\pi R\omega$$

The JKR theory was not the first to investigate the adhesion of two spheres. In 1932,

Bradley [120] showed that the adhesion P_c between two rigid, incompressible spheres in

contact was

$$P_c = 2\pi R\omega$$

The primary difference between the two theories is that Bradley theory is only valid for

incompressible materials, whereas the elastic modulus, while affecting the contact area,

has no effect on adhesion in the JKR model. The solution to this conflict was later

explained by Tabor [121], who created a dimensionless parameter called the Tabor

number μ to act as a guide for the transition between the two conflicting theories. The

Tabor number is defined as:

$$\mu = \left(\frac{R\omega^2}{E^{*2}\varepsilon^3}\right)^{\frac{1}{3}}$$

Where E* is the equivalent Young's modulus $\frac{1}{E^*} = \frac{1-v_1^2}{E_1} + \frac{1-v_2^2}{E_2}$, and ε is the interatomic

spacing.

The Tabor number is used to determine which theory to use, with small values of μ ($\mu <$

0.1) resulting in negligible deformation, and thus the Bradley theory is used [122]. For

larger values ($\mu > 5$) the JKR theory is more appropriate. Most synthetic gecko adhesion

materials are very soft, resulting in high values of μ, so the JKR theory will often be

appropriate [123]. For very stiff materials, or cases where the contact area of the fibers is

rigid with a soft backing, the Bradley theory may be applicable. For values of μ between

0.1 and 5, which corresponds to hard materials with low energy of adhesion, a third

theory is needed. Derjaguin, Muller, and Toporov developed a theory for this range of

materials that considers the attractive forces outside the area of contact in addition to the

contact forces known as DMT theory [124]. The theory builds off the Bradley theory by

considering effect of contact deformation which increases the elastic contact area. The

corresponding values for contact radius and pull-off force are

$$a = \frac{RP}{K} + \frac{2\pi\omega R^2}{K}$$

$$P_c = 2\pi\omega R$$

The resulting pull-off force for the increased contact area ends up being identical to that

predicted by the Bradley theory, and thus DMT theory is normally used as a replacement.

As such the range of tabor number values between 0.1 and 5 is considered to be in

transition between DMT and JKR theory, although contact scenarios with values of $\mu < 5$

are generally evaluated using DMT theory.

While these theories are useful for many MEMS applications [125], they have

inaccuracies when applied to many of the common materials used for gecko inspired

adhesives. The polymer adhesives often more closely resemble a flat punch rather than a

sphere, and are often viscoelastic and/or hyperelastic materials rather than linear elastic.

Furthermore, these adhesion theories likely cannot be scaled up to accurately predict the

adhesion of a large area of dry adhesive as point flaws in the surface or adhesive fibers

themselves cause lower adhesive values than what theory would predict. Manufacturing

defects will normally reduce the real adhesion when compared to values predicted by

theory and an adhesive sheet may only need to fail in a single location before a crack can

rapidly propagate through the contacting surface. An improved theory considering the

likelihood and distribution of manufacturing defects may be necessary in the future.

Kendall also investigated the adhesion between a flat punch and infinite plane in 1971

[126]. This theory considers a rigid disk of radius a contacting an infinite plane of

Young's modulus E. By balancing surface, stored elastic, and potential energy the pull-

off force at a constant load P will be achieved when:

$$P = \sqrt{\frac{8\pi}{1 - v^2} E \omega a^3}$$

Kendall noted that this is similar to the Griffith theory of the brittle fracture of solids

[127]. Unfortunately this scenario does not accurately describe typical gecko adhesive

scenarios. The rigid disk in the theory can represent a structured adhesive, but the

adhesive material will rarely be perfectly rigid. The notable difference between the pull-

off force for a flat punch compared to spherical contacts is the proportionality of P to ω

with $P \propto \omega$ for the JKR and DMT theories while $P \propto \sqrt{\omega}$ for the flat punch. The difference

between these values demonstrates that the geometry of the contacts plays a key role in determining adhesion of identical structural materials. The lesson learned is that the contacts flatness may play an important role in the adhesion and should be investigated as a method of optimizing the adhesive strength of the synthetic adhesives.

Elastomer flat punches and their adhesion to rigid flat surfaces has been investigated and compared with mushroom-shaped geometry [128]. A flat punch of 15 mm diameter was compared to a punch of 11mm diameter with a 15mm plate at the terminal end. The overhanging flat cap significantly improves adhesion strength compared to a simple flat punch. The failure mode for the flat punch is a crack started at the edge of the punch contact that propagates through to the other side, likely started by the stress concentration. The primary failure method with the overhanging cap is a void formation in the center of the fiber that grows until it reaches the edge of the plate. The suction component in these large scale mushroom shaped fibers plays a role in adhesion, but the suction effect may be diminished at the microscale.

The superiority of the mushroom shape was further investigated by Carbone [39,74,75,129]. They found that the flat punch had a stress concentration at the edge which was the primary cause of crack initiation. An overhanging cap removes this stress singularity at the edge of the cylinder and forces the pillar to detach by either mode II (crack propagation from an internal defect) or mode III (failure due to the achievement of theoretical maximum adhesion strength) failure mechanisms, both of which produce much higher adhesion.

1.3.7   *Adhesion Optimization*

Much research has been done on the ideal shape of the gecko adhesive structures. The ideal shape will often depend on the intended application and for elastomeric fibrillar adhesives, the designer primarily considers the AR, pillar spacing, pillar radius, and cap geometry. Early analysis suggested that a flat punch or toroidal shape is best for achieving high adhesion [123]. As discussed in Section 1.3.6, it was found that a mushroom like fiber geometry was best for adhesion [74,129]. This has been confirmed with many mushroom shaped adhesives showing very high adhesive strength [109,130]. Adhesion was found to increase with decreasing pillar radius and increasing AR [77] but there is a limit to this as manufacturing defects will often begin to outweigh the benefits from this trend [131]. Increasing AR will also make the fibers more susceptible to collapse and clumping [63,65,132], ultimately reducing adhesion with increasing AR, although a higher AR is needed to enhance the adhesive's ability to handle off-axis loads [131]. Pillar spacing is best chosen to maximize the apparent contact area of the caps while preventing the pillars from clumping or self-adhering to neighboring pillars. In our work, the apparent contact area of 50% has been effective [131].

Finite Element Modeling (FEM) on adhesive fibers and stamps has been investigated by other researchers [133,134], but almost exclusively have used a linear elastic model, and the hyperelastic behavior of typical synthetic gecko adhesive materials is neglected. Materials such as ST-1060 can elongate as much as 590% without plastic deformation, and such elongation will change the elastic properties and shape of the fibers [110]. As a result these FEM models of non-elongated fibers may provide inaccurate results for the critical moments before failure. A more accurate model will be needed before predictions of adhesive behavior will be relevant.

1.3.8   Adhesion Testing

There is currently no standardized method for testing these bioinspired adhesives [35]. The general adhesion testing process is to bring a probe into contact with the adhesive with a defined preload, then withdraw the probe measuring the adhesion forces. Normal adhesion can be tested by withdrawing from the sample parallel to the preloading direction, while shear tests withdraw the probe perpendicular to the preload direction [135].

A flat-flat contact adhesion test has the benefit of even load sharing and unchanging contact area. This makes finding the adhesive pressure relatively simple. There are two similar methods for this test, either putting the rigid backed adhesive in contact with a flat surface[46,48,73,136,137], or bringing a flat punch in contact with the adhesive [91,108,112,138,139]. The primary problem associated with this testing method is the issue of careful alignment. The test requires either a self-aligning joint or very careful manual alignment. Misalignments of greater than 0.2^{o} can reduce adhesion by more than 30% [140].

To avoid the problems of misalignment a hemispherical indenter can be used instead of a flat punch [66-68,77,88,90,94-97,131,141-144]. The curved indenter introduces new issues however, notably an uneven distribution of pressure when applying a preload, sometimes resulting in central adhesive fibers buckling while outermost fibers have a minimal compressive force [145] as seen in Figure 7. These bucking fibers, in combination with the backing layer, store elastic energy which opposes the preload and affects the adhesion data. Increasing the preload will compress the adhesive and allow the probe to further indent into the adhesive surface. This allows another ring of outermost fibers to come into contact and increasing the resulting adhesion. Increasing preload will

26

have diminishing returns, as the probe can only compress the adhesive a finite distance. The effect is reflected in the data of preload versus adhesion; the adhesion will increase with preload until reaching a plateau of adhesive strength [66,79,131]. During the pull-off motion, the outermost fibers will be in tension while the inner fibers initially remain in compression. The fibers will be under a gradient of compressive and tensile forces which results in a stepped detachment, somewhat resembling a peeling motion with the outermost fibers losing contact first. Under high preload forces, the outer perimeter of fibers will adhere to the probe at a sharper angle than those contacting the center, resulting in an off axis load. These outer fibers can experience a combination of shear and normal forces during pull-off, further complicating the adhesive data. All these factors result in data which is difficult to characterize and convert to adhesion pressure. Very low preloads most closely resemble a flat-flat contact scenario due to the lack of significant buckling at the central contact point, and thus they are used for most hemispherical probe adhesive pressure calculations.

27
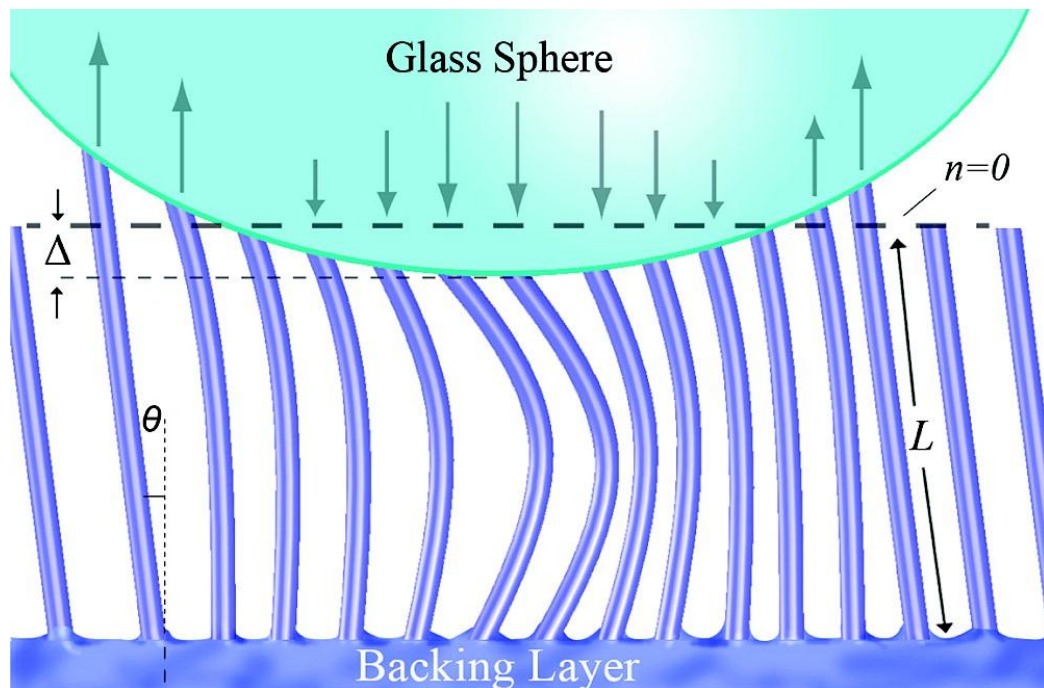
Figure 7: Effect of a glass sphere on adhesion tests. Central fibers buckle while the outermost fibers are in tension resulting in a gradient of forces from the center to edge of the contact radius. Although the fibers in this image are angled, the same effect will be seen with straight fibers. Reprinted with permission from [68]. Copyright 2007 American Chemical Society

Peel tests can be done by attaching the adhesive to a flat surface and pulling one edge from the surface similar to the way elastic thin film peel tests are done [146]. The adhesive is peeled from the surface at a particular angle while the force is measured [50,55,82,100] and both isotropic and anisotropic adhesion behavior can be studied. For many applications the peel test is the most common failure mechanism and thus should be investigated in detail. Peel tests have the added benefit of easy comparison to an unstructured surface of the same material.

1.3.9   *Transfer Printing and Micromanipulation*

The strong, controllable adhesive qualities of the gecko adhesion system have spurred interest in using the technology for micromanipulation. Transfer printing using elastomeric stamps or fibers [7-10,134,147-150] has been done to move inks and small silicon platelets. The adhesion mechanism is the same as standard synthetic gecko adhesives, with individual fibers moving individual inks or platelets instead of considering a larger adhesive area with multiple fibers in contact. Larger structures have been successfully manipulated as well, notably large glass panels with a gecko-like adhesive [78].

Using a variety of fabrication and actuation techniques, microtweezers and microgrippers have been used to manipulate micro objects or biological cells [151-159]. These tweezers and grippers can be used for microassembly of MEMS structures, and are well characterized. However, micromanipulation has not been scaled up to the size of an entire

28

MEMS die. The success of these devices and the transfer printing techniques demonstrate the feasibility of using these adhesives in a silicon environment, but scaling up from the microscale could have unforeseen challenges that will need to be addressed.

The picking and placing motions for inks and platelets can potentially be scaled up as a way of controlling adhesion on larger MEMS die. Cheng details a technique for controlling adhesion [149]; maximum adhesion is achieved by rapidly withdrawing the stamp in the normal direction, followed by placement to the receiver substrate, a slight shear, and slow withdraw speed to reduce adhesion to the stamp as seen in Figure 8.
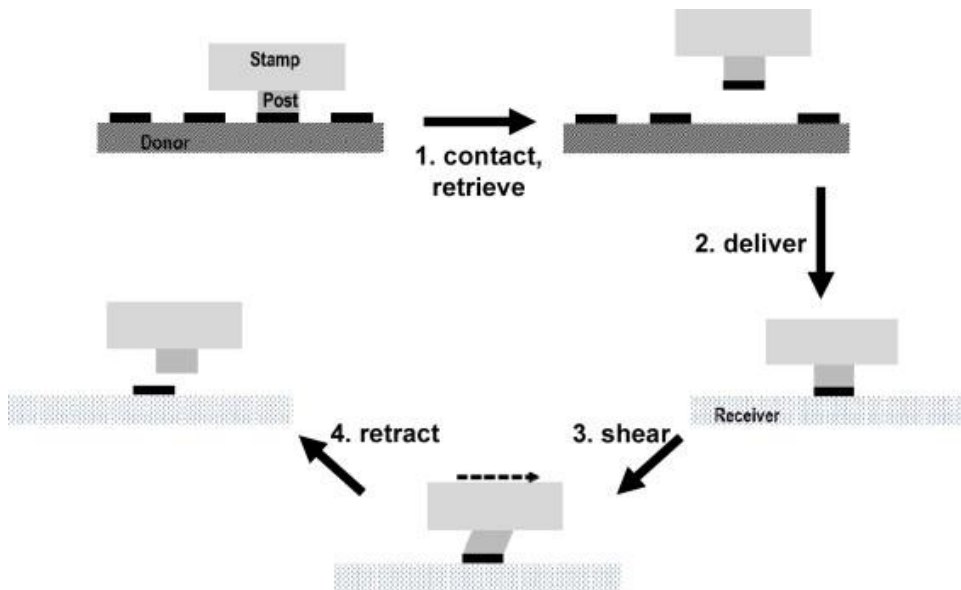
Figure 8: Pick and place operation for elastomeric stamps. A shearing motion in combination with a slow withdraw speed is enough to release the sample. Reprinted from Elsevier, 43, Cheng, Huanyu; Wu, Jian; Yu, Qingmin; Kim-Lee, Hyun-Joon; Carlson, Andrew; Turner, Kevin T.; Hwang, Keh-Chih; Huang, Yonggang; Rogers, John A., An analytical model for shear-enhanced adhesiveless transfer printing, 46-49, Copyright 2012, with permission from Elsevier. [149]

These early results provide the foundation for scaling up gecko adhesion based pick and place to move larger objects such as MEMS devices. A strong, controllable, reliable

adhesive should have the ability to move larger objects and act against stronger forces than just van der Waals interactions as demonstrated in the earlier pick and place of silicon platelets for example.

2   FABRICATION

2.1   Introduction

The fabrication is based off a method described previously [109] as seen in Figure 9. In the original process the focus was on developing very small fibers with high AR (height:width) to demonstrate the capabilities of the technology. It was established however that very small features were fragile and prone to breakage during fabrication and that the high AR structures were not significantly improving the adhesion to smooth surfaces. As a result, some process variations were required to improve the adhesion strength and fabrication yields. The fabrication in this study is a highly optimized version of this previously established method.

Fabrication begins in a class 1000 cleanroom where the master copy of the adhesive is made from Polymethylmethacrylate (PMMA) and SU-8. Following this, all subsequent fabrication steps are done within our lab. Up to eight similar versions can be manufactured in the cleanroom at one time in a span of three to five hours. Multiple versions of the master copy can be used to make hundreds of copies of the final adhesive since each casting step can be repeated numerous times. The result is a very large sampling group for any one type of adhesive making characterization more accurate.
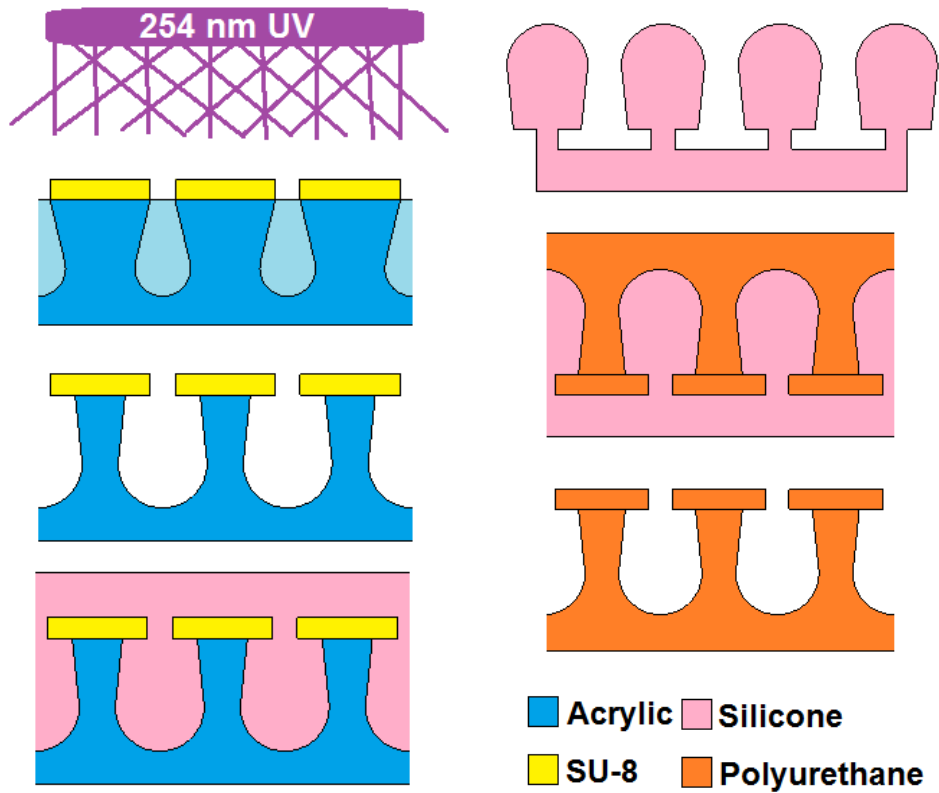
Figure 9: Simplified fabrication steps for the standard fabrication method as described in [109]**. The SU-8 acts as a secondary mask for DUV exposure. Development in SU-8 developer leaves the completed fibers which are cast in silicone rubber. The polyurethane adhesive is cast from the silicone rubber mold.**

2.2   Substrate Preparation

A commercial version of PMMA, known as OPTIX®, manufactured by Plaskolite [160], is first purchased from Home Depot as large sheets. The greatest advantage of using the PMMA sheets is that the material cost per unit area is very low compared to silicon which will allow mold sizes to be scaled up significantly in the future. In addition, the PMMA fabrication process produces many unique features, including extremely smooth sidewalls, rounded corners and overhanging structures, that are far more challenging to manufacture in a silicon based process. This material was first used for patterning

microfluidics [161], and later adapted to gecko adhesives [109]. The sheets are scored and broken into smaller 12" x 24" sections that can be fit into a commercial laser engraver (Versa Engraver VLS3.50). The engraver then accurately cuts the PMMA into 5" x 5" substrates, which is the maximum size compatible with the University of Alberta lithography equipment. After cutting, the substrates are brought into the cleanroom and the protective covering is removed just prior to fabrication. A disadvantage of using the laser engraver is that the heat generated during cutting can cause the PMMA to bow slightly, resulting in a convex side and concave side. If the concave side is used, the photomask may not have adequate contact in the center of the substrate during exposure. This will result in poor quality, bloated features that are not usable for an adhesive. The solution is to use the convex side, since the bow shape can improve contact over the critical central areas. To determine the convex side, the acrylic substrate is held against a glass substrate of equal size. Newton rings become visible with the areas of close contact at the center of the rings. The PMMA often is not perfectly convex, and can be warped with a slight wave shape, but the visible Newton rings allow easy recognition of the more convex side.

Once the convex side has been determined, the substrates can be marked on the backside for identification (usually by scratching with a knife), and then cleaned with isopropyl alcohol (IPA), de-ionized water, and pressurized nitrogen. Substrates can be processed one at a time, but for efficiency, between four and eight were processed during each fabrication session. Manufacturing multiple substrates at once also ensures that nearly identical processing conditions are used, and different conditions can be tested to determine their effect on the adhesive more accurately.

2.2.1   *Substrate Warping Issue*

As mentioned previously, the PMMA sheets purchased from a local hardware store are often slightly warped. The surface warp is often exacerbated when the sheet is cut with the laser engraver. This non-flatness causes a serious issue during the exposure step. The exposure mask material is glass with chrome patterned on one side, which is normally used for extremely flat silicon substrates. The two flat surfaces can make excellent contact using the aligner in the University of Alberta Nanofab, resulting in very sharp features. If there is an air gap between the photomask and photoresist, the UV light will scatter and bend slightly when passing the chrome mask. The mask features will be projected as an unfocused image onto the photoresist, resulting in a bloated image with uneven and poorly defined edges as seen in Figure 10. Thus if the PMMA substrate is too warped, portions of the resulting SU-8 caps will be unusable as an adhesive.
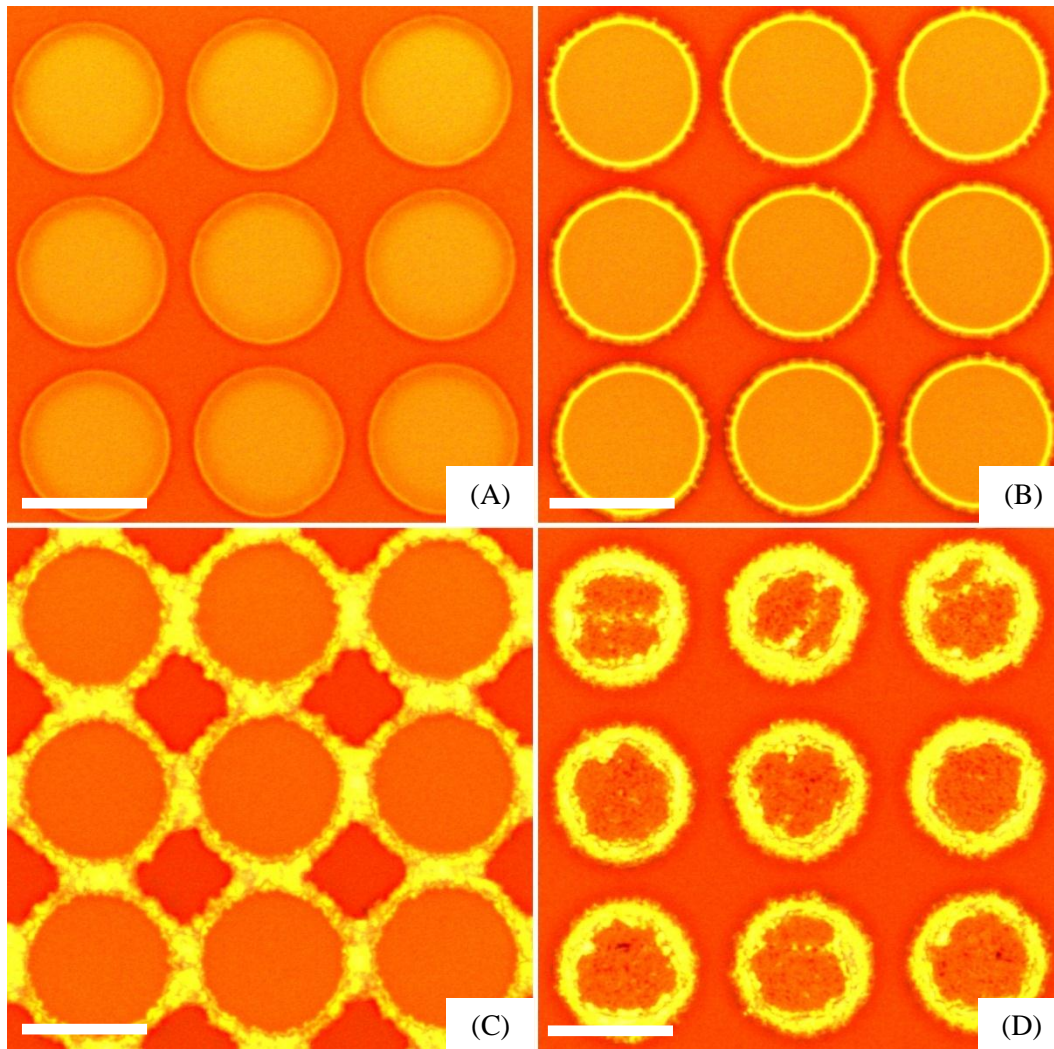
Figure 10: A comparison of various levels of exposure for identical sizes of 24 μm SU-8 caps on a PMMA substrate including: excellent contact between the mask and photoresist (A), slightly bloated features (B), extremely bloated, merged features (C), and an insufficient exposure dose (D). All images were taken from different sections of the same substrate. Debris was present on the pre-exposed photoresist, resulting in a large air gap between the mask and resist causing the merged features in (C), but poor features due to mask warping normally resemble (B). A felt marker was used to partially block UV light, resulting in the underexposure present in (D). Scale bars represent 20 μm.

2.3   Cleanroom Fabrication

2.3.1   *Spin Coating*

Fabrication begins with the spin coating of a layer of SU-8 2002 photoresist onto the

PMMA. SU-8 2002 was chosen to achieve the desired SU-8 thickness of between 2 and 3

µm at typical spin-coating speeds. The thickness of the SU-8 will define the thickness of

the final adhesive caps. The spin speed was chosen to be 3000 RPM, which is the

manufacturers recommended spin speed for a thickness of 2 µm [162]. A 5 second ramp

up to 500 RPM, followed by a 5 second ramp up to the full 3000 RPM was used to ease

the square substrate up to the higher speeds and reduce the likelihood of a loss of contact

with the spinning chuck. The SU-8 thickness often varies slightly across the substrate,

with a thinner layer in the center and thicker near the edges as the spinning forces gently

draw the photoresist from the center to the edges. There is no evidence to date however

that this slight change in thickness significantly affects the performance of the adhesives.

Following spin coating, the substrates are baked in a convection oven at 90°C for 3

minutes to help drive out the solvents before exposure, which is close to the maximum

temperature before PMMA begins to warp. This is different than the SU-8 manufacturers

recommended time of 1 minute at 95°C using a hotplate, which risks warping the PMMA,

and is impractical for repeatable performance due to the poor thermal conductivity of the

substrate. The extra prebaking time is to compensate for using the convection oven at a

lower temperature as the substrate may take longer to heat.

2.3.2   *Exposure*

Despite the attempt to improve photomask contact through using the convex side of the

substrate, additional measures were needed to more uniformly distribute contact.

Originally bulldog clips were used around the perimeter of the substrate and photomask, sometimes with a second blank glass plate below the PMMA substrate to help flatten it. In addition to these clips, neodymium magnets were placed in the center of the substrate such that they acted to squeeze the mask and substrate together. The magnets provided a good force for squeezing the vulnerable central area of the mask furthest from the bulldog clips, but created a problem by blocking a small section of UV light. A second technique to replace the magnets was developed, which involved using flat-ended polymer screws to apply pressure at key areas of poor contact. A 5" x 5" plate that contained an array of holes and flat-ended plastic screws is placed below the substrate such that the screws will apply pressure to the substrate from below as seen in Figure 11.

Figure 11: Adjustable screw apparatus for increasing mask contact. The screw array (right) is being used to apply pressure at strategic points of poor contact between the mask and substrate (left). Each screw can be individually turned to apply upwards pressure while the eight bull dog clips squeeze the mask, substrate, and screw apparatus together. The rigid glass mask remains stationary while the more flexible PMMA substrate conforms to flatten against it when being assisted by one or multiple screws.

Since each screw is individually adjustable, the user can visually check for locations of poor contact and apply more pressure strategically. By observing the same newton rings as used to find the convex side of the substrate, areas of poor contact become visible as seen in Figure 12. The poor contact can be corrected by twisting the screw upwards at

that location, which forces the PMMA to conform to the more rigid glass mask. This technique helped to further improve contact and thus feature quality, making the inexpensive PMMA more viable for these adhesives. The system requires more cleanroom time to adjust each of the screws, but our past work has suggested that exposure is the most critical manufacturing step to ensure good performing adhesives [131]. The system does not guarantee perfect contact, as sometimes the substrate is too warped to be corrected, but it has shown to be significantly better than only using the bulldog clips.

Figure 12: Newton rings can be seen indicating varying levels of photomask and substrate contact. The darker, wider rings indicate good contact while closely packed rings indicate poor contact or debris separating the photomask and photoresist. The sample is a test structure photomask on a PMMA substrate with SU-8 photoresist identical to the gecko adhesive processing conditions.

Exposure was done at a range of doses with a minimum of 280 mJ cm^{-2}, which is above the manufacturers recommended dosage for this SU-8 thickness of 80 mJ cm^{-2}. The reason for this is that it is better to overexpose the negative SU-8 photoresist to improve adhesion to the substrate [109]. The acrylic substrate should not have any topography that will reflect the UV light and cause problems during extra exposure, and thus increasing the exposure dose to maximize SU-8 crosslinking and adhesion is worthwhile. The quality of the SU-8 is significantly more dependent on the quality of contact between the mask and substrate rather than exposure dose, therefore variations in exposure dosage was not investigated in depth. Approximately 20 seconds of exposure was enough to ensure good quality caps at all exposure intensities over the course of fabrication trials.

2.3.3   *Deep UV Exposure*

Deep UV (DUV) exposure is done to decrease the molecular weight of the PMMA in order to increase the development rate in SU-8 developer [109]. The SU-8 acts as a secondary photomask, blocking the DUV light on the areas of PMMA that will eventually become the fiber structures. This step can be done in the cleanroom, but to reduce fabrication costs it was done in our own lab in a 254 nm DUV exposure source (Stratalinker 2400) that is normally used for DNA crosslinking. The box uses four mercury arc lamp bulbs to produce the light, and as a result has an inconsistent intensity of light throughout the box. To give the substrate a relatively even exposure dose, it was placed upon a rotating battery powered pedestal (AUTOArt 8" rotary display) during exposure. The intensity of the UV light also depends on the separation distance of the bulbs to the substrate. The substrate was raised such that it was 44.5 mm from the bulbs during exposure. The intensity of light at this distance was measured with a UV intensity meter, and it was found to have an intensity of 4.4 ± 0.2 mW cm^{-2}. The light can be

partially collimated as well by placing a 1:1 plastic grid between the bulbs and the substrate [109]. With the grid used in our early trials, the UV intensity was reduced to 1.5 $\pm$ 0.4 mW cm^{-2}. As a result the substrate will need to be exposed nearly three times as long for an equivalent dose if partial collimation is desired. Typical uncollimated exposure times to achieve an approximate AR of 1:2 are 5-8 hours depending on the diameter of the SU-8 fiber caps. Thus a collimated dose needs to be approximately 15-24 hours. This should produce about the same AR, and to achieve a higher AR, significantly longer exposure doses can be expected.

During exposure, the chemistry of the acrylic is changing. One result of this is an increase in tensile stress in the exposed acrylic which warps the substrate. If the sample is not developed shortly after exposure, cracks can appear in the acrylic and adversely affect the performance of the adhesive produced from these molds. The solution to this stress problem is to anneal the substrate after exposure at 80°C overnight to remove the internal stresses.

DUV exposure is one of the core steps of the fabrication process that will define the shape of the underlying fibers, but not necessarily the performance. The presence of an overhanging cap has been proven to be much more important in determining adhesion [129], but the underlying structures still play a role, especially in determining the adhesive's ability of conform to off-axis loads [131]. The dimensions of the overhanging cap are a function of the development time as discussed in the next section.

2.3.4 *Development*

The final stage in the fabrication of the master copy of the adhesive is the second development of the substrate. Development is done with SU-8 developer, which is an

organic solvent solution consisting of 98-100% 1-methoxy-2-propyl acetate, and 0-2% 2-methoxyl-1-propanol acetate [163]. Submerging the substrate in SU-8 developer will begin to etch the PMMA, while leaving the SU-8 features intact [109]. The development rate of the PMMA is a function of its molecular weight, and thus the exposed PMMA, with a lower molecular weight, will be dissolved significantly faster that the unexposed PMMA. Within the first few minutes the exposed PMMA will be entirely dissolved, and the remaining unexposed PMMA will be dissolved at approximately 100 nm min^{-1} at 21°C. Preliminary fabrication was done at 21°C, but current cleanroom temperatures are closer to 18°C, which decreases dissolution rates considerably.

The use of uncollimated light complicates the developed depths, as the dose in between closely packed features is much lower than that in wide open areas. Measuring the depth between closely packed features is difficult, and an estimate is found by using a profilometer in the open areas. For a more accurate estimate, a basic calibration of depth for exposure dose, development times, and feature spacing at 18°C is shown in Figure 13.

10 Minutes

Development Depth (μm) vs Feature Separation Distance (μm)

Legend:
- 0 hours
- 5 hours
- 6 hours
- 7 hours
- 8 hours

20 Minutes

Development Depth (μm) vs Feature Separation Distance (μm)

Legend:
- 0 hours
- 5 hours
- 6 hour
- 7 hours
- 8 hours
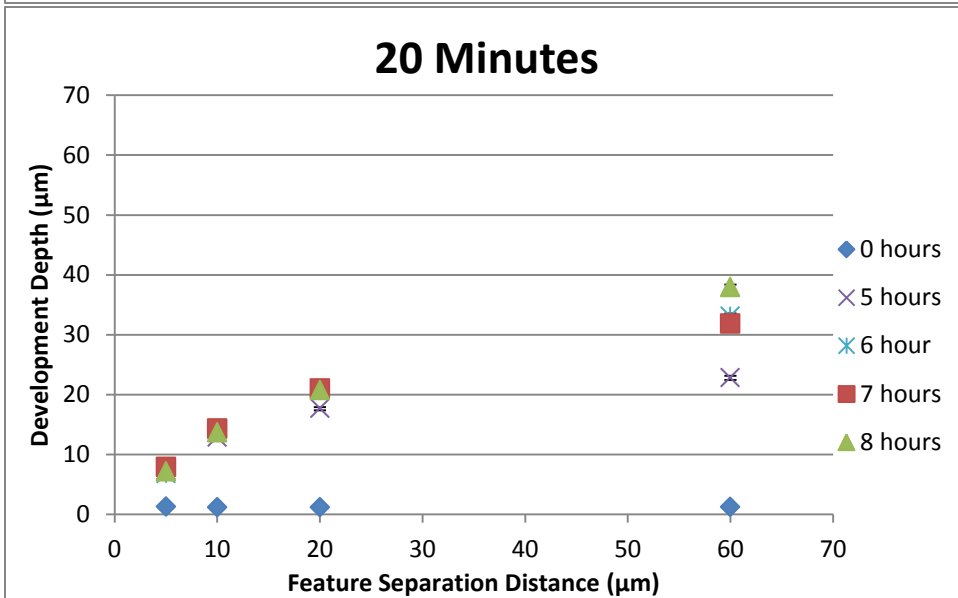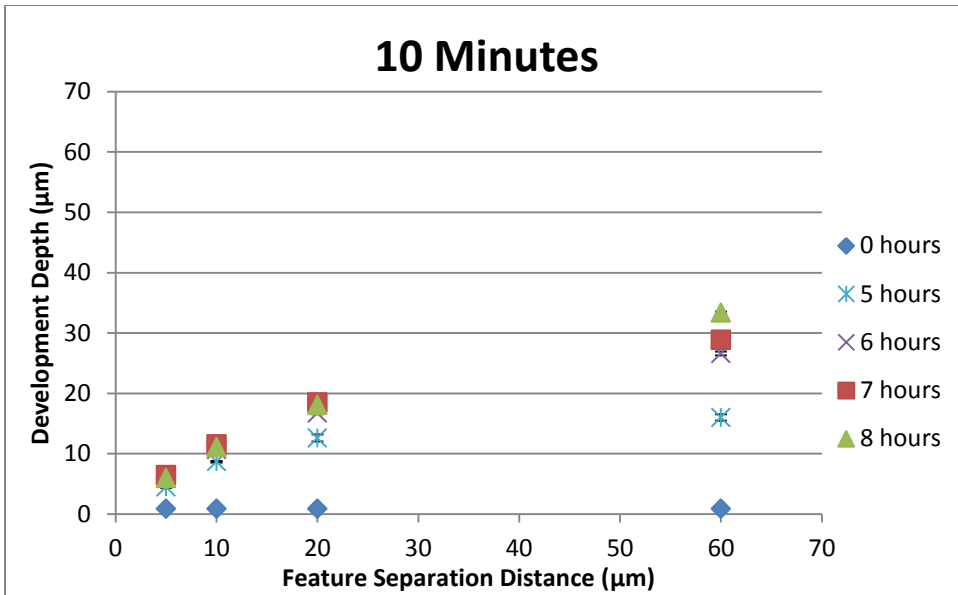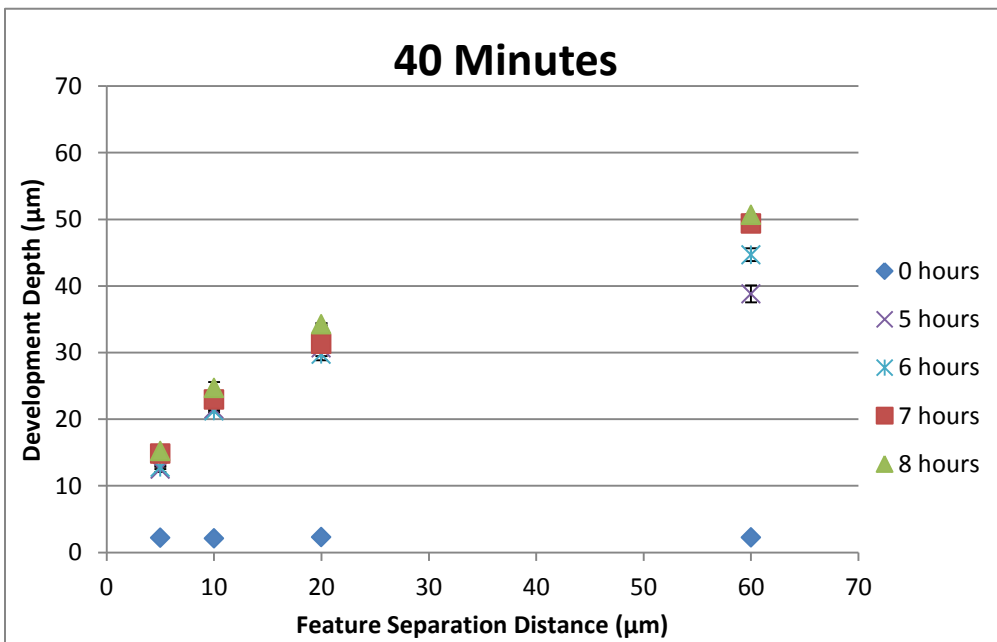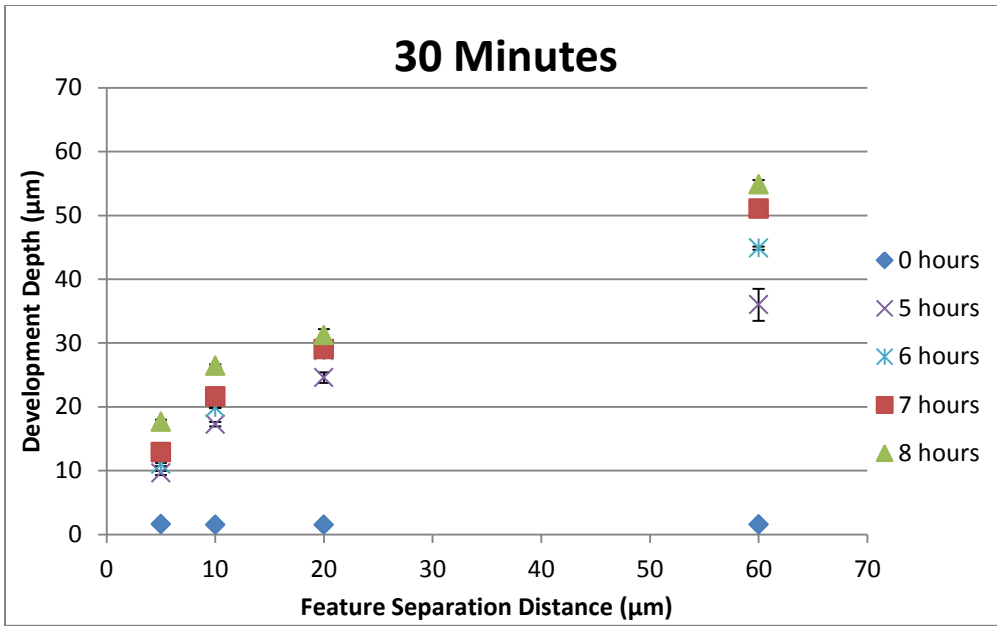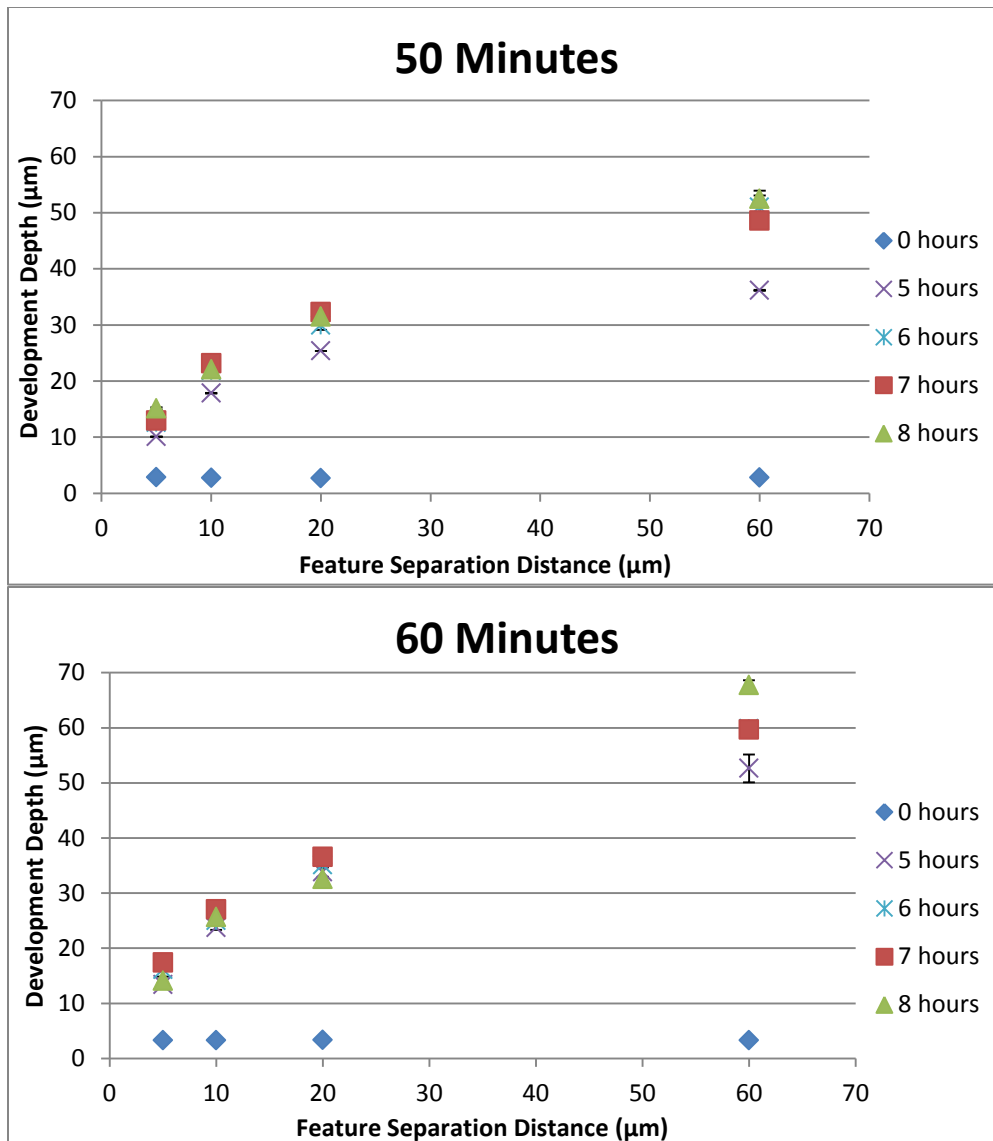
Figure 13: Development depth as a function of feature separation distance for various exposure doses and development times. Each graph represents one substrate that was developed approximately the time shown in the title. Each data set represents a section of the substrate that was under DUV exposure for the indicated time. The features were approximately 2 μm thin SU-8 strips separated by the distances indicated. The 60 μm distance represents an infinite plane where adjacent features do not affect the development depth. The vertical axis has been kept at the same scale for comparison.

This characterization was done on a number of substrates fabricated from a mask that consists of various test structures. Measurements were taken by scanning electron

microscope (SEM) images on features that resemble the gecko adhesive, as seen in Figure 14. SU-8 strips of varying widths and separation distances were present on the substrates, and it can be clearly seen that the separation distance of features affects the development depth. Closer features reduce the developed depth more drastically, and as a result, a closely packed array of fibers may need a longer development time to reach the desired fiber height. This is an important consideration when designing future gecko fiber arrays and trying to predict their geometry from fabrication processing parameters.
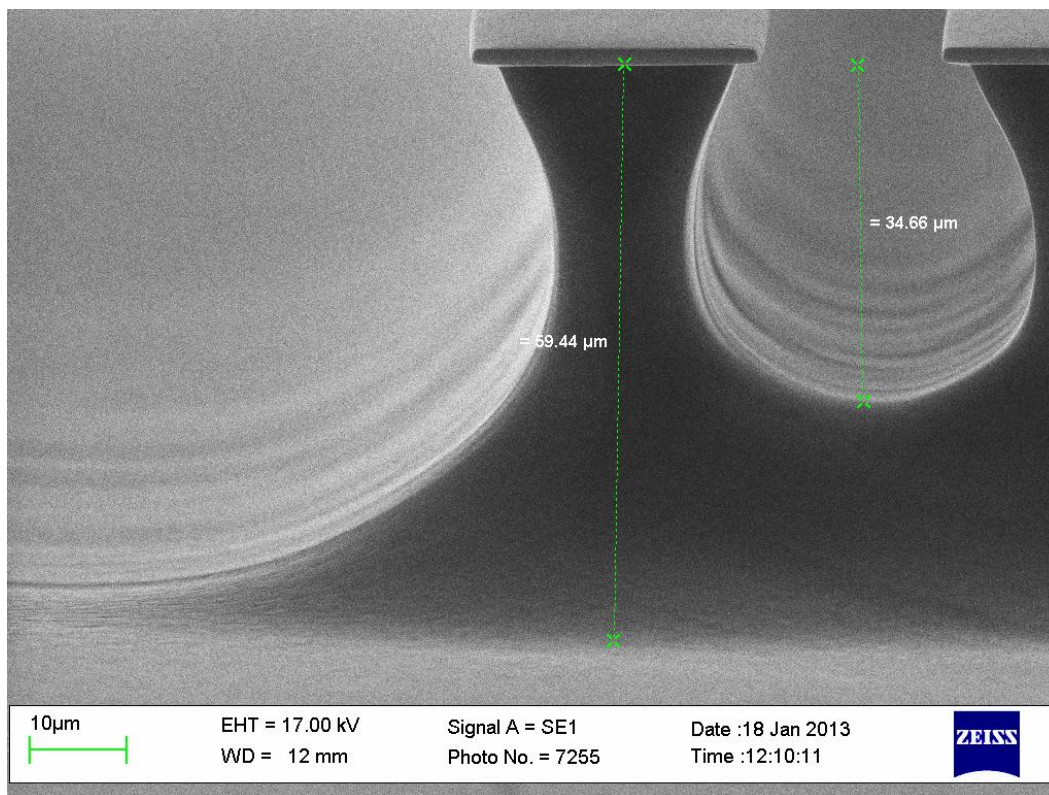
Figure 14: Sample image from the depth characterization SEM imaging. It is clear that the close proximity of the SU-8 strips is reducing the total development depth compared to the unrestricted development on the left.

The substrate will rarely be given 0 hours of DUV exposure, but knowledge of the unexposed PMMA dissolution rate is still valuable. The fiber undercut, which defines the cap overhang, is created by the development of the PMMA directly under the SU-8

features, which were not exposed to DUV light. Therefore the unexposed development rate will be approximately the undercut development rate. For 0 hours of exposure, the development rate is 58 ± 7 nm min^{-1}. Based on this rate, an undercut of 3 μm will be achieved with approximately 50 minutes of development. SEM imaging of substrates developed in a 21°C cleanroom indicate a much higher development rate, which is expected since these development trials were done at18°C, and development rate is highly dependent on temperature.

It is important to estimate the undercut from development time and etch rate, but also to supplement this estimate by periodically removing the sample from developer to visually confirm the undercut. By removing the sample from the developer and observing it under an optical microscope, the undercut can be clearly seen through the SU-8 cap and the manufacturer can determine whether or not to continue with development. The substrate can also be returned to the cleanroom for additional development after it has been replicated numerous times and the adhesive tested. Overdevelopment risks the fiber necks becoming too narrow, which can result in them fracturing during replica molding, or breaking away from the substrate during development. These stray fibers in the developer solution can damage the fibers still anchored to the substrate. Careful attention to development time is important to prevent damaging the substrate and losing the cumulative fabrication time.

This is the final step in creating the master adhesive structures, and all subsequent copies of the adhesive will be replicas of these structures, thus it is essential to handle the substrate extremely carefully after fabrication to prevent damage.

2.4   Replica Molding

Replica molding is used for fabricating the final adhesive. Replica molding is a widely used fabrication technique that is well characterized [62,109]. Our process begins by casting the negative mold of the completed master adhesive copy in silicone rubber. TC-5045 silicone rubber (BJB Enterprises) was used for its strength and durability (Shore A hardness 45, Tensile Strength 756 psi). TC-5045 can be used repeatedly over a number of weeks or months with little degradation of the mold for multiple castings. However, during some fabrication it is sometimes desirable to have a transparent mold to view the microstructures filling. Thus a translucent silicone rubber, TC-5030 (BJB Enterprises), was used to replace TC-5045 for most fabrication in later work. TC-5030 is slightly softer and less durable (Shore A hardness 30, Tensile Strength 700 psi), but this reduced stiffness can help with demolding from both the master copy and the final adhesive. Sylgard 184, the most commonly used silicone rubber in microfabrication research, was also been considered as a mold material, but was quickly rejected since it is much more susceptible to tearing compared to the silicone rubbers TC-5030 or TC-5045. A tear in the edge of a mold will quickly propagate, making the molds very fragile. Thus the more durable TC-5030 was selected as the primary mold material.

Casting for both silicone rubbers is done using standard mixing parameters given by the manufacturer. Mixing is followed by applying the liquid prepolymer to the mold and degassing in a vacuum oven for approximately 10 minutes. Curing is complete in approximately 3 hours if the polymer is put into the 80°C oven, otherwise 24 hours at room temperature.

Once the polymer mold is created, the master adhesive substrate is safely stored away and the final adhesives are created from these reusable molds. One of the most common

polymers used for the adhesive, and the one primarily used within our lab, is ST-1060 from BJB Enterprises. Preparation is similar to how the silicone rubber molds are made, and involves mixing the part A and B polymer together at the manufacturers given ratio – in the case of ST-1060, a 100:55 weight ratio of part A to part B. The prepolymer is applied to the negative mold and degassed in a vacuum oven for at least 10 minutes. During degassing, ST-1060 will often expand with bubbles far more than TC-5030, and thus the vacuum must be carefully monitored to prevent the polymer from thinning out too much and overflowing the mold. Curing is done at room temperature for 24 hours, followed by 24 hours in an oven at 80°C. The adhesives are ready to be used after they have been removed from the oven, cooled, and demolded. A similar process can be used to cast polymers with different properties, and BJB Enterprises' polymers such as ST-1087 and TC-854 have been fabricated with the same molds.

This replica molding process has a multiplicative effect on the volume of samples that can be created. Multiple molds (20+) can be cast from the original master with minimal degradation if proper handling procedures are followed. From each negative silicone mold, multiple adhesives (20+) can be cast resulting in a possible 400+ samples from a single PMMA master. This greatly reduces the cost per sample of the final adhesive making this method viable for commercialization.

2.4.1   *Viscous Polymer Molding Issues*

For some materials, such as polymers with very short working times or polymer composites with an additive, the prepolymer can be extremely viscous. A vacuum degas step will not be sufficient to draw the material into the microstructures once the viscosity reaches a critical value; the prepolymer will simply remain on the upper surface of the mold and not consistently fill the microstructures. Even if the prepolymer is able to

48

partially or fully fill the mold through vacuum, the backing layer of the adhesive will be uneven as seen with the viscous prepolymer of Figure 15. A new fabrication technique was needed to handle these viscous polymers.
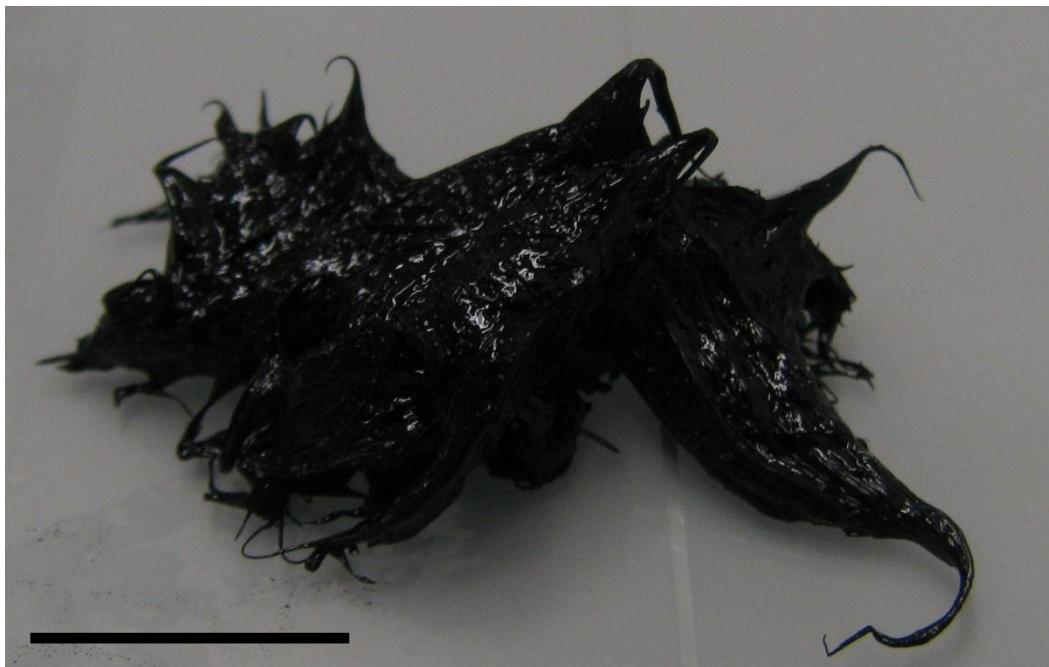
Figure 15: Extremely viscous prepolymer made from ST-1060 (antistatic version) and 12% by weight carbon black composite. Exposure to vacuum did not assist in filling the mold and the adhesive was left with a very rough, uneven backing layer. Scale bar represents 5 mm.

2.4.2   *Squeegee Solution*

The first solution to this problem of filling silicone molds with viscous materials was to use a spatula to manually force the material into the mold. This was a good temporary solution for testing viscous polymers as adhesives, but still left an uneven backing layer, and occasionally only partially filled the mold as it is difficult to apply even pressure by hand. A more automated and characterized process was needed as a spatula could one day be scaled up into a fully automated squeegee in a roll to roll manufacturing setting. As further detailed in Appendix A, an apparatus was built to test the effectiveness of the

49

squeegee at various pressures (Figure 16). The apparatus is customizable for different pressures and angles of the squeegee.
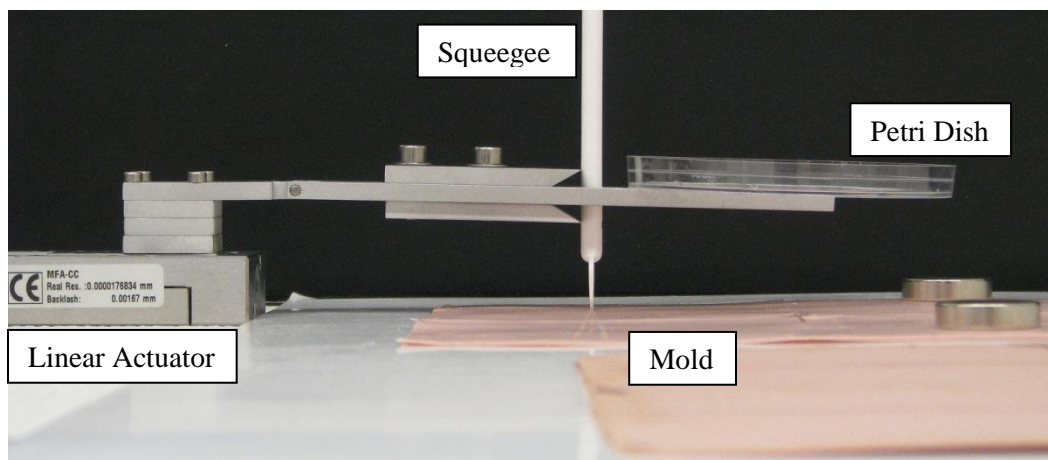
Figure 16: Squeegee testing apparatus for evaluating the effectiveness of the squeegee at different pressures and angles. The apparatus is pulled by a linear actuator while weights are placed in the petri dish to apply pressure to the mold while it drags across the prepolymer (not pictured). The three point hold in the center of the apparatus allows the squeegee to be placed at a range of angles. Magnets hold the mold in place to a steel table under the mold during the dragging motion.

It was found that increasing pressure typically increases the percentage of filled fibers as seen in Figure 17. The sharp reduction in filling after 537.2 kPa is most likely caused by the higher pressure forcing polyurethane out of the mold after it has filled. The study also visually inspected the molds as they were being filled by creating clear molds from TC-5030 and positioning the system under an inverted microscope. The surprising result was that the micro-cavities of the mold are fully collapsed under the pressure of the spatula, and as they regain their shape when the pressure is released, a vacuum is created that draws the polyurethane into the mold. This means that the trail of polyurethane following the spatula is critical for effective filling. If this trail is removed, either from the applied pressure being too high or an inadequate volume of prepolymer, then the vacuum created

50

upon regaining the mold shape will only draw in air. The higher pressure trials may have been removing this critical polyurethane trail and reducing the fill percentage.
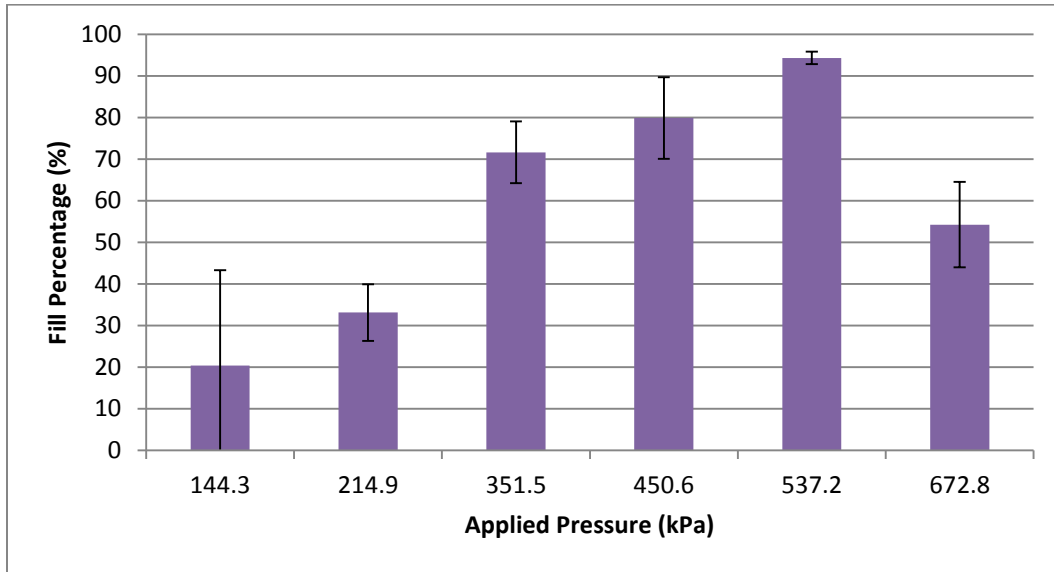
Figure 17: Applied squeegee pressure versus fill percentage of the squeegeed area. The sharp drop after 537.2 kPa is likely due to a lack of prepolymer trailing the squeegee.

Although a promising initial result, the squeegee method still does not achieve 100% fill rates consistently, and it is difficult to arrange the setup for accurate robotic use in a laboratory setting. A more effective compression molding technique is desired, one that is simple to use and reliable, and works for a variety of polymers.

2.4.3   *Lamination Method*

With the success of using a spatula to apply viscous polymer to a mold, a more effective, large scale technique was desired. A roll to roll manufacturing system was considered, but due to equipment limitations a simpler approach was needed. Micralyne Inc. was able to provide a commercial photoresist laminator (Think and Tinker 1200df, Figure 18) that consists of two rubber rollers with adjustable separation distance. These rollers are able to

apply smooth, even pressure to a sample as it is drawn through them. A lamination

technique was a potential compression molding technique for these adhesives.
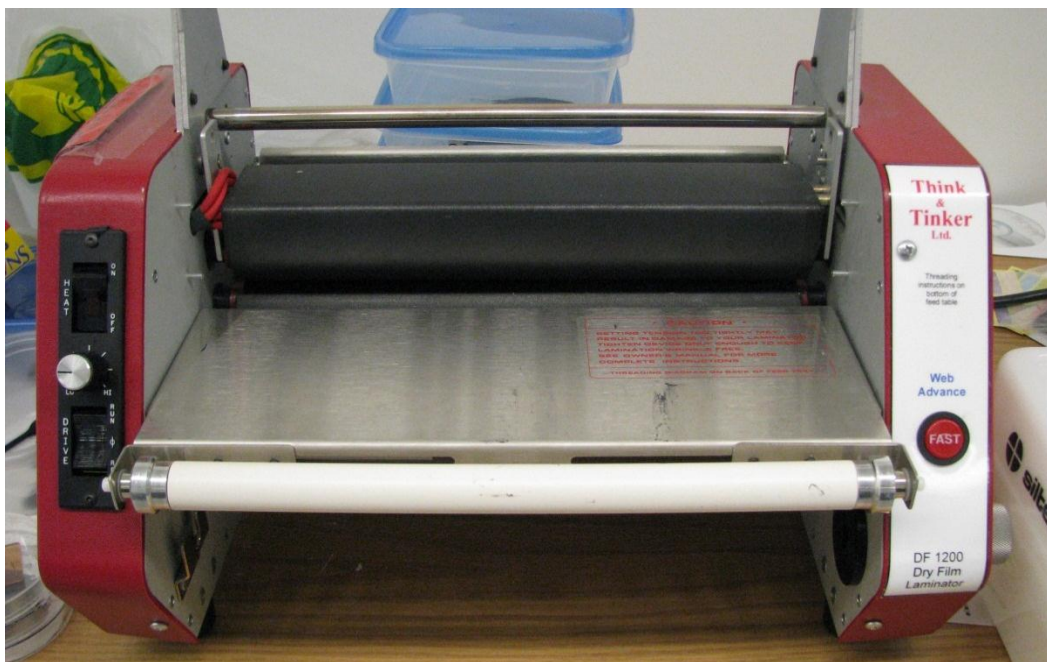
Figure 18: Commercial laminator Think and Tinker 1200df. Normally used for laminating photoresist, the adjustable rollers are excellent for laminating viscous polymers into gecko adhesive molds.

The technique begins with applying a small amount of prepolymer to a thin sheet of stiff

polyethylene (which makes an excellent release material for all the polyurethanes used in

this work). The mold is placed on top of the prepolymer such that the prepolymer is next

to the edge of the mold that will first enter the laminator. The sample is placed in a

polyethylene bag (Zip-lock freezer bags) to protect the laminator from any polymer

overflow, and then run through the laminator to compress the prepolymer into the mold.

The entire process can be seen in Figure 19. The roller's separation distance can be

adjusted to reach the desired backing layer thickness of the cured adhesive. After waiting

the appropriate time for a complete cure, the adhesive can be removed from the bag and demolded.
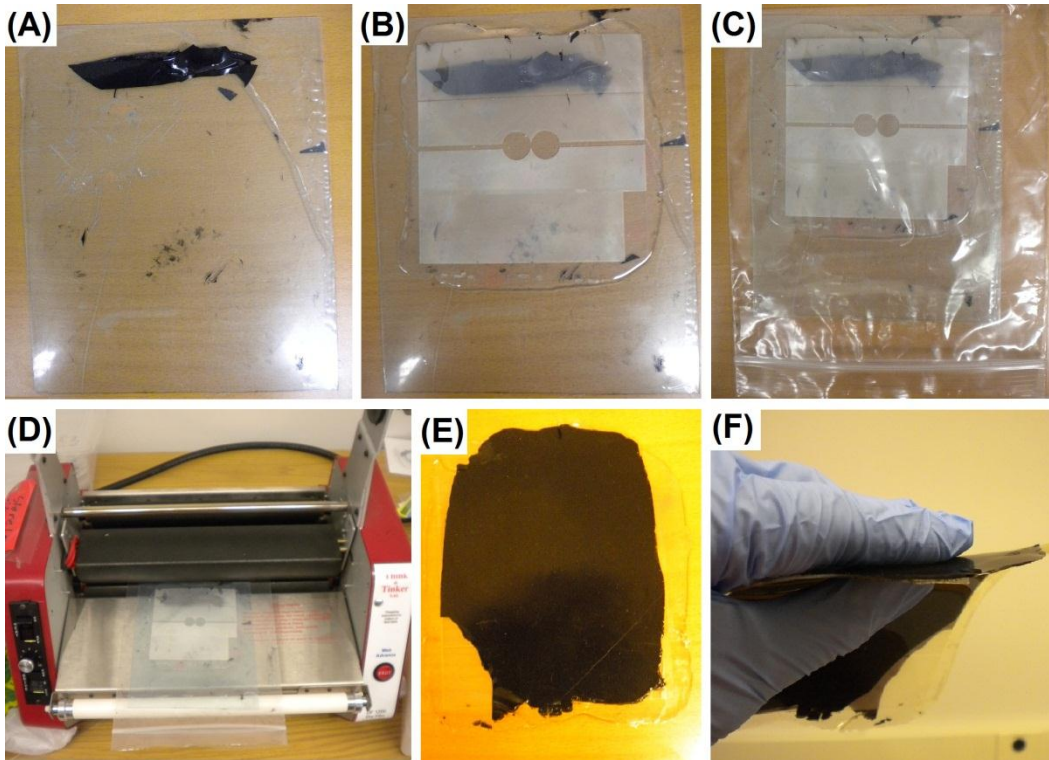
Figure 19: Process flow for laminating an adhesive sample. Prepolymer is first applied to one end of the stiff polyethylene sheet (A). The mold is set overtop and both are put into a Zip-lock bag (B,C). The setup is pushed through the laminator (D). After curing for 24 hours, the laminated sample can be removed from the bag (E). The thin backing layer (F) can be easily applied to other surfaces. A small section of the laminated adhesive was removed prior to taking the image in (E).

The lamination technique removes the need for a vacuum degas step during fabrication. This is especially valuable for dealing with extremely viscous materials that cannot be vacuum degassed, but also will remove the need for expensive degassing equipment, reducing the total manufacturing cost.

The ability to accurately customize the backing layer thickness is another significant advantage of using a laminator. This method can produce backing layers as thin as 100 µm, and, by having the adhesive between two molds, it is possible to make thin, double sided adhesives as seen in Figure 20. Adhesives such as this can potentially be used as a sealing layer or soft connection joint. The thinly laminated adhesive can easily be applied to other surfaces, either with traditional pressure based adhesives, glues, or by curing another layer of the identical polymer between the cured adhesive and desired surface. An easy method of applying the adhesive to other objects opens a wide range of possible applications for temporary adhesives in fields such as sports, household products, or electronics. The lamination method is an excellent proof of concept for compressive molding and can one day be scaled up for continuous roll to roll applications.
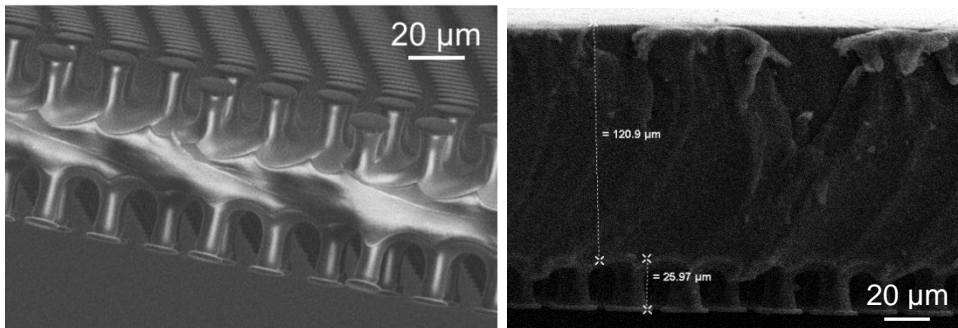
Figure 20: Adhesives fabricated by lamination. A double sided adhesive (left) is produced by applying the polyurethane between two molds, and an adhesive with 120.9 µm backing layer is produced (left). The thin backing layer assists in applying the adhesive to other surfaces.

3   ADHESION TESTING

3.1   Introduction

Determining adhesive strength is crucial in order to properly design an effective pick and place tool. Knowing the adhesive strength will allow the pick and place tool to minimize the required adhesive contact area and optimize the design. The adhesive strength can also be compared to conventional adhesives.

3.1.1   Work of Adhesion as a Characterization Tool

The work of adhesion can quantify the adhesive force needed to separate two surfaces and is a valid method of reporting adhesion forces [79]. Work of adhesion can be calculated from the surface energy of flat materials, but it does not consider fibrillar interfaces. Instead the effective work of adhesion, W_{ad}, can be found as a function of the maximum tensile load, F_{max}, achieved during an adhesion test [65]:

$$W_{ad} = \frac{-2F_{max}}{3\pi R_s}$$

Where R_s is the radius of a hemispherical indenter.

While work of adhesion is valid for predicting adhesion against an identical hemisphere, it is easier to compare adhesion over a wider range of surfaces when it is reported as adhesion pressure. Thus this work will focus on reporting adhesion as a force or pressure rather than effective work of adhesion.

3.2   Testing Equipment and Methodology

A testing apparatus is needed to carry out the adhesion tests. It should include a high accuracy load cell for effective data collection, be customizable and upgradable for future

tests, and be as autonomous as possible to make data collection efficient. The ideal apparatus should not require an operator to be present for the trials as this will allow the system to run unattended for hours or overnight if desired. The adhesive tests done in this work were conducted using the custom built testing apparatus as seen in Figure 21. The adhesion test system consists of a linear actuator, a load cell to measure forces, and a 6mm diameter sapphire hemisphere which contacts the adhesive samples. Using a hemispherical indenter is commonplace for testing such adhesives and has been done successfully in our group previously [131]. The linear actuator is a MFA-CC model controlled by ESP301 motion controller from Newport Corporation. Up to three actuators can be controlled simultaneously with fully customizable acceleration, speed, and timing settings with a maximum speed of 2.5 mm s^{-1}. The actuator shown in Figure 21 was mounted to a second actuator (not pictured) that controls lateral motion. The load cell is a GSO-25 model from Transducer Techniques, which has a range from 25 g of compression to 25 g of tension. The adaptor was custom made from aluminum. The hemisphere used was a 6 mm sapphire half ball NT49-556 from Edmund Optics. The hemisphere can be easily switched for one of a different size or entirely separate type of indenter. The entire apparatus is controlled with custom written LabVIEW software. The software samples data from the load cell and collects data at 10 Hz and the adhesion testing system can simply extract the preload and adhesion values, and/or record the full, real time data. The test system has customizable testing parameters and more complex characterization is possible, but for the purposes of this project, data from the following two tests is sufficient.

56
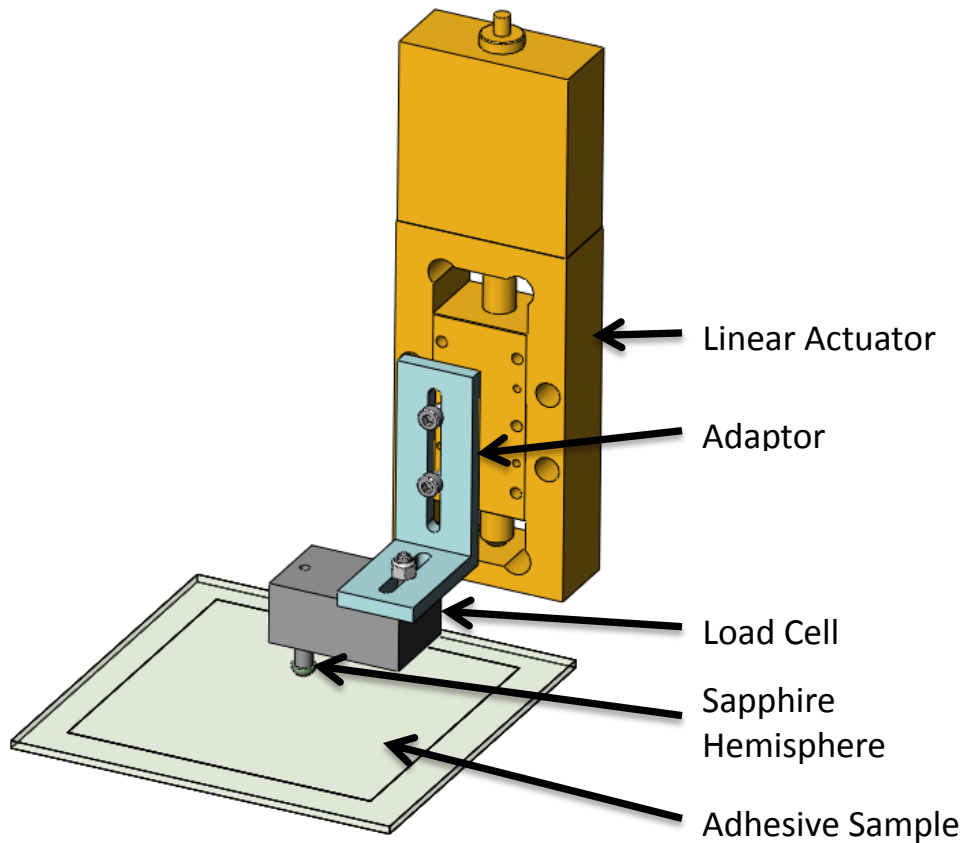
Figure 21: Custom built testing apparatus. The linear actuator is anchored on a second linear actuator (not pictured) placed perpendicular to the first actuator to enable horizontal movement. The adjustable adaptor allows the load cell to be positioned appropriately for testing the sample. Electronics and wiring is not shown.

3.2.1 Normal Adhesion Tests

The procedure for a normal adhesion test is shown in Figure 22. It involves applying a small preload to the sample, and withdrawing the indenter to record the maximum adhesion force. The standard adhesion test was programmed for a range of preloads from 2 mN to 60 mN, although the actual preloads were slightly higher (~0.5 mN) due to feedback time delay of the load cell and actuator. All tests were done with the 6 mm glass hemisphere moving towards, and withdrawing from, the sample at a speed of 5 μm s^{-1}. It is known that increasing retraction speed will increase adhesion [164], and thus a low

speed of 5 μm s^{-1} is a good balance of simulating quasi-static behavior and having the tests finish in a reasonable time while not affecting adhesion. A location was tested starting from 2 mN and ending at 60 mN and tests were usually done after repeated preloads in that location. Testing the same area simulates repeated attachment/detachment cycles that the adhesive will most likely encounter, and thus gives a more conservative measurement for the adhesive strength. The software is able to test a pristine location for each trial, but this was not done for most data presented.
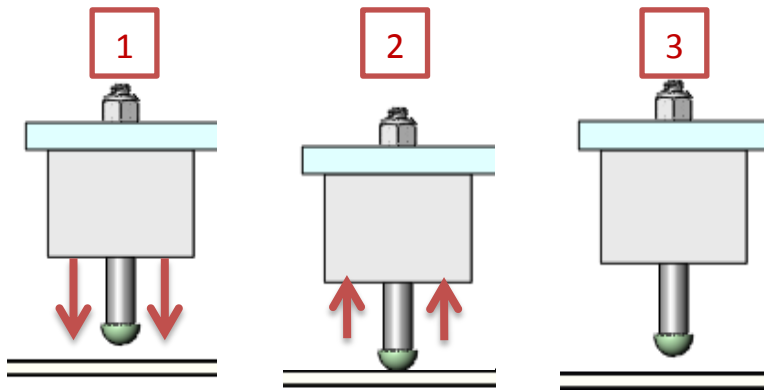
Figure 22: Normal adhesion testing procedure. Step 1: Impact the adhesive with a known preload measured with the load cell. Step 2: Stop the linear actuator and reverse direction, recording the adhesion during pull-off. Step 3: Restart the test with either the same or higher preload.

3.2.2 *Load Drag Pull Tests*

A load-drag-pull (LDP) test can show how the adhesive performs in shear loading [135]. The testing apparatus was left unchanged for LDP tests, and only the software was modified. Since the load cell gives no feedback in the horizontal plane, the testing system can only show a reduction in normal adhesion caused by a horizontal dragging motion, rather than the shear force the adhesive can withstand. However, knowing the shear force adhesion reduction is still valuable data as it can be applied to a release mechanism for

turning off adhesion. The standard procedure for a LDP test is to move the load cell a specified distance laterally while in contact with the adhesive as seen in Figure 23.
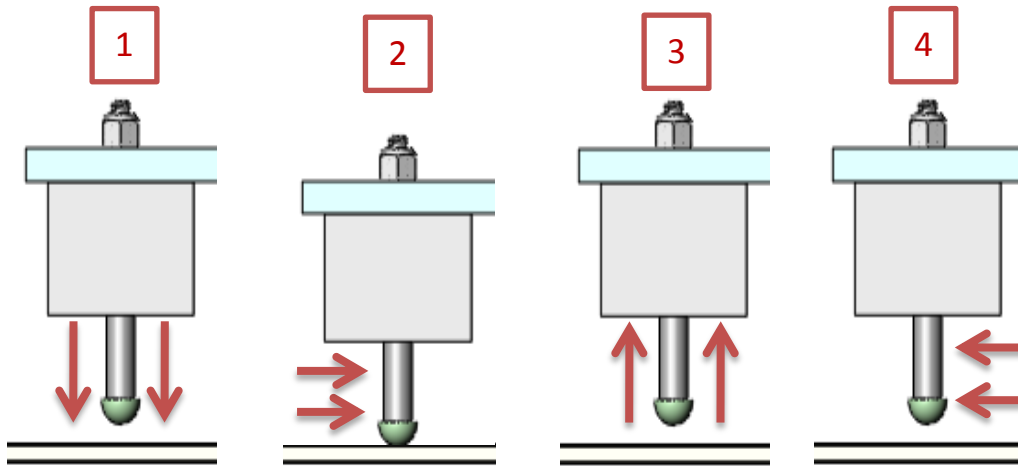
Figure 23: Load-drag-pull testing procedure. Step 1: Impact adhesive with a 2 mN preload. Step 2: Move hemisphere laterally a specified distance while still in contact. Step 3: Move hemisphere out of contact while recording pull-off adhesion. Step 4: Reverse drag distance to ensure the same area is being tested.

3.3 LabVIEW Software

3.3.1 Objectives

Software design and programming was a significant challenge due to the LabVIEW environment and the need to interface with multiple tools. The system must be fully automated requiring no user input during testing. This feature greatly increases the volume of tests as they can be run overnight and when the user is occupied with other tasks. To achieve this, the system must be able to control the linear stages purely based on the feedback data given from the load cell. Earlier research within the group has produced real time adhesion graphs with a characteristic shape [109]. The preload and adhesion is distinguishable as the maximum and minimum of the graph for one cycle and thus are the primary two data points that the software should capture (Figure 24).
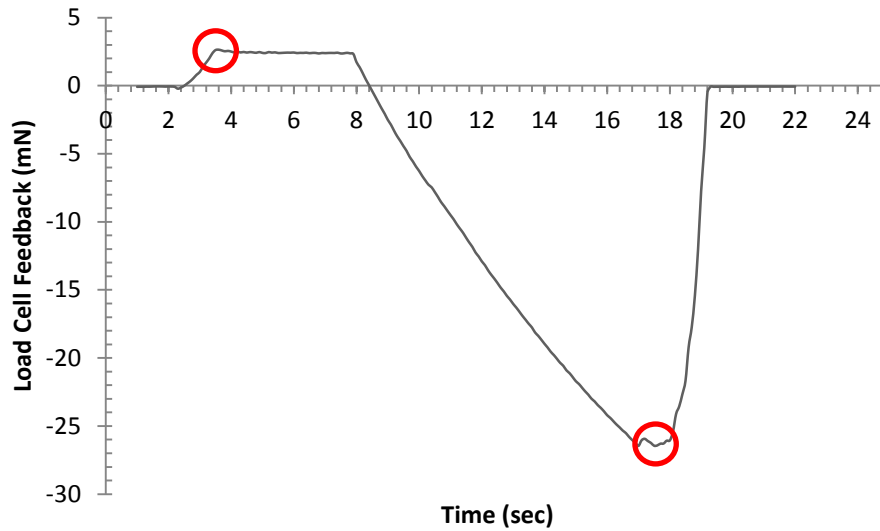
Figure 24: Typical graph of load cell feedback versus time. The maximum and minimum force values, highlighted with circles, represent the preload and maximum adhesion respectively. These are the primary data points the program will extract for each attach-detach cycle.

The system captures the preload and its corresponding adhesion value and outputs all the values to an excel file for easy viewing. For LDP tests, each preload and adhesion value is accompanied by the drag distance. There are normally ten different preloads per test, each of which can be tested nearly unlimited times at multiple locations on the sample. The program also has an option to capture every data point (10 Hz) and output it to an additional excel file to rebuild the test data if necessary. The system will rest upon an inverted microscope with the indenter coming in contact over the microscope viewpoint. The program can make use of the microscope-mounted camera to take an image at any point during testing.

It is crucial that the program has safeguards to prevent uncontrolled movements of the linear stage. If the stage is not stopped, it can cause damage to the equipment, especially the sensitive instrumentation on the load cell.

3.3.2   Methods & Results

The program has the capabilities to accomplish all the aforementioned tasks along with a few extra tools to enhance functionality. The Newport Corporation supplied a set of premade LabVIEW programs that send individual commands to the motion controller. These single programs, along with many additional programming techniques, were combined in the software to create the specific instructions for the two linear stages.

To extract the maximum and minimum values the program uses a combination of triggers and timers. For a basic test, the user will input the velocity of the linear stage, the preload(s), the number of cycles at each preload, the distance to withdraw from the sample, and the drag distance if a LDP test is desired. To determine the distance to withdraw, the user should first try a single trial at the maximum preload and witness how far the load cell needs to withdraw to fully break contact from the sample; the defined withdraw distance should be slightly greater. As the linear stage is moving towards the adhesive for the first preload, the program's first trigger waits till the load cell value reaches 80% of the preload. The program then begins storing every value from the load cell in a "maximum value array". After the preload is reached, the indenter begins to withdraw from the sample. When the load cell value drops below 80% of the preload the program finds the maximum value in the array (which is the exact preload) and outputs it to a second array, which will eventually be output to an excel file summarizing the test. The minimum value data collection works based on timing rather than triggers. Since the velocity and withdraw distance of the linear stage is known, the program calculates the time until the stage is fully withdrawn and, for the duration, stores all values from the load cell in a "minimum value array". Once motion has ceased, the minimum value (which is the maximum adhesion for that trial) is taken from the array and stored in the

same secondary array as the exact preload. As the test progresses, the data points are plotted on a graph of adhesion vs. preload as seen in Figure 25. The vertical stage is instructed to stop briefly when in contact, this gives the program a chance to perform a lateral motion with the horizontal stage for a LDP test, and/or take an image of the indenter in contact. The upper limit of testing cycles has not been determined, although 8 hour tests with 500 data points have been done.
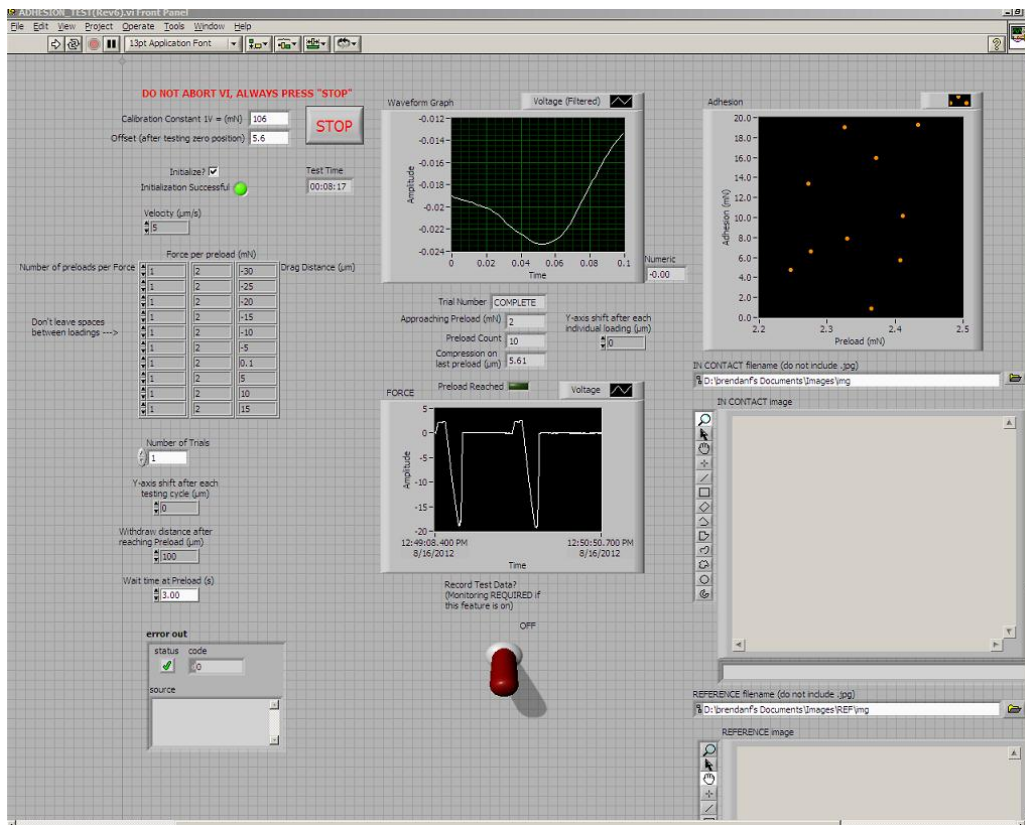
Figure 25: Image of the adhesion testing software interface. The adhesion vs. preload graph is in the upper right corner. Intended preloads and drag distances are input in the three column table on the left. The real time data scrolls across the two middle charts.

In addition to tests at different preloads and multiple cycles per preload, the program can move the indenter to a pristine location on the adhesive after each contact cycle. As an alternative, the system can do a full test of all different preloads on one location, and then

shift to another location for an identical test. The program is capable of testing up to ten different locations, with ten different preloads for each location without any user input after pressing "start".

3.3.3 *Software Issues*

There are a number of significant issues in the software that can potentially ruin data or damage the equipment. These issues can be overcome, but it is essential that the operator be made aware of them before running tests. Details about software problems can be found in Appendix B.

3.4 Gecko Adhesive Testing

3.4.1 *Testing Parameters*

Multiple versions of the gecko adhesive were fabricated and tested. All batches were fabricated with the same mask, which included four different square arrays of circles with 16, 24, 32, and 40 μm diameters and with center to center spacings of 20, 30, 40 and 50 μm respectively to produce fill factors of approximately 50%. These different diameters can have different DUV doses on the same substrate since the arrays of fibers are spaced enough apart that some sections can be covered during exposures. However, each array of fibers on individual substrates had identical development times. Three batches of eight substrates per batch were fabricated with slightly different fabrication settings as seen in Table 1. Within each batch, some samples would be discarded for a variety of possible reasons including irreparable damage during fabrication, having poor mask contact resulting in bloated or merged features (many being produced before the final contact system was developed), being overdeveloped, or other issues. As a result, only a few samples from each batch made it to the final stages of adhesion testing and, within this

subset, only some of the fiber sizes were tested. The original labeling conventions have been kept the same, with the letter indicating the batch, and the following Roman numeral indicating the specific substrate within the batch. For some substrates, their development time may have been satisfactory for the larger fibers (32 and 40 µm diameter), but too long for smaller fibers (16 and 24 µm diameter), causing fiber fractures for these smaller structures. As a result, the AIV and EI samples only have the larger fiber sizes reported.

Table 1: Processing parameters for gecko adhesive variations. Exposure time for AIV and CVIII is collimated (1:1) and for EI and CII uncollimated.

Substrate number	Fiber size (µm)	Exposure time (hours)	Development time (minutes)
AIV	32	7	20
AIV	32	8	20
AIV	40	8	20
EI	32	8	20
EI	40	8	20
CVIII	16	15	20
CVIII	16	20	20
CVIII	16	25	20
CVIII	16	30	20
CVIII	32	15	20
CVIII	32	30	20
CVIII	40	15	20
CVIII	40	20	20
CVIII	40	25	20
CVIII	40	30	20
CII	16	5	28
CII	24	6	28
CII	32	7	28
CII	40	8	28

3.4.2 Results

The adhesion testing results are summarized in Figure 26.
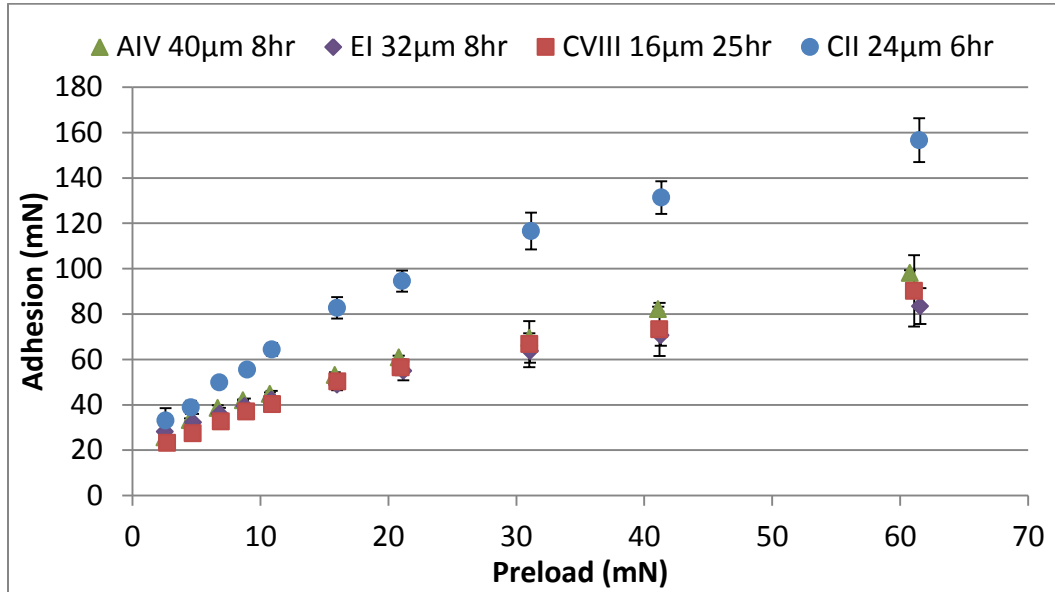
Figure 26: Adhesion testing results of preliminary fabrication trials. For clarity, only the best performing adhesive from each substrate is shown. The CII 24μm fibers are overall the highest performing for normal adhesion strength. The hours in the legend represent UV exposure time, which for AIV and CVIII is collimated (1:1) and for EI and CII uncollimated.

It is clear that the 24 μm fibers from the CII mold are superior in normal adhesion. Although not shown, all fiber sizes of the CII mold were superior to the highest performing fibers of the 2nd best mold. The collimation of UV light does not seem to have a strong effect on adhesion, although uncollimated light in general performs better within these four substrates, as suggested by earlier work [109]. The primary difference between the CII and AIV mold is the development time. The extra 8 minutes of development time seems to have given the fibers of the CII mold the ideal amount of undercut. The CII mold also had better mask contact than the AIV mold as observed during fabrication. Four neodymium magnets were placed in the center of the CII mold such that they

compressed the mask and substrate together to maximize the contact quality. Thus the

likely reason for the high adhesion is a combination of the ideal development time and

excellent contact between the mask and substrate. The CII mold will be the primary

adhesive used for the remainder of this document, and it is investigated in more detail in

the next chapter.

4   HIGH ADHESION CHARACTERIZATION

A version of this chapter has been submitted for publication in Smart Materials and Structures

4.1   Fabrication

The basic fabrication process is detailed in Section 2. Specific fabrication steps are as follows.

The PMMA substrate was marked for identification then cleaned with IPA and compressed nitrogen. A 2.2 ± 0.1 µm layer of SU-8 2002 was deposited onto the PMMA using a spin speed of 500 RPM for 5 seconds, followed by a 5 second ramp to 3000 RPM for 40 seconds. The substrate was baked for 3 minutes at 90°C, and then exposed to UV light through the mask with a total dose of 444 mJ cm^{-2}. This was followed with a 20 minute post exposure bake at 90°C. Development of the SU-8 was done by spinning the substrate at 2500 RPM for 40 seconds while applying an alternating spray of SU-8 developer and IPA. Uncollimated DUV exposure of intensity 4.4 ± 0.2 mW cm^{-2} was completed for 5, 6, 7, and 8 hours on the 16, 24, 32, and 40 µm diameter fibers respectively. The PMMA was developed in SU-8 developer for a total of 28 minutes at approximately 21°C. The development was done in three steps of 10, 10, and 8 minutes with a spin rinse and inspection in between each. Replica molding was done to produce the final working adhesive in a manner identical to that discussed in Section 2.4.

4.2   Adhesion Testing

The strongest performing adhesive was subjected to further characterization beyond a single preliminary set of adhesion tests. Accurate knowledge of the adhesive performance is essential to the proper design of a pick and place system.

4.2.1   *Methodology*

Normal adhesion strength tests were done using the same parameters as described in

Section 3.2.1. In addition, a 2 mm diameter sapphire hemispherical lens (Edmund Optics

NT48-429) was tested along with the 6 mm diameter hemisphere. Using both a large and

small diameter indenter provides information on fiber behavior on surfaces with different

"roughnesses" and pull-off behavior can change from quasi-continuous to discreet

depending on the number of fibers in contact [100]. Larger diameter indenters tend to

load fibers in the contact area more equally, and when a critical pull-off displacement is

reached, the fibers will lose adhesion very quickly. The smaller radius indenter will have

fibers pull-off over a longer period of time as those in the perimeter of the contact area

fail at much earlier times due to the extra linear displacement and angular displacement

the tips must maintain during pull-off. Multiple samples and multiple locations on each

sample were tested to account for local changes in adhesion strength caused by defects or

other issues. The sapphire tip was left uncleaned between trials to maximize the chance

for oligomer equilibrium to occur [165] and the adhesive was tested both immediately

after fabrication, and up to two weeks following. This caused more variability in the data

but also gives a more realistic view of how the adhesive will perform in working

conditions over time. Beyond two weeks the adhesive still performed well, but it may be

necessary to replace the adhesive once the adhesion drops beyond a critical value.

4.2.2   *Results*

The extended adhesion data is shown as preload versus adhesion strength in Figure 27.

The adhesion values are slightly lower than the original tests in Figure 26, and this is

attributed to the older samples beginning to degrade. Full adhesion data was also

collected for many tests as seen in Figure 28. Except for the 24 μm fibers, all the sizes

have essentially identical maximum adhesion, but the larger diameter fibers generally require more energy to overcome adhesion (using the 6 mm diameter probe) as seen with a larger area under the adhesion versus time curve. This can generally be attributed to the fact that there can be more energy stored in the larger fibers before the maximum adhesion strength is reached. A number of different adhesive samples were fabricated for testing and the backing layer thickness was slightly different for each sample (average 1 mm thick), but not enough that adhesion will be noticeably affected [139,166].
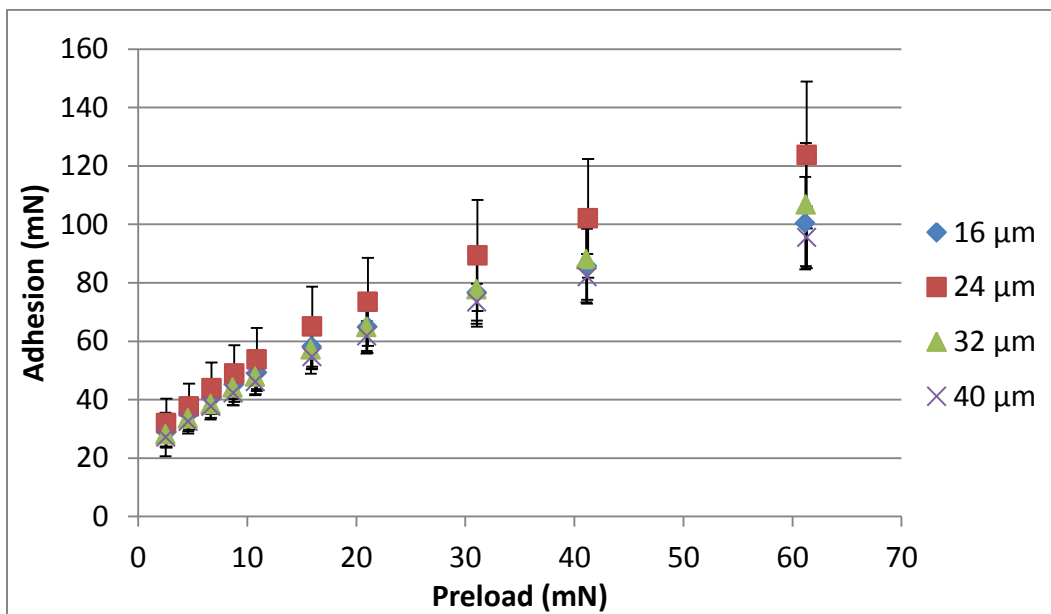
Figure 27: Adhesion data for various preloads and fiber cap diameters. The 24 μm fibers have the highest adhesion.
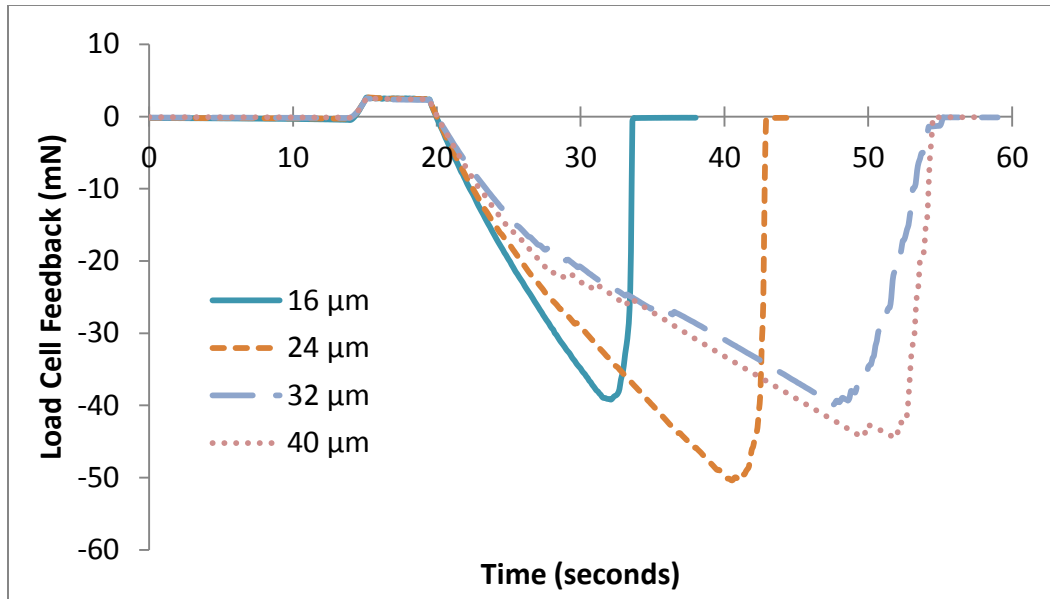
Figure 28: Sample real time date for different fiber sizes. It is evident that the larger fibers require more energy to remove them with the increased time to release adhesion.

Another dramatic difference in the performance of the adhesives can be seen with the 24 and 40 μm diameter fibers compared in real-time during pull-off with 6 and 2 mm diameter indenters as seen in Figure 29. The indenter with smaller radius initially can make contact with many individual fibers, but the 24 μm diameter designs maintain contact more readily, until a final, relatively quick failure occurs at maximum adhesion strength. In contrast, the 40 μm diameter fibers initially maintain contact with the 2 mm diameter probe, but adhesion failures begin much earlier, resulting in a slower, steady peeling from the perimeter as individual fibers lose contact and lower maximum adhesion strength results. Those 40 μm fibers near the center of the probe maintain contact for longer than the 24 μm diameter designs (as estimated by the time elapsed from the beginning of the pull-off) but in general, these fibers were less able to maintain contact on rounded surfaces at larger tilt angles to the pure normal loading scenario, showing them to be less adaptable to "rough" surfaces. This needs to be considered when selecting

a fiber size, as the topography of the MEMS devices can affect the adhesion performance.
It is unlikely that a MEMS device will ever have a rounded surface for the adhesive to
contact, but the roughness needs to be considered.
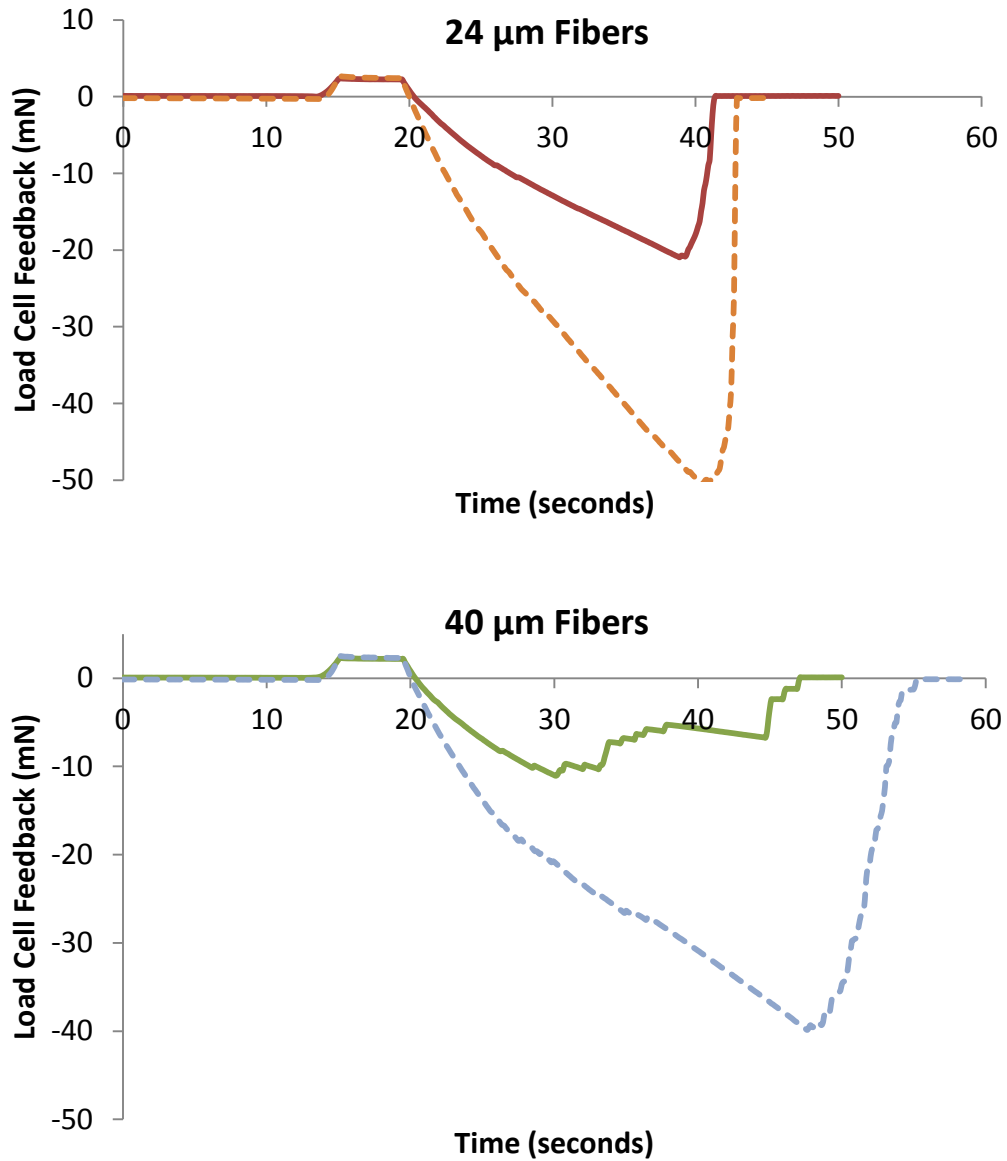
**Figure 29: Comparison of the real-time pull-off data for the 24 µm and 40 µm diameter
fibers. Solid lines and dashed lines represent 2 mm and 6 mm diameter glass hemisphere
respectively.**

At the lowest preload (2 mN) with the 6 mm indenter, there is minimal vertical distance between the center and edge of the contact area and thus most closely resembles the flat-flat contact scenario; therefore this is the preload where the estimate of adhesion pressure is found. The best performing adhesive using the 6 mm tip was the 24 μm caps, with an adhesive pressure of 557 ± 146 kPa. The pressure is estimated from the observed circular area of contact of the hemispherical indenter (average diameter 270 μm) rather than the specific area of the adhesive caps in contact as seen in Figure 30. Using only the in-contact fiber cap areas, the adhesion pressures approach 1 MPa. Despite the excellent performance of these adhesives, there is evidence that adhesion can be further improved. It was often observed that adhesion is not first lost from the outer perimeter of the contact area, but from specific fibers under test in the same location repeatedly. Small, sub-optical defects, such as minor scratches and imperfections can dramatically reduce adhesion compared with the theoretically flat, ideal caps. If the entire adhesive consisted of these near perfect "super-fibers" then the total adhesion strength may be far higher still than the ~1 MPa limit.
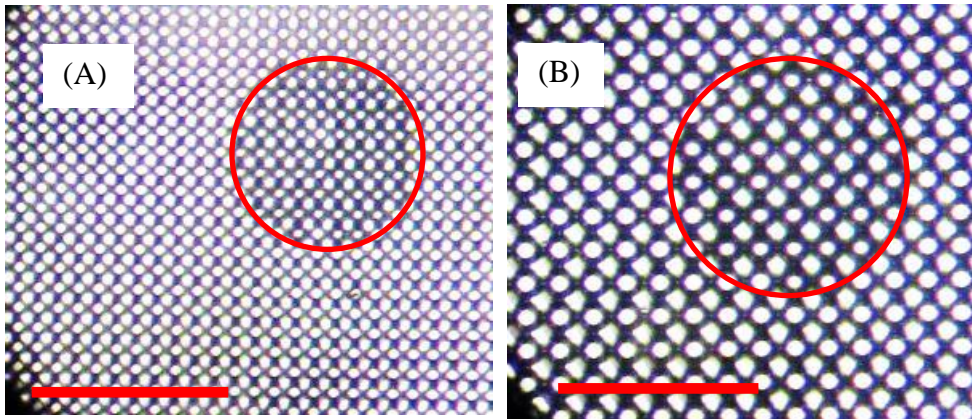
Figure 30: Inverted microscope images of two areas of fibers under test. (a) and (b) shows 24 μm and 40 μm diameter fibers respectively as they are being pulled off. The red circle represents a projected area in contact, although the actual area is the number of discrete fibers multiplied by the area per fiber. For the 24 μm fibers, this trial had an adhesion pressure of 770 kPa per fiber, while the 40 μm fibers had an adhesion pressure of 704 kPa per fiber. Scale bars represent 300 μm.

4.2.3   *Upper Adhesion Limits*

Not shown in the figures is the significant reduction in adhesion after the first adhesion test on a pristine area. The first test often has approximately 150-180% of the average adhesion for a particular preload as seen in Figure 31. This will increase the measured microscale adhesion pressure to upwards of 2-3 MPa, which to the authors knowledge is the highest ever reported in literature [35] for normal adhesion strength for gecko-inspired fibers. The adhesion rapidly drops off after repeated loads, but these initial extremely high adhesion values help suggest an ultimate upper limit for these particular adhesive designs. In respect to a pick and place operation, it may be necessary to "prime" the adhesive by attaching and removing it from a smooth surface to ensure that the higher than average adhesion does not affect the first die that is moved. The reduction in adhesion is likely due to surface degradation, damage to the fibers [91], or the adhesive shedding oligomers on the indenter [165]. There are methods by which active cleaning

steps can help restore these materials to close to their original adhesion strength

[143,167], but for a small adhesive area it may be more cost effective to simply replace

the adhesive.
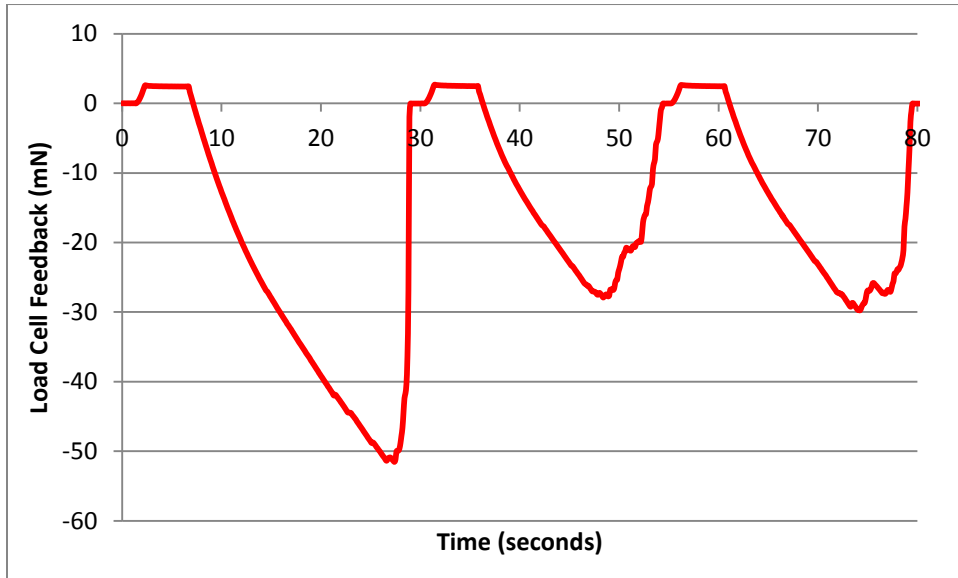
Figure 31: Example real time data showing a drastically higher adhesion for the first test on a new area. The adhesion of 51 mN is nearly 190% of the approximate adhesion of 27 mN for the second and third adhesion tests. The actual trials had a longer delay between each adhesion test (30-40 seconds), but the delays were removed from the graph for clarity.

4.3   Antistatic Adhesive

4.3.1   Introduction

During adhesion testing tribocharging was detected from multiple attachment/detachment

cycles. The charging is detectable by the load cell as an attraction between the

hemispherical indenter and adhesive during adhesion trials as seen in Figure 32. This

charge is measurable at separation distances as large as 150 μm (as estimated by the

approach velocity and time) and therefore is unlikely to be caused by attractive van der

Waals forces.
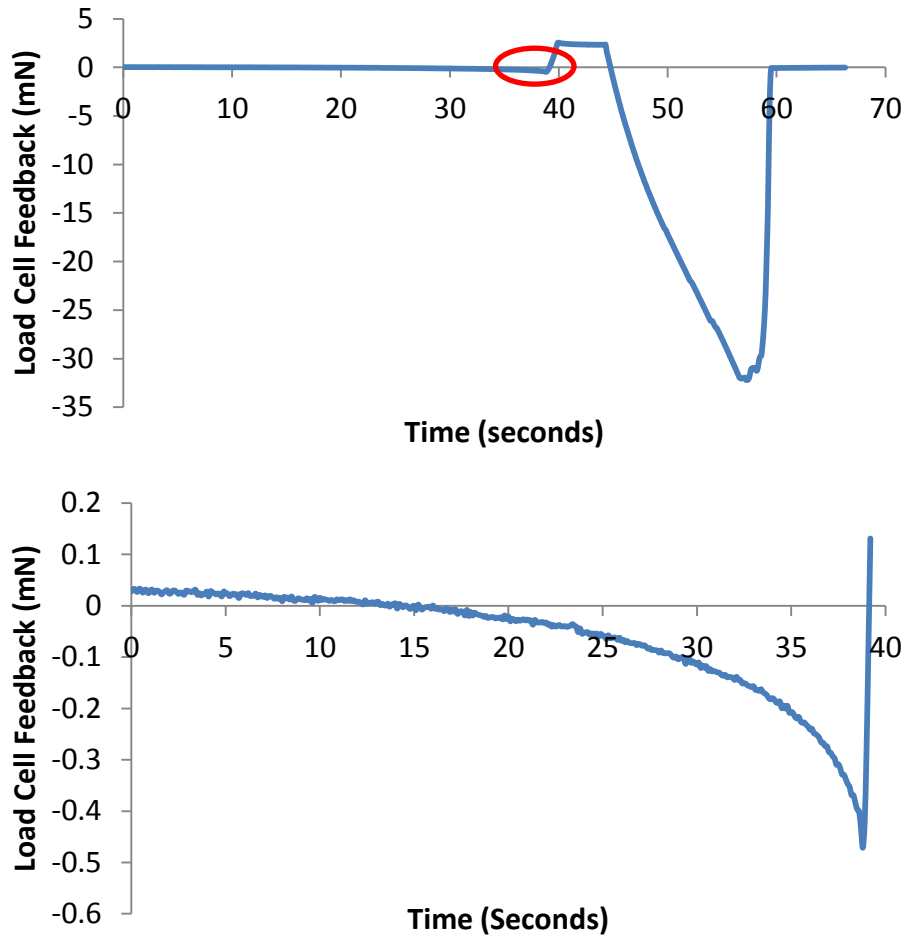
Figure 32: Evidence for electrostatic tribocharging during adhesion trials. The lower graph represents the circled section of the upper graph. A negative force represents attraction and positive is repulsion. It can be clearly seen that as the hemisphere approaches the adhesive, it is being attracted to the adhesive with a measurable force. The hemispherical probe is approaching the adhesive at 5 μm s⁻¹.

This charging may be assisting in bringing the adhesive in contact with surfaces, but it is dangerous when dealing with electronic components. The charge may build up and discharge into a MEMS die causing damage. This is not acceptable for a commercial setting, and an antistatic version of the adhesive is desirable. Creating an anti-static adhesive device was not a core part of this work and is primarily being developed by

Walid Bin Khaled as part of his MSc work, but some preliminary results are presented here.

4.3.2   *Carbon Black Composite Polymer*

ST-1060 polyurethane from BJB Enterprises has an alternative, antistatic version. BJB Enterprises claims that the antistatic ST-1060 has nearly identical properties to regular ST-1060 with slightly different mixing parameters, but creating the adhesive from the antistatic version revealed that the cured polymer is usually softer than standard ST-1060. The reduced stiffness makes the antistatic version less effective as an adhesive, since the fibers are more susceptible to collapse, in particular the overhanging caps which were designed to work with the standard ST-1060 formulation. As a result the antistatic ST-1060 alone was not considered for an antistatic material. An alternative technology was considered, which involves creating a nanoparticle/polymer composite. The nanoparticle added to form the composite was carbon black (Cabot Vulcan XC72R).

The following is the standard technique for making sufficiently conductive adhesives. The prepolymer is first prepared using standard mixing techniques, followed by degassing in the vacuum oven. It is then transferred to a glove box where carbon black is measured out separately at 12% of the weight of prepolymer. Many weight ratios were tested, and 12% was found to be the minimum threshold for ensuring conductivity. The carbon black is added to the prepolymer in small portions with vigorous mixing between each addition of the nanoparticle to even the distribution of nanoparticles. Instead of standard ST-1060, the ST-1060 antistatic version is used for the composite. This is not to achieve higher conductivity, but because additional time is needed for the slow manual mixing process. Standard ST-1060 has a working time of approximately 25 minutes, while the antistatic version is approximately twice as long. The standard ST-1060 often

76

would become too viscous to work with before the carbon black was fully mixed. The added time from the antistatic version was usually enough to ensure adequate mixing.

After mixing is complete, the polymer becomes too viscous to effectively degas or mold with traditional techniques. The solution is the lamination technique as described in Section 2.4.3. Lamination produces a smooth, even backing layer similar to the one seen in Figure 33.
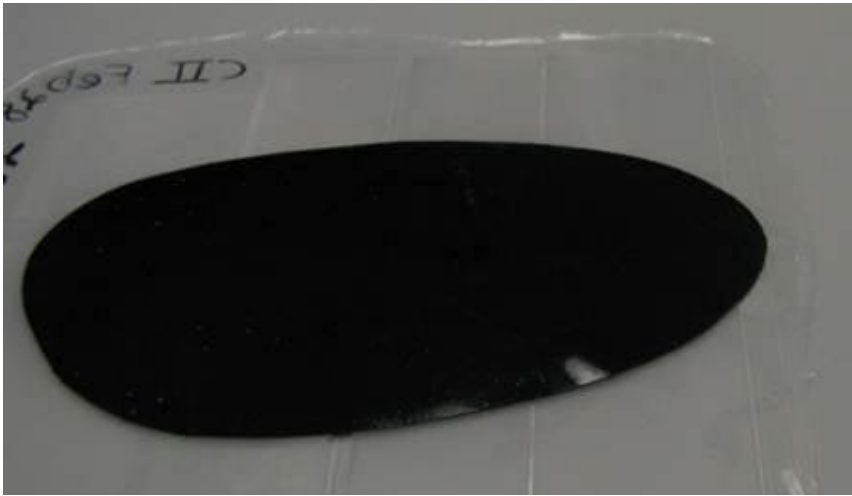
Figure 33: Result of laminating the viscous polymer/nanoparticle composite. A smooth, even backing layer is produced with fully formed adhesive structures.

4.3.3   *Adhesion and Reliability*

Adhesion tests were performed on the antistatic composite to ensure adhesion is not reduced when the nanoparticle is present for identical fibers shapes as described in Section 4.2.2. A standard adhesion test was done for the composite and the results were compared to the non-conducting adhesive as shown in Figure 34. Conductivity tests were also carried out using a four point probe, and the unstructured polymer achieved conductivity on the order of 500 Ω cm^{-1}. The conductivity tests also revealed that the

77

nanoparticle mixing is uneven, and different locations on the same sample had widely

varying levels of conductivity.
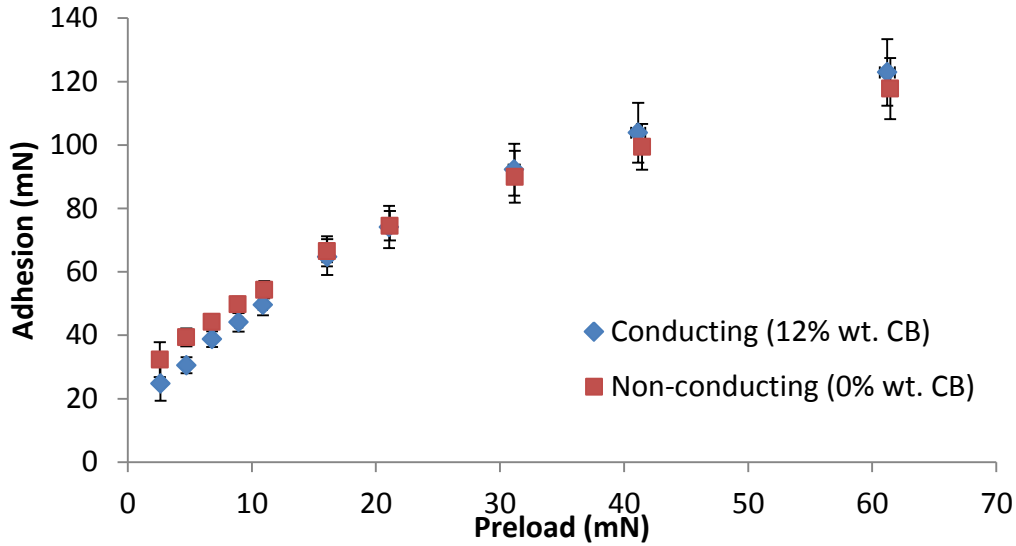
Figure 34: Standard adhesion test for comparison of conducting and non-conducting polymers. There is negligible difference between the two variants. The 16 μm diameter fibers were tested.

The conducting polymer proves to have similar adhesive properties to the non-conducting

variant, but proper design of a pick and place system will need to know how long it will

last before degradation renders the adhesive unusable. A reliability test was done on the

conducting polymer using the same adhesive testing apparatus. 500

attachment/detachment cycles were done in the same location with a preload of 60 mN

and the results are shown in Figure 35. Approximately 28% of adhesion is lost by the end

of the trial. Most of the loss in adhesion occurs within the first few cycles, which is the

expected trend as mentioned in Section 4.2.3.
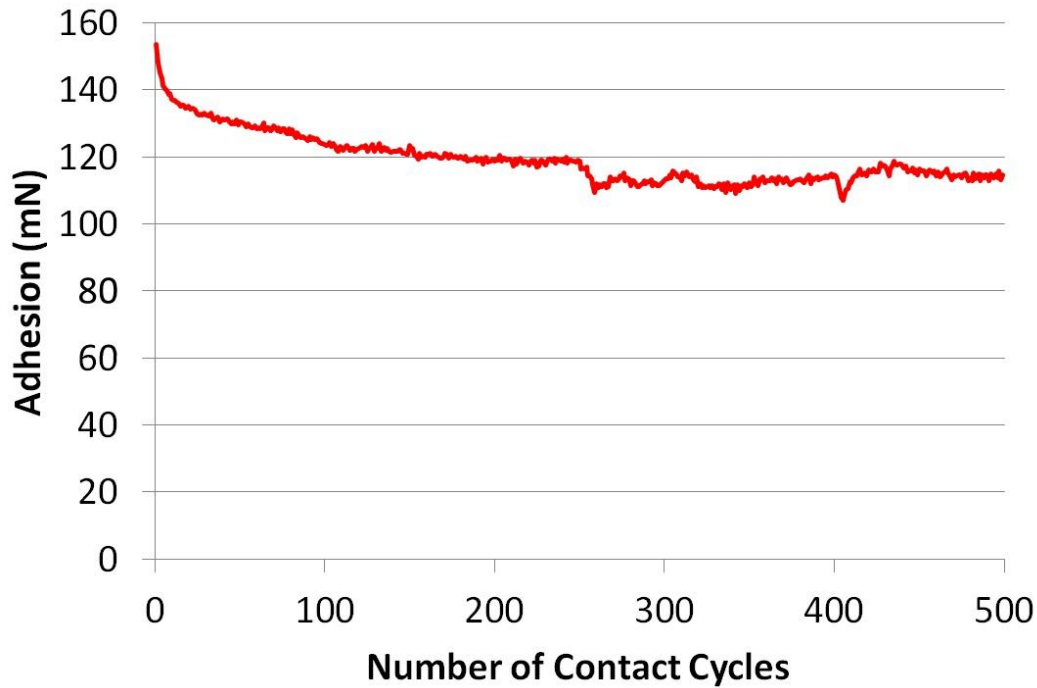
Figure 35: Reliability test for the ST-1060 (antistatic version) carbon black composite. 500 trials were done in the same location at a preload of 60 mN. The 16 μm diameter adhesive was tested.

4.4   Material Characterization

4.4.1   Introduction

Finite Element Modeling (FEM) has been used to predict and enhance adhesive performance [133], but often uses only the initially fabricated device geometry and relatively restrictive boundary conditions. Frequently, synthetic dry adhesives are simulated using linear elastic assumptions [168] despite often being made from hyperelastic materials such as polyurethane or silicone rubber. This can fail to accurately capture the fiber behavior in the critical moments just before adhesion is lost. A Mooney-Rivlin hyperelastic model was selected to simulate the adhesive materials beyond 100% elongation [169]. The model requires two strain energy constants that can be found from

a stress-strain curve, which had not yet been done for these polyurethanes in the academic literature prior to this work.

4.4.2 _Tensile Tests_

Standard tensile tests for these polyurethanes are based on ASTM D412 tests for rubber in tension. The uniaxial test involves breaking a dog bone shaped specimen within an Instron testing machine.

To create the specimens, a two-step molding process was used that was similar to fabricating the dry adhesive. First a positive mold was fabricated from PMMA as seen in Figure 36. The PMMA was cut using the laser engraver and subsequently bonded with acetone in a recessed mold to form the positive mold shape. Silicone rubber (TC-5045, BJB Enterprises) was then cast in the PMMA mold to form a negative rubber mold. A similar negative PMMA mold was also fabricated for polymers that would adhere to silicone rubber. Finally both the standard ST-1060 and ST-1060 (antistatic version) carbon black composite was cast in the dog bone shape mold.

Figure 36: Various molds and casts for the dog bone test specimens. Upper left shows two PMMA positive molds, upper right shows the resulting TC-5045 silicone rubber negative molds, Lower right shows various dog bone specimen, lower left shows two negative PMMA molds. The PMMA molds were made using a laser engraver with scrap Acrylic, and thus the outer edges are slightly irregular.

Care was needed to ensure there were no air bubbles within the thin testing area. Samples with bubbles were discarded, as the bubble changes the smallest cross sectional area of the sample causing failure to occur much sooner than expected. After the prepolymer part A and B was mixed, the material was degassed in the vacuum oven to remove air. Pouring the prepolymer into the mold can also form air pockets, and the best solution to minimize this was to pour the prepolymer into one of the wells, then tilt the mold to allow gravity to draw the material through the neck. For the extremely viscous composite material, it was best to carefully apply it to the mold with a spatula, and remove the excess by drawing a clean edge across the top surface of the mold. A secondary sheet of

PMMA or similar material can be placed over the mold to create a flat edge for the side of the specimen not contacting an edge of the mold. However, this second sheet often created an extra flap of ST-1060 material that formed from the imperfect seal between the mold and second sheet. The extra material needs to be cut away, but the action of cutting can also affect the test.

Although care was taken to cut the PMMA with as vertical side wall as possible, the heat from the laser cutter will still cause a slight angle. The result is a dog bone sample with a trapezoid-shaped cross section. During testing, the Instron machine assumes a square or rectangular cross section, and, to compensate for the trapezoid, the width was taken as approximately the average between the upper and lower edges of the trapezoid shape. Although not exact, this provides a good approximation for data collection.

Tensile testing was done for a number of different materials including:

- PDMS

- PDMS with 4% wt. Carbon Black (CB)

- PDMS with 8% wt. CB

- PDMS with 10% wt. CB

- PDMS with 12% wt. CB

- ST-1060

- ST-1060 (antistatic version) with 4% wt. CB

- ST-1060 (antistatic version) with 8% wt. CB

- TC-854

- TC-8740

The primary materials of interest are ST-1060 and the ST-1060 anti-static composite, but knowledge of a number of materials can assist modeling in the future.

The Instron machine used was model 5943 with 2713-001 self-tightening grips. Samples were loaded into the machine and held with just enough force to prevent sagging of the neck. The dimensions of the sample were entered and the machine reset to prepare for testing. The ends of the sample were slowly pulled apart at a constant speed until the sample fractured. The Instron gives data in the form of an extension versus load curve, which is easily converted to a stress-strain graph. The Instron also gives an estimate of the Young's Modulus.

4.4.3   *SEM Imaging*

The dimensions of the fibers are needed in order to create an accurate model. Optical microscope and SEM images (Figure 37) were taken of all fiber sizes in order to accurately determine their shape.
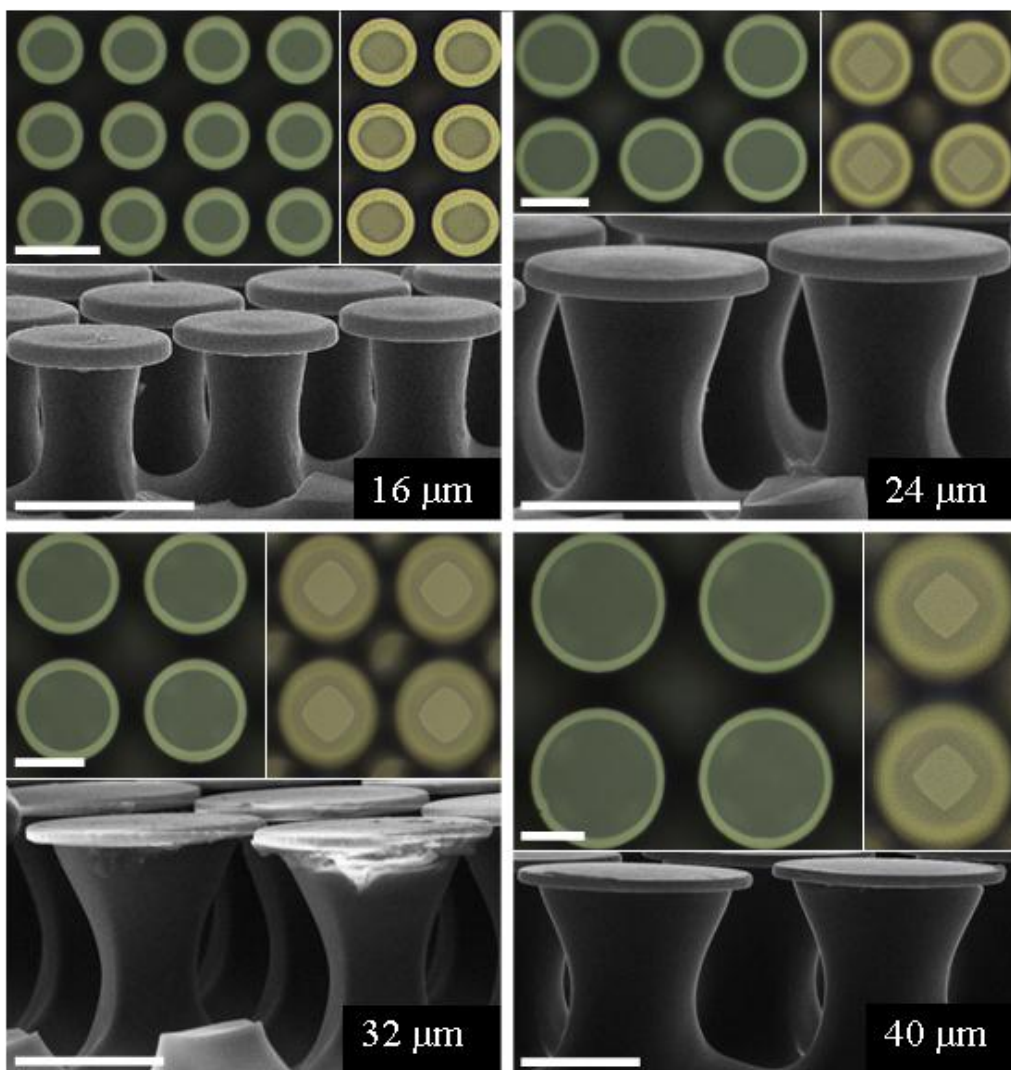
Figure 37: Optical and SEM images of the four fiber sizes cast from the best performing mold. Optical images are taken looking from above at the SU-8 caps on an acrylic backing. The optical image on the left for each size is focused on the cap, while the image on the right focuses on the fiber neck which emphasizes the cross section. SEM images are ST-1060 fibers of the final adhesive. The diamond shape is visible on both the optical and SEM image. Some debris is visible on the 32 μm fibers. Scale bars represent 20 μm.

Unlike most mushroom-shaped fibers discussed in literature [35], these fibers have an hourglass shape with a square cross section which is more pronounced as the fiber size increases. The shape is the result of the DUV exposure step during fabrication. Less light

passes by adjacent SU-8 caps at their closest point, resulting in a shallower depth compared to the more open areas. This means the distance between the edge of the square cross section shape and the edge of the cap is an indication of the amount of light that area has received. The lowest point of the underlying fibers is at the central point between four fibers because that point receives the largest dose of DUV light. The hourglass shape is a result of using uncollimated UV light. The negative sidewall angle represents the maximum angle the light can penetrate between the SU-8 caps while retaining the level of intensity needed to affect the molecular weight of the PMMA.

The negative sidewall angle of the fibers increases with increasing fiber diameter for these dimensions. This is a result of the caps being spaced proportionally further apart as their size increases (to keep the fill factor constant across all designs). Light can penetrate at a sharper angle with a larger cap separation distance, and thus the sidewall angle of the caps is larger.

These images were used as the basis for creating a 3D model of a 24 µm fiber within Solidworks. The result closely matches the SEM image as seen in Figure 38. This was the primary model used for the hyperelastic FEM simulation [169]. Similar models were also created to investigate the effect of a pure cylindrical shape, and a circular cross section rather than square.
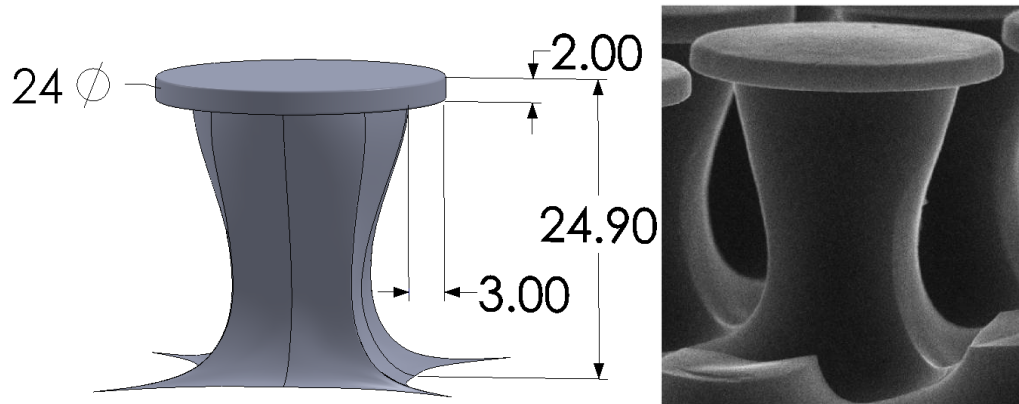
Figure 38: Comparison of the 3D fiber model in Solidworks to the SEM image of the 24 μm fiber. Dimensions of the fiber were taken in SEM (not shown) and closely match the 3D model.

4.4.4   Data Extraction and Finite Element Modeling

Using the data from the tensile tests, the Mooney-Rivlin strain energy constants were found for ST-1060 and a ST-1060 (antistatic version) carbon black composite [169]. Using the constants, a simulation of the adhesive fibers was prepared using COMSOL Multiphysics 4.2 by Ben Bschaden as part of his MSc work. The extended fiber simulation can be seen in Figure 39 with an SEM image for comparison. It is clear that the simulation closely matches the hyperelastic behavior of the fiber, confirming the validity of the material tests.
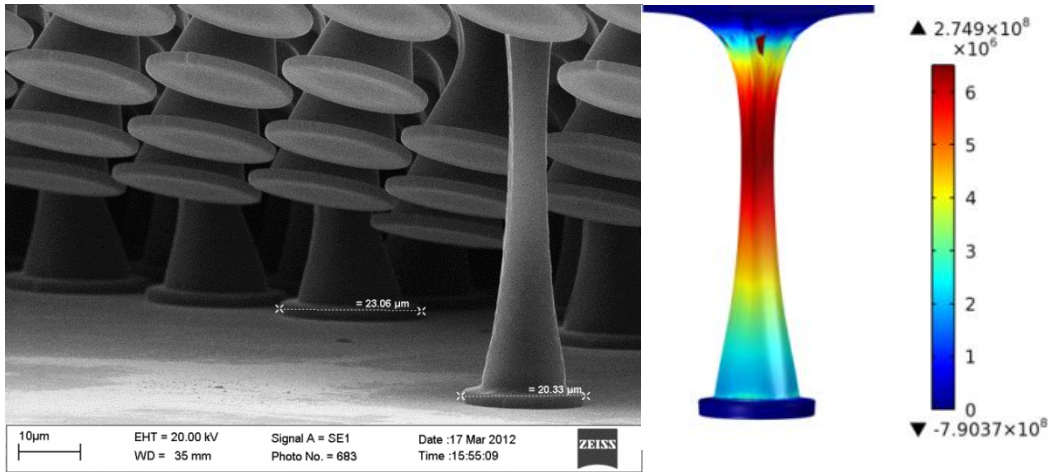
Figure 39: Cross-section stress distribution and SEM image for shape comparison. The simulation is in good agreement with the SEM image.

A roller boundary condition was used at the top interface of the fiber cap, giving comparable cap shrinkage/fiber elongation ratios as observed in SEM imaging of loaded fibers. Fiber elongation was approximately 144% in both simulation and observational measurements. For modeling, a force of 0.4 mN was subjected to a 100 μm thick rectangular block with dimensions equal to the pitch of the fibers representing the adhesive backing layer.

FEM can also reveal other behaviors that are not clear from SEM images. When compared to a pure cylindrical fiber with the same cap diameter and overhang, FEM shows that the hourglass shaped fibers direct maximum surface stresses at the contact interface to the center of the fiber cap (Figure 40). The reduced volume due to the curved sidewalls causes increased elongation and higher absolute stresses in the center, which makes the fiber more likely to first lose contact from the center of the cap, rather than peeling from the more vulnerable cap edge. Particularly in the case of non-axial loading, directing the stress well away from the perimeter may reduce the odds of early peel

failure for an individual fiber. This delayed peel failure results in greatly increased

adhesion strength when compared to an unstructured material.
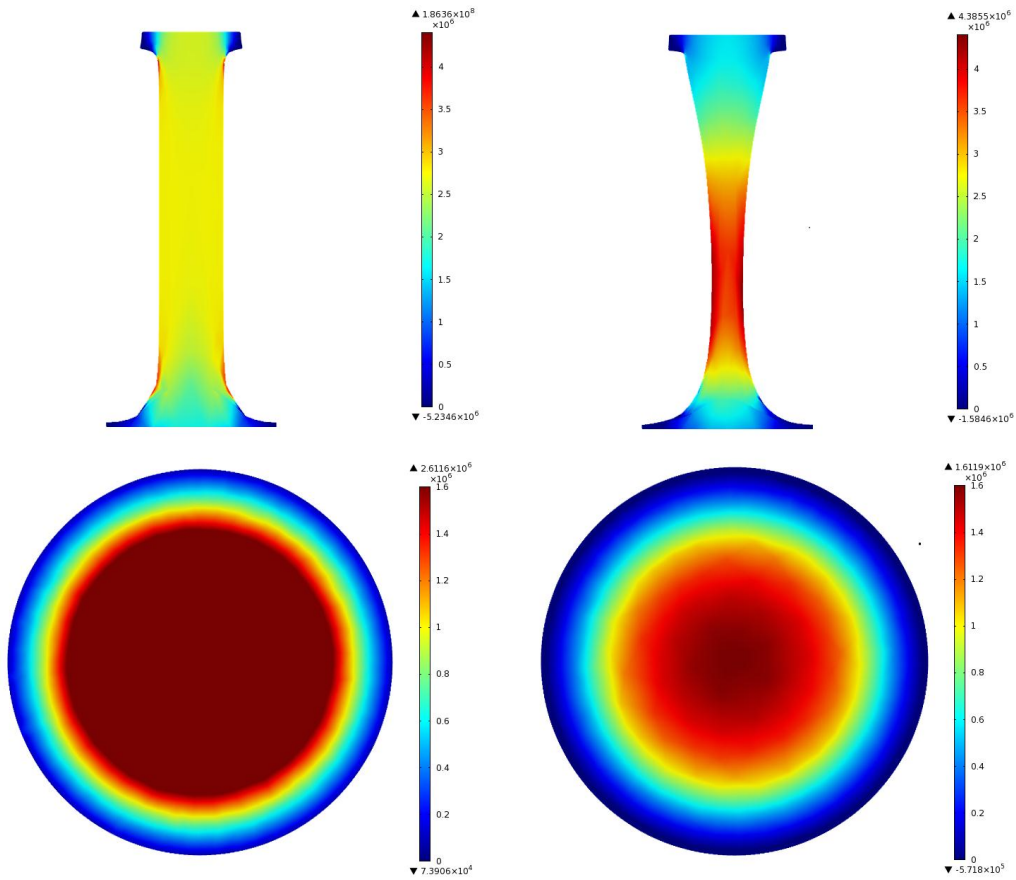
Figure 40: FEM simulations: Cross sectional stress distribution and cap stress for a pure cylindrical fiber (left) and hourglass shaped fiber cap (right). The hourglass shape directs maximum surface stresses to the center of the fiber, rather than the more vulnerable edges, delaying the onset of peel failure and making the adhesive more robust and able to handle off axis loads.

For comparison, the fiber neck was modeled with both a circular and square cross section

in addition to the hourglass shape (Figure 41). FEM shows a nearly identical force

distribution on the fiber cap and neck, suggesting that the square cross section does not

have a significant effect on the performance of the fiber. Therefore the more complex

square cross section could be eliminated in favor of computational savings from using a circular cross section with axisymmetric model.
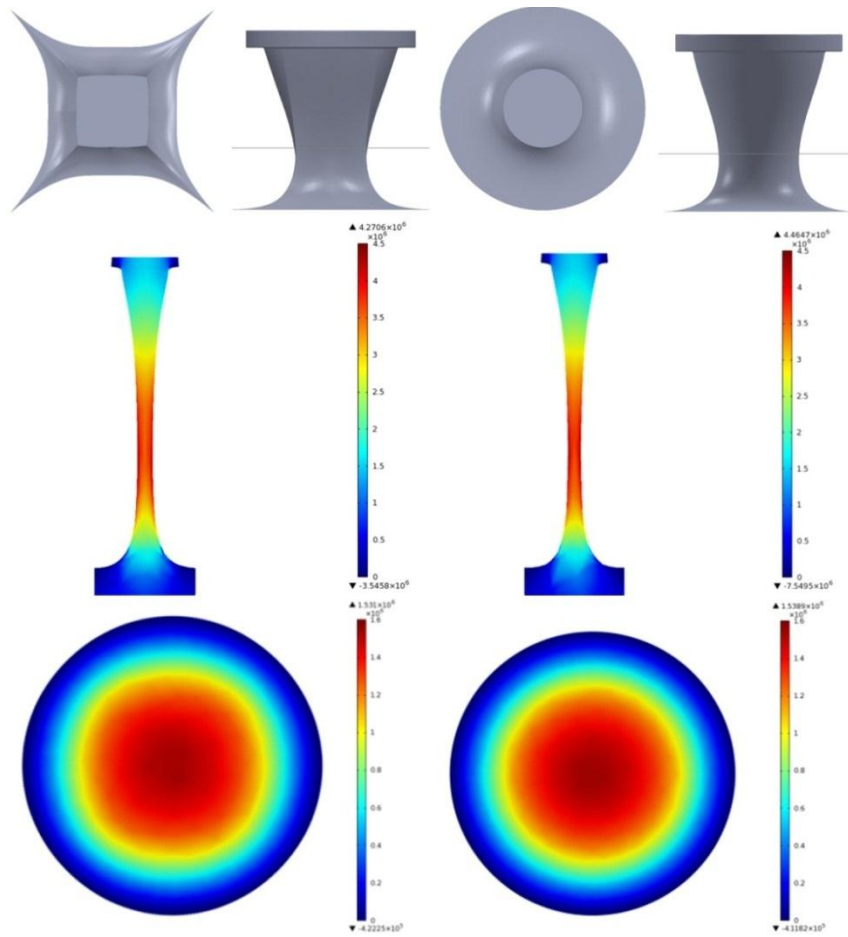
Figure 41: Comparison of a square cross-section (left column) to a circular cross section (right column). Top images show the cross-sectional profile and its location on the model, mid images show internal stress and elongation, bottom images show stress distribution on the cap surface. FEM demonstrates there are nearly identical maximum and minimum forces despite the very different cross sectional profiles.

As seen in Figure 42, the fiber cap shrinks as the fiber is stretched. The cap shrinkage of the FEM (17.2%) closely approximates the observed shrinkage in the SEM images (15%), validating the use of a roller boundary at the cap interface. The real fibers shrink less; likely due to friction between the two surfaces in contact.
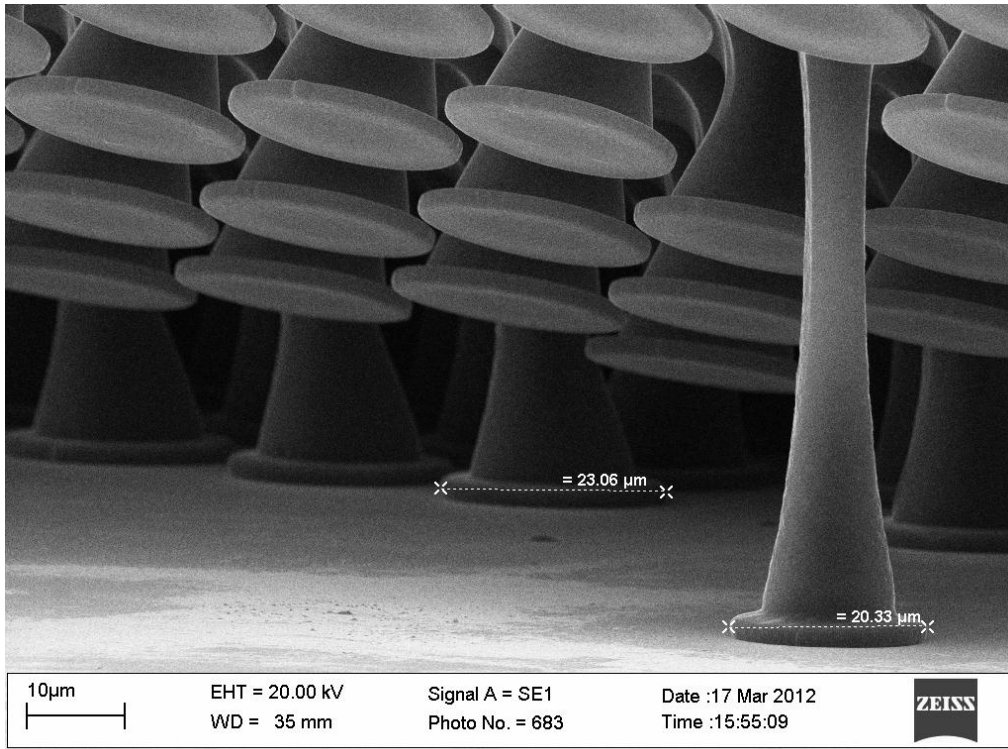
Figure 42: SEM image of a stretched fiber. The original cap width is approximately 24 μm, showing a reduction in diameter of nearly 4 μm. The reduction would likely be greater than this, but friction between the cap and the adhering surface (silicon) is likely creating resistance to further shrinkage. These results suggest that a roller interface with friction is a valid boundary condition for further FEM.

4.5   Summary

The newest generation of these adhesive have numerous improvements over the best performing adhesives first produced in the original work [109]:

- The adhesion is significantly improved. Under near identical testing contitions, the original adhesive achieved adhesion on the order of 60 mN, while the new adhesives achieve nearly double with 120 mN under identical testing conditions.

- The fabrication time has been reduced. The post exposure baking time has been reduced from several hours to 20 minutes, and the lack of collimation increases the DUV intensity, decreasing the required exposure time.

- Fabrication techniques have been improved. The lamination technique eliminates the need for a vacuum degas step while improving control over the backing layer thickness.

- Adhesive material has been improved. With the addition of carbon black nanoparticles, the adhesive can dissipate a buildup of charge compared to the standard electrically insulating polyurethane.

The optimized adhesive can now begin integration into useful applications. The high adhesion reduces the required adhesive contact area for a desired adhesion force, and more material choices allow a wider range of possible applications. The next step is to develop an end effector and pick and place procedure for manipulating die.

5   PICK AND PLACE TECHNOLOGY

5.1   Introduction

With a strong adhesive developed, the final task is to design an end effector for use with transporting MEMS die. The solution must meet the following requirements as best as possible:

- Simple, inexpensive, easy to manufacture

- Reliable

- Highly controllable

- Easy to use by hand or robotics

- Customizable for different tasks

This chapter will focus on material considerations, manufacturing techniques, design iterations, and testing of the final solution.

5.2   End Effector Material

Materials for both prototyping and the final product were considered. Metal and plastic prototypes were considered as both could be designed using SolidWorks and manufactured at the local machine shop. Metals are more expensive and take time to form, especially with the fine tolerances necessary for MEMS pick and place. They are electrically conductive, but this was disregarded in favour of a simple alternative as the requirement for complete grounding/anti-static performance is being addressed by another individual participating in the project. Plastics are a more viable option, as they are cheaper, lighter, and potentially faster to prototype. Commercial Acrylic (PMMA) has been used by our group in the past as well as throughout this project; it is well

characterized and thus is an excellent choice for prototyping. The same laser engraver that was used for cutting the original PMMA substrates can be used for more complex design patterns. With appropriate settings the laser engraver can complete patterns very quickly, allowing a wide variety of designs to be tested. Polyurethane can adhere to PMMA relatively well, providing a good option for bonding the adhesive to end effector prototypes.

The final end effector material must be robust, relatively inexpensive, easy to manufacture, and easy to integrate with robotics. Since the final adhesive will likely have anti-static capabilities, the end-effector will need to share these properties to provide a grounding source. Metals again may be a good option, but if a disposable end effector is desired, metals may be too expensive. Plastics remain a good choice if sufficient electrical conductivity for grounding can be achieved. For Micralyne Inc.'s purposes, plastic end effectors can be manufactured in order to provide an inexpensive, disposable option. A special coating or conducting plastic can be used to provide grounding, or, for non-conducting plastics, a supplementary grounding system can potentially be installed and incorporated with the robotic system.

5.3   Laser Engraver Characterization for Rapid Prototyping

All preliminary end effector designs were fabricated from 5 mm thick PMMA sheets using a Versa Laser Engraver (VLS 3.50) [170]. The designs were created in SolidWorks and exported to the engraver as a two-dimensional vector image. Characterization of the laser engraver was done beforehand to determine the best power and speed settings to effectively cut through the PMMA and achieve the desired structures. The raster calibration chart is shown in Figure 43. If the power is too high, the PMMA will become excessively heated and burn off more material than is intended. Excess heat can also

warp the PMMA, rendering the prototype unusable. Low power will not fully cut through the PMMA, but this can be rectified by having the laser do multiple passes over the PMMA to deepen the cut. For thick PMMA (>3 mm), multiple passes are often required to have a high quality through cut. Simply increasing the laser power level and decreasing the cut speed will produce a deep trench with angled sidewalls from the high heat, potentially ruining delicate features. When using multiple passes to cut thick PMMA, the laser may need to be refocused to the cutting plane rather than the top surface of the PMMA to prevent the same trench problem previously mentioned. Using the minimum power settings needed to cut through the PMMA will ensure sharp features with minimal burning and warping.
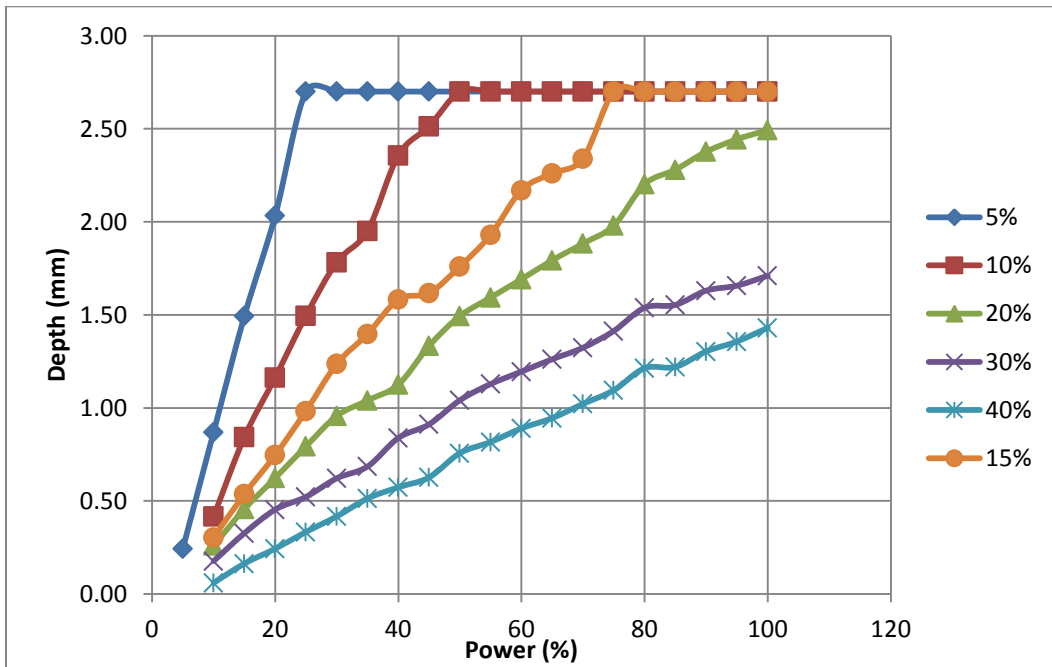
Figure 43: Versa Laser Engraver PMMA calibration guide with power and speed versus depth. To ensure a complete cut of a 5 mm thick sample, power level 50% and speed 5% was most often used with two or three passes of the laser.

5.4   Tape Drum Removal Designs

As discussed in Section 1, tape drums consist of adhesive tape pulled taught within a metal ring. MEMS foundries normally use a combination of UV or heat release tapes and pushing die from below with an array of needles as a mechanism for separating devices from a diced wafer in commercial processes [6]. A handheld device for removing die from large tape drums was first considered.

5.4.1   *Push Pin for Assisted Removal*

Preliminary investigation into a release mechanism incorporating gecko adhesives considered raising the die off the tape to assist removal. This can be accomplished in a number of different ways. One option is to slide a prodding device below the tape from the back to front of the die. The wave motion will begin to peel the die from the tape in a relatively predictable manner that the handheld device can complement. Another option is to push against the die from below using a three or four point pin similar to what is done in industry today. A prototype of the push pin design can be seen in Figure 44. This method will position the die more predictably than a sliding prod, but it relies more on the accuracy of the push pin. A slight misalignment will only peel the tape from one edge.
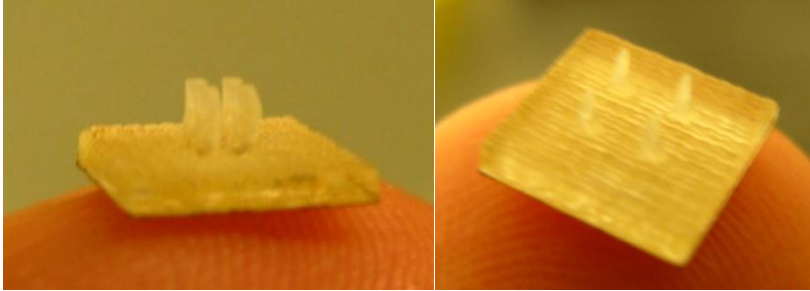
Figure 44: Push pin examples for removing dies from tape drums. The points are pressed into the tape below the die that is to be moved. The pressure points cause the tape to release from the die at the edges, significantly reducing adhesion to the tape by initiating the peel failure and allowing a device to pick the die off the tape drum more easily. The push pin on the right has more widely spaced pins.

5.4.2   *Handheld Tweezer Designs*

A handheld device to remove die from tape drums was first considered. The device, referred to as tweezers, would have two prongs, one above the tape intended for grabbing the die, and one below the tape assisting its removal. The lower prong will have the four point probe or prodding mechanism, and the upper prong will contain the gecko adhesive.

A number of tweezer designs were fabricated in 1/8" thick PMMA as seen in Figure 45. Early failures were caused primarily by lack of ergonomics. A lack of grip and flimsy joint made controlling the tweezers very difficult. Handles and grips were added to the design, and the connection joint between the upper and lower sections was optimized for proper stiffness. The latest design allows for the end effecter grasping mechanism to be changed based on what is required for the current job. This gives increased flexibility for multiple die types.
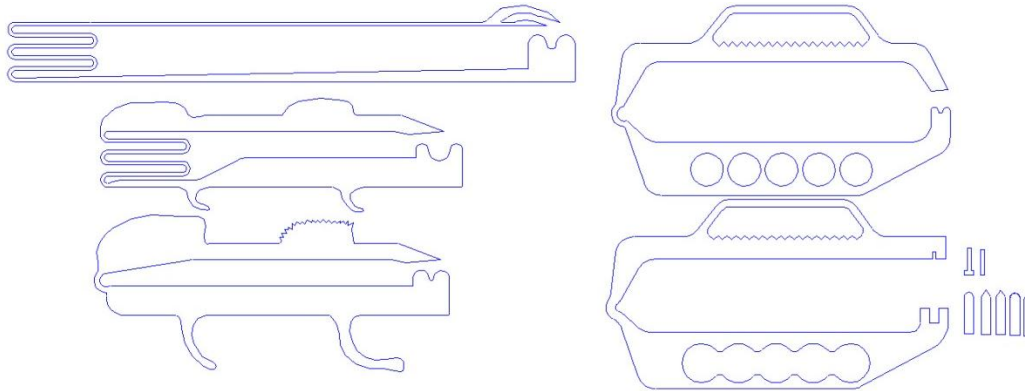
Figure 45: Laser instructions for cutting the tape drum tweezer designs. These designs were fabricated from PMMA using the Versa Laser Engraver. Various links between the upper and lower sections produced different amounts of flexibility. Various finger grasps were also tested for ease of use.

The push pin was affixed to the lower prong of some tweezer designs for testing. As expected, proper alignment to the die was very difficult and most die only detached from the tape on one edge. Sliding a shallow wedge also proved to be ineffective as the die often slipped off the tape entirely. However, sliding the push pin proved to be the most reliable method of raising the die from the tape drum.

A sample of gecko adhesive was affixed to the upper prong of the tweezers for testing with 5 mm x 5 mm x 1 mm die. The device was very difficult to use and was unable to effectively remove die from the tape drum. Not only is it difficult to raise the die with the push pins, aligning the adhesive with the raised die was also extremely difficult. The large, bulky tool has very poor lateral stability because of the thin acrylic. This problem could be remedied by reinforcing the joint connecting the upper and lower segments, but this will only add more bulk to the device. Picking up small MEMS devices requires a high level of accuracy and operator skill, and a smaller, lighter device would make this task easier. A larger device may work with the accuracy of a robotic system, but these

systems already exist [3]. The failure of the complex tweezer design is the reason for pursuing a design that is as simple as possible, as discussed in the following sections.

5.5   Gel-Pak Removal Designs

As discussed in Section 1, Gel-Paks are small, durable boxes contain a specialized polymer material that is tacky enough to reversibly adhere to the backside of a die or wafer. Available with different adhesion strengths, they ensure that the device does not come loose within the box, even when dropped or shaken. The gel material is strong in normal and shear adhesion but weak in peel strength, so a peeling motion is normally needed to remove devices from the gel.

5.5.1   *Gel-Pak Testing and Comparison to the Adhesive*

Normal and LDP tests were conducted in order to compare the adhesion of the Gel-Paks to that of the gecko adhesive. Identical testing conditions to the gecko adhesion tests were used for two Gel-Pak durometers, X0 and X4. As expected, the lower durometer Gel-Pak X4 has the highest adhesion strength as seen in Figure 46.
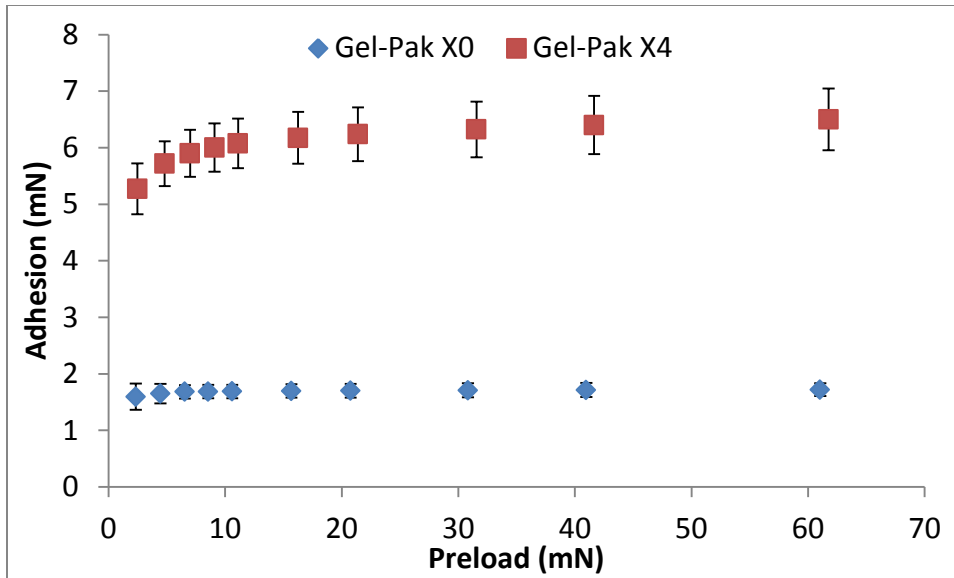
Figure 46: Gel-Pak X0 and X4 adhesion data. Tests were done with a 6 mm hemispherical indenter and the same standard conditions that were used for testing the gecko adhesive.

LDP tests were also done on both Gel-Paks. The hemispherical indenter was dragged a number of different distances ranging from 0 to 80 μm while in contact with the Gel-Pak and the results are summarized in Figure 47. There is some slight anisotropic behavior for Gel-Pak X0 which is attributed to the Gel-Pak shifting slightly when moving in the negative direction. A larger error accounts for the slightly higher adhesion values. This reduced adhesion with drag distance provided a means by which a simple control mechanism could pick and place devices on these Gel-Paks without requiring complex adhesion anisotropy.
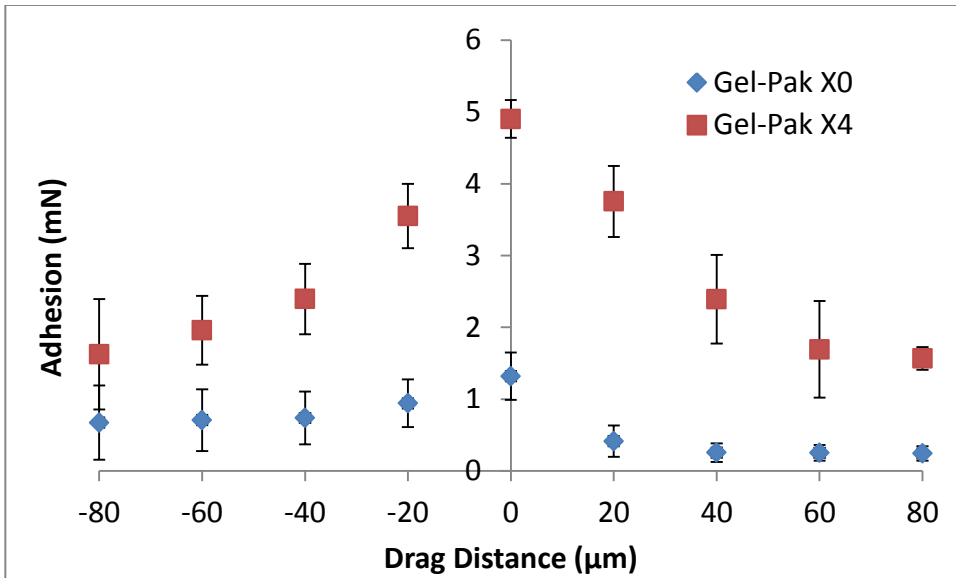
Figure 47: Gel-Pak X0 and X4 LDP test results. The slight anisotropic behavior is likely due to the Gel-Pak slipping during the drag motion.

5.5.2   *End Effector Wedge Prototypes*

The first generation of manual end effectors were simply wedges as seen in Figure 48.
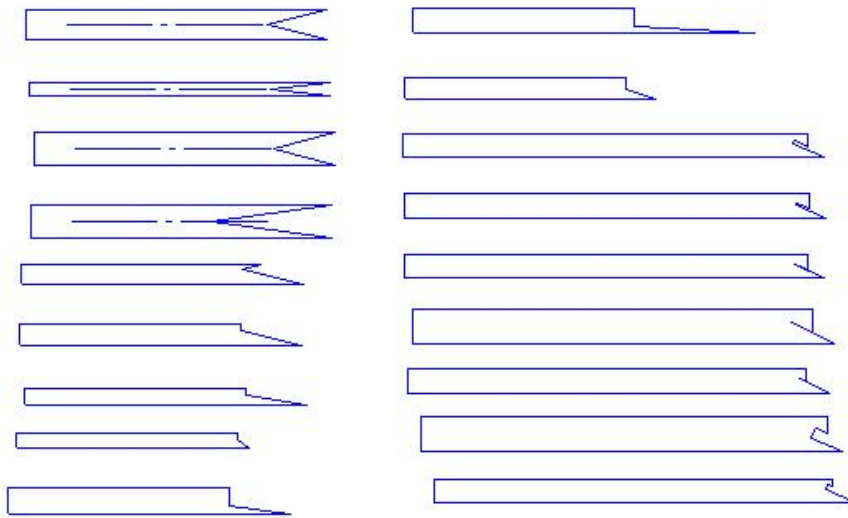
Figure 48: Gel-Pak end effector designs. Various wedge shapes were cut from 1/8" acrylic using the laser engraver.

Surprisingly, the simple wedge shape design was sufficient to manually remove the die from the Gel-Pak nearly every time with high accuracy and speed. Alignment is important, and the size of the wedge needs to be custom made to the size of the die, but an operator can remove the die with relative ease. The main advantage of this technique is that the top surface of the die is not contacted, so there is very little risk of contamination. The main challenge with this adhesive-less method is the stability of the die during movement. The die can easily slip off the wedge, making this method worse than manual tweezers in this respect. To supplement a simple wedge, the gecko adhesive can be placed on a sidewall at the thick end of the wedge as seen in Figure 49. This technique solved the issue of holding the die secure during transport, but it created new problems.
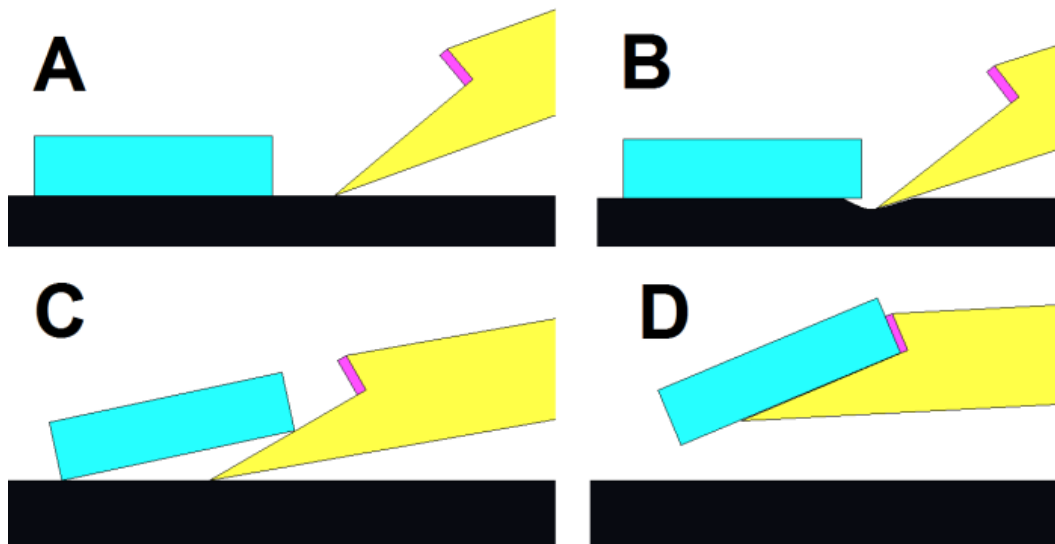
Figure 49: Sequence of picking a die from a Gel-Pak using a wedge with pink gecko adhesive. The adhesive holds the die at the edge during transport. Compressing the Gel-Pak at the edge of the die creates a gap for the wedge to enter (B). This gap initiates the peel failure of the Gel-Pak, and the die lifts away easily.

To engage the adhesive, a preload is applied by lightly pressing the die against the Gel-Pak at its edge. This is an awkward movement that can easily damage the die and/or have

it come loose from the Gel-Pak before adhering to the gecko adhesive. Currently there is no reliable method for releasing the die. Attempting to adhere the die to a second Gel-Pak often resulted in it spinning or flipping since the adhesive can remain attached along one edge. A secondary tool may be viable, but that would add more complexity to the design and likely cause more issues. These control problems lead to abandoning the simple wedge design in favor of a surface contact method.

5.5.3   *End Effector Shear Ledge Prototype*

A method of controlling adhesion was now the most important consideration for these designs.The results of the LDP tests on both the gecko adhesive and Gel-Pak demonstrated that a lateral shear movement is a good candidate for controlling adhesion. Shearing was able to reduce the normal adhesion of both the gecko adhesive and Gel-Paks, and thus the issue was when and how to shear them to create the simplest pick and place technique.

Since contacting the top surface of the die must be minimized, the first design intended to take advantage of normal adhesion force reduction through shearing the Gel-Pak and reduce the required gecko adhesive contact area. The gecko adhesive will have weaker normal adhesion than the underlying Gel-Pak and will remove the die after the gel has been sheared to reduce its normal adhesive strength. This makes placing the die simple, as the die only needs to be adhered to the gel, then withdrawing the end effector will break the gecko adhesion.

The only requirement is a small ledge extending from one side of the end effector as seen in Figure 50. After contacting and preloading the gecko adhesive, a shearing motion would have the ledge apply pressure to one edge of the die, shearing the underlying gel.

The shear will lower the gel's adhesion strength enough so that the gecko adhesive can overcome it, and remove the die from the Gel-Pak. For placement, the end effector simply needs to attach the die against another medium with higher adhesion than the gecko adhesive.
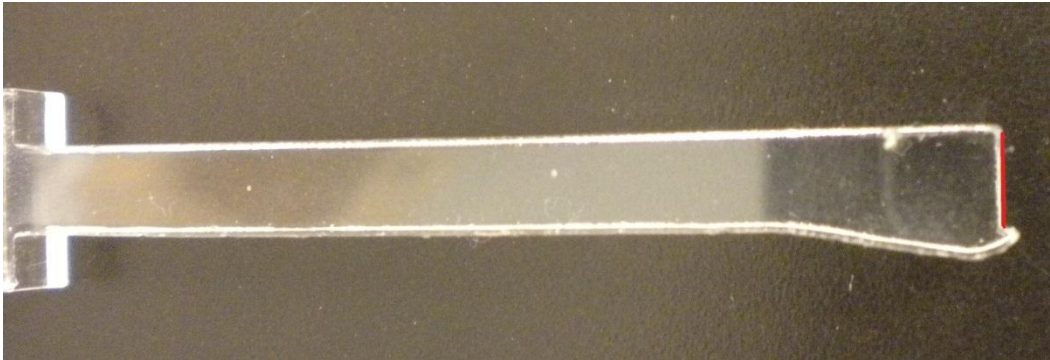
Figure 50: Early end effector prototype with a ledge for shearing the die. The adhesive, 5 mm x 5 mm, is affixed at the red line in the image with the ledge just next to it.

Preliminary tests were done by hand. The end effector was difficult to use, and had very few successful pick and place cycles. The failures were assumed to be caused by the inaccuracy of manual operation. A robotic system was needed to perform more accurate testing.

5.6   Linear Actuator Stage Design

A testing apparatus that could simulate a MEMS manufacturer's robotics system was needed. Two leadscrew linear actuators were used to simulate the robotic pick and place system. The linear actuators are the same ones used for the adhesion testing apparatus, an MFA-CC model controlled by ESP301 motion controller from Newport Corporation. These actuators and the LabVIEW software that controls them have been extensively used throughout this project, and thus programming a pick and place robotic system was a trivial task. The actuators have a high level of accuracy, allowing precise movements as

small as 0.1 μm. The actuators allow the pick and place testing to be done with only the

end effector being a variable, rather than the accuracy of the robotics affecting the results.

The pick and place system is shown in Figure 51.
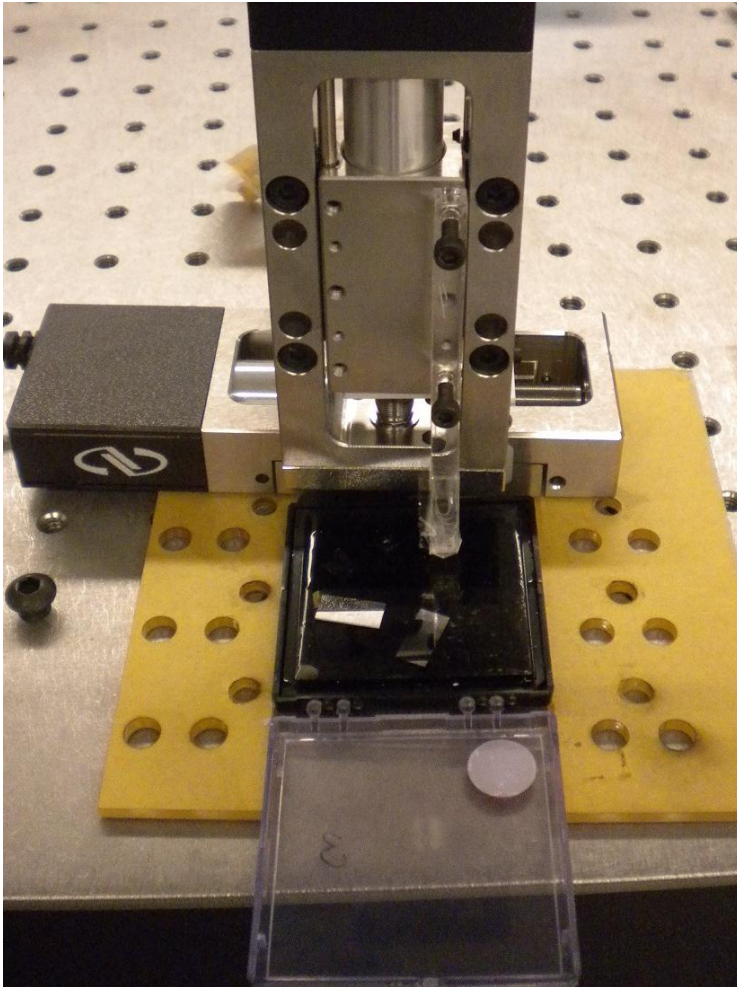
Figure 51: Pick and place testing apparatus. Two coupled linear stages provide x and z directional movement. The system is anchored to the table with screws. A Gel-Pak fits firmly just below the end effector.

5.7 Shear Ledge Prototype Testing

Preliminary robotic testing was less successful than handheld tests, and after multiple testing attempts, the die was almost never successfully moved. Many robotic failures were attributed to the lack of force feedback or cushioning on the end effector. The pressure would often be too high, causing too much friction to move the die along the Gel-Pak. The gecko adhesive is known to reduce its adhesion if it is crushed as well [171], and the increased pressure could also contribute to the die being repeatedly left behind. As a result, a new end effector was designed that reduced the pressure on the die.

5.7.1 End effector Springs

The new end effector has a spring that will constantly apply a light amount of pressure to the gecko adhesive as seen in Figure 52.
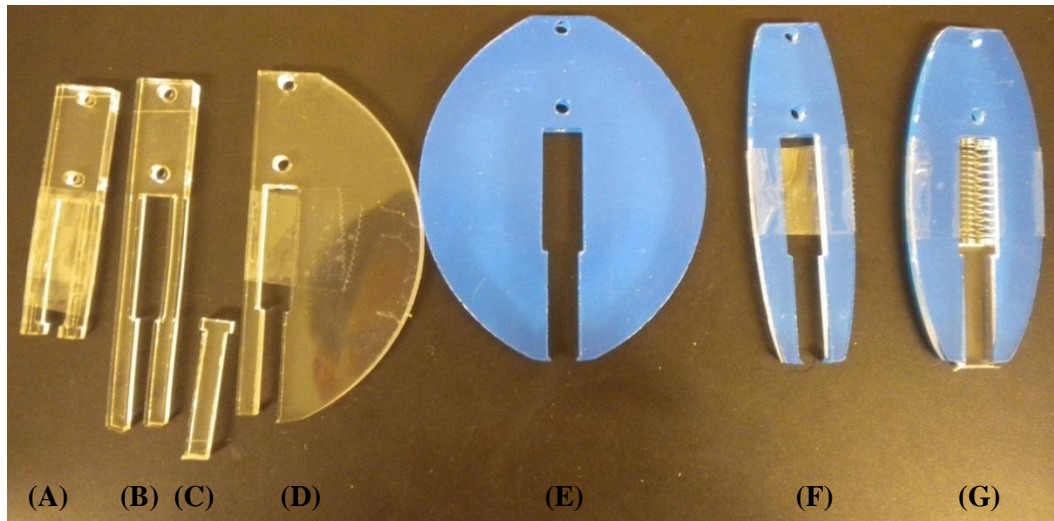
Figure 52: Multiple end effector designs using a spring to reduce the maximum possible pressure on the top surface of the die and gecko adhesive. The spring is only shown in design G. From left, the original model (A), extended guides for punch stability (B), example punch with adhesive at its tip (C), rounded wall for added stiffness (D), two walls for shearing either direction (E), reduced material for reduced stiffness (F), slightly increased material for stiffness (G).

The spring pushed against a flat punch with the gecko adhesive at the opposite end. The ledge within the channel allows the punch to be slightly extended from the channel when no pressure is applied to the spring. The system will work with the punch first contacting the die, causing the springs to compress and the punch to withdraw into the channel. The compression will stop when the channel extends just beyond the gecko adhesive contact point. The edge of the channel will then function as the ledge in the earlier model, and the system will be sheared to release the die from the Gel-Pak. The first model of the spring system was unable to control the path of the flat punch and thus the extended channel walls were added. The next models did not have enough stiffness to shear the Gel-Pak, resulting in the channel walls significantly deflecting. Rounded edges were added instead of the thin edges to give the required stiffness to move the Gel-Pak.

The spring solved the issues of excess pressure, but introduced an equally troubling issue. After shearing the Gel-Pak, the pressure from the spring would often reapply the die to the gel before it was removed, and thus the modification was unsuccessful.

5.7.2   *Ledge End Effector Discussion*

There are serious problems that prevent the ledge design from working. First and foremost, alignment is very difficult. The gap between the ledge and the edge of the die must be less than the drag distance that affects the gecko adhesive's adhesion strength. This value is approximately 40 μm, which is extremely difficult to achieve by hand or without complex robotic alignment systems. The result is that, regardless of manual or robotic positioning, the gecko adhesive is nearly always inadvertently sheared. If positioned too close, the ledge can press on the surface or one edge of the die, possibly damaging it or shifting the die causing misalignment. The robotic system reduced the severity of this problem, but inaccuracy of the robotics still caused problems.

106

The size of the ledge is an equally important parameter. There is a small margin of error for the length that it extends from the contact plane of the gecko adhesive. It should extend enough to align very closely to the Gel-Pak without contacting it. If the ledge extends too far, it will simply press into the Gel-Pak and prevent the gecko adhesive from contacting the die. Even if the gecko adhesive is in contact with the die, if the ledge is contacting the Gel-Pak, the shearing motion will be significantly hindered due to friction between the ledge and Gel-Pak. When the lateral motion takes place with robotics, this extra point of contact can store energy similar to a spring; when the end effector is retracted, it will release this energy by flicking the die, potentially damaging or dropping it. If the ledge is too short, or pointed with a non-vertical sidewall, it may slip and rub the top surface of the die. Each die must have its own custom build ledge based on the thickness of the die. The ledge also must account for the compression distance of the gecko adhesive when applying the preload.

Finally the heavy shearing forces need to be resisted by the Gel-Pak, but frequent shearing can cause damage to the Gel-Pak, which in turn risks damage to the devices being transported. The gel layer was seen to come loose from to the underlying stiff backing later after a number of cycles. This will change the gel's resistance to shearing which can affect the shearing release mechanism and potentially prevent the proper picking or placement of the die.

The issues listed previous all contribute to this ledge design being too complex with not enough room for error, and another, simpler solution was needed.

5.8 Flat Punch Model

A new theory was devised based on the performance of the gecko adhesive and Gel-Pak X4 as seen in Figure 53 and Figure 54. The gecko adhesive is superior in normal strength, while the Gel-Pak, when having a higher area in contact, will have a higher resistance to shear. In practice there will be a ratio of the two contact areas in which the gecko adhesive will remain superior in normal adhesion, but inferior in shear loading.
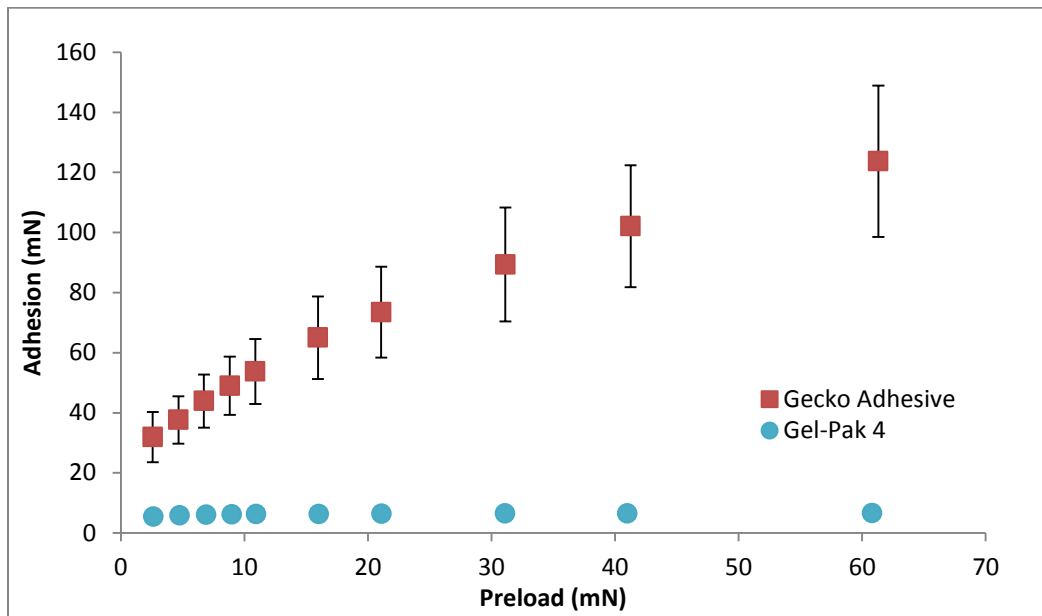
Figure 53: Normal adhesion strength comparison of the strongest performing gecko adhesive and Gel-Pak X4. Tests were done with identical testing parameters and a 6mm diameter probe.
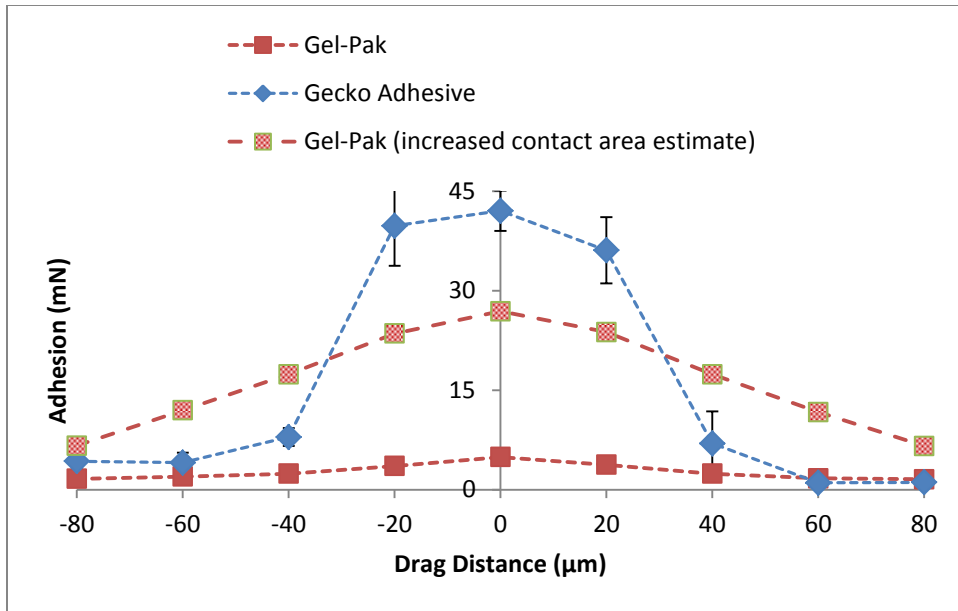
Figure 54: LDP test comparison for the gecko adhesive and Gel-Pak X4. The tests were performed with identical settings. The second Gel-Pak dataset represents an estimate of adhesion force if the Gel-Pak had a significantly higher area in contact. The high area Gel-Pak would better resist shear loading if both the gecko adhesive and Gel-Pak were sheared simultaneously.

The new design is a simple flat punch with the gecko adhesive arranged around the perimeter, or with two parallel strips as seen in Figure 55. The design was first tested with gecko adhesive covering the entire top surface of the test die as proof of concept. The original tests involved attaching the gecko adhesive to the end effector with standard adhesive tape, with subsequent models fabricated by curing the polyurethane adhesive directly to the end effector.
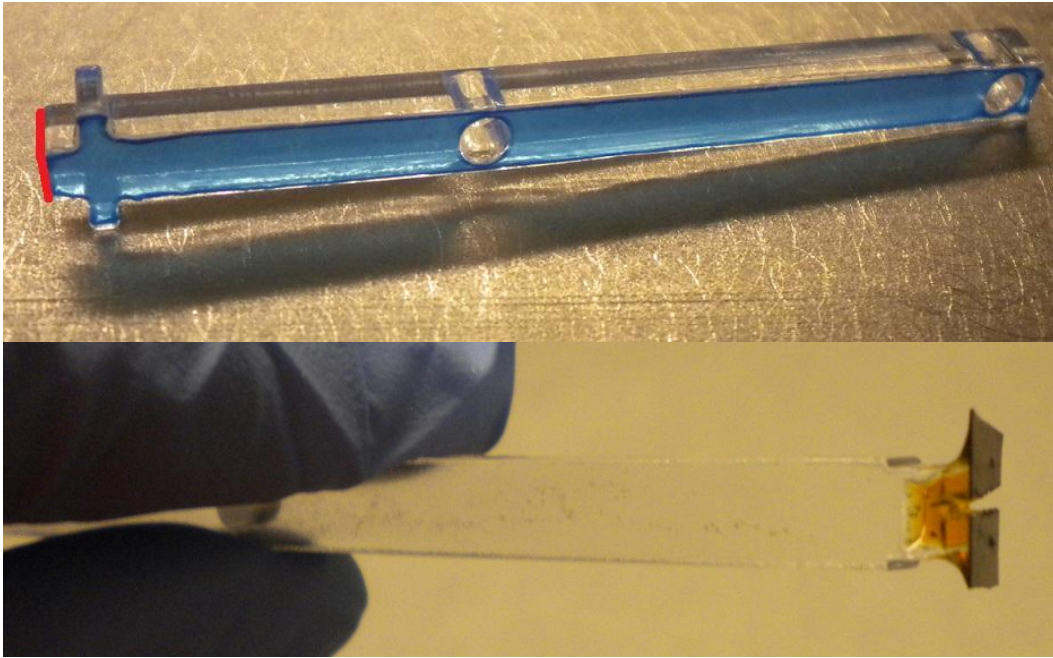
Figure 55: Flat punch end effectors with adhesive covering a square tip (top) or two parallel strips of adhesive (bottom). The bottom end effector had the polyurethane cured directly to the PMMA. The parallel adhesives will only touch the edges of the die. It is possible to use these designs either by hand or attach them to the linear stages for robotic pick and place.

5.8.1   *End Effector Fabrication*

The final end effectors needed to be fabricated in such a way that the central area of the MEMS die would not be contacted. The first prototypes, where the adhesive was attached with standard adhesive tape, had the central section simply cut away with a blade. This worked well, but the tape often slipped, and a more durable, permanent solution was needed.

The polyurethane can be cured directly onto the PMMA end effectors. The application can be done at the same time as the original molding of the adhesive, but it was deemed that the presence of the end effector may affect the formation of the microstructures. As an alternative, a two part fabrication method was chosen. The prepolymer would first be

110

laminated into the mold to produce a working adhesive with a thin backing layer. The polymer can be standard ST-1060, or the ST-1060 (antistatic version) and carbon black composite. Next, a second batch of polyurethane prepolymer was prepared and applied to the cured backing layer before demolding the original laminated adhesive. The end effector was placed in contact with the prepolymer such that it will cure directly to the PMMA. Once cured, the adhesive is demolded, and trimmed away with a blade to form the final end effector.

The adhesion of polyurethane to PMMA turned out to be a problem for manufacturing end effectors with an empty central contact point; polyurethane could rarely be removed without damaging the surrounding adhesive. The solution was to fabricate the end effectors such that they had two extended fins for bonding to the polyurethane. After curing, the central material could more easily be cut away from the PMMA as it did not contact any point of it. This resulted in a design with adhesive not around the entire perimeter, but only along two parallel strips as seen in Figure 55. Further testing was needed to validate the slightly modified design.

5.8.2 _Manual End Effector Preliminary Trials_

The first flat punch prototypes were fabricated and tested with adhesive covering the entire surface, rather than the two parallel strips mentioned in the previous section. Preliminary tests on Gel-Pak X0 demonstrated that the end effector is very effective when used manually; the gecko adhesive is strong enough to remove a small 5 mm x 5 mm die withdrawing in the normal direction. The die can then be placed back on the Gel-Pak by applying normal pressure and a slight shearing motion as seen by the procedure detailed in Figure 56. By hand a lateral shear is difficult to perform accurately, and it proved to be considerably easier and more controllable to instead twist the end effector to

111

apply the shearing motion. The twisting motion was not 100% effective, but the failed

release could be corrected after repeated attempts. These failures often occurred when

dealing with a pristine sample of the adhesive, suggesting the device will function with

less adhesive area in contact.

A larger die, measuring 13 mm x 6 mm x 1 mm was also tested. The end effector was

able to remove the die on most attempts. There was noticeably more adhesion from the

gel with the larger surface area in contact, suggesting that the adhesive may have

difficulty removing the die should it only be contacting the perimeter.
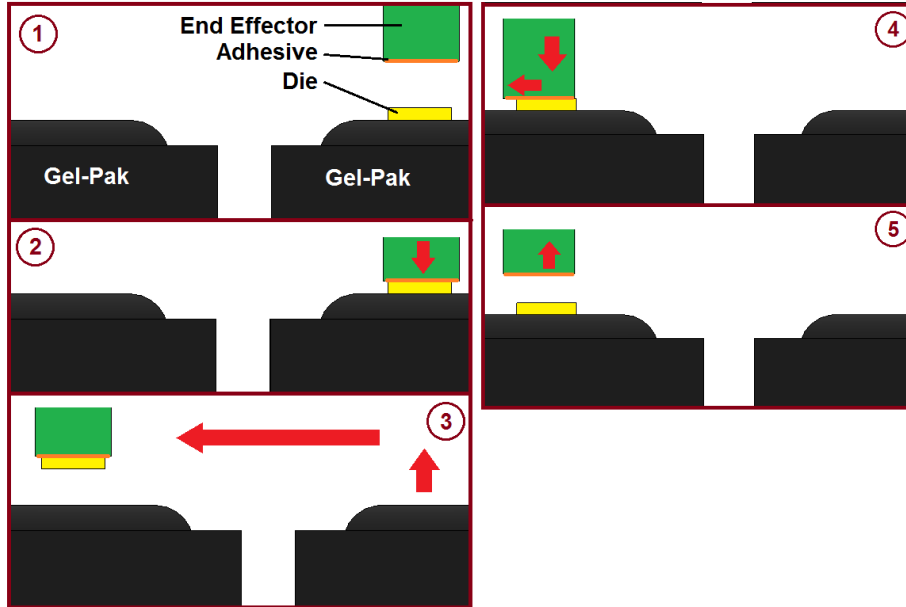
Figure 56: Process flow of moving the die with a flat punch. The end effector initiates contact with the die (2), withdraws and moves above the desired placement location (3), applies light pressure to the location and a slight shear to disengage the adhesive (4), with the gecko adhesive disengaged the end effector simply retracts to place the die (5).

As the gecko adhesive on the first prototypes began to degrade from mishandling damage,

overuse, and dust, the normal strength of the adhesive was not always enough to remove

the die on the first attempt; however, this problem lead to the discovery of a simple trick

that can assist in removal of the die. Applying slightly more pressure to one edge of the die while it is still attached to the Gel-Pak would raise the opposing edge. Applying this slight torque initiates the peel failure of the Gel-Pak, greatly reducing the force required to break contact. This strategy, should the die have the strength to endure it safely, can ensure the safe pickup of the die nearly 100% of the time if the adhesive is in good condition.

Once the die is on the end effector it is nearly impossible to drop. Violent shaking and motion of the handheld end effector has no effect on the die if it is properly adhered to the gecko adhesive. A trained operator under normal conditions will rarely apply anything more than gentle lateral movements, and thus the die should never be dropped, unless the end effector itself is dropped. This is far superior to manual tweezers which are susceptible to dropping or squeezing the die should the operator change the strength of their grip.

Following the trials with a full contact area of gecko adhesive, end effectors were fabricated only with the adhesive around the perimeter or two edges of the die. The perimeter adhesion end effectors were also very effective when operated by hand. For the stronger, pristine adhesive the perimeter end effectors were more effective since the reduced adhesive area will require less shearing and release the die more easily. However, the larger die became nearly impossible to remove with the reduced gecko adhesive contact area, suggesting there may be a maximum size of die, or minimum relative contact area for this device to be successful.

5.8.3 Robotic End Effector Preliminary Trials

With the success of the handheld end effectors, the robotic system was tested. The motions were the same except the robotics applied a lateral shear like that in Figure 56 rather than a twisting motion. The lateral shear is less effective by hand, but with the precision of the robotics, it is similar in effectiveness compared with the twisting motion. In addition, the robotic system used in this study does not have the necessary degrees of freedom to perform a twisting motion, or a torqueing motion to assist picking the die. Micralyne Inc. may wish to upgrade their robotic system to perform these more complex movements should they be deemed necessary.

The robotics was successful in picking and placing the small die with adhesive covering the entire die or only having two parallel adhesive strips. The larger die had no successful pick and place cycles with a reduced area of adhesive. Thus the end effector design for larger die was abandoned pending adhesive improvements. This larger die is close to the upper limit of die that Micralyne Inc. manufactures and thus the adhesive system may not be usable for the whole range of their products. There will be a maximum die size that this technology can be used with.

5.8.4 Reliability Testing Procedures

Reliability tests were performed on both Gel-Pak X0 and Gel-Pak X4 using the robotic system. The test die used was a 5 mm x 5 mm x 1 mm silicon piece supplied by Micralyne Inc. The adhesive used is shown in Figure 55, and consists of two strips of the adhesive that will attach to the outer edges of the die. The standard test is carried out by the method of pick and place shown in Figure 56. The die was removed and placed on a different location of the same Gel-Pak, using the apparatus in Figure 51. Trials were done in groups of five, meaning the die was lifted and moved five times per trial. The actuators

114

were set to 2.5 mm s^{-1} and each trial lasted about 2 minutes. After each trial the alignment of the die was inspected and corrected before continuing with the next, and a trial was considered a failure if the end effector failed to either remove or place the die. 20 trials were done for a total of 100 consecutive pick and place cycles.

Manual reliability testing was also done on the Gel-Paks. Testing procedure was simply to continue removing and placing the die until the adhesive was degraded enough to prevent adhesion. Trials were only considered failures if the die was moved in an erratic and unpredictable manner and multiple attempts to pick or place the die were deemed acceptable.

5.9   Results and Discussion

Early robotic trials on Gel-Pak X0 were promising, but began to have significant failures, completing only 15/20 movements. The failures were quickly attributed to the orientation of the gecko adhesive with respect to the shear direction. If the end effector was dragged perpendicular to the orientation of the two parallel strips of gecko adhesive, the sharp edges of the die would damage the adhesive. This method would also position one strip of the adhesive closer to the center of the die, potentially damaging the central components. The solution was to reorient the gecko adhesive strips such that they are parallel to the shearing direction. This doesn't prevent the die edges from damaging the adhesive, but it significantly reduces the damaged area. This also prevents the adhesive from moving any further towards the center of the die, reducing the risk of damage to the die.

Subsequent testing on Gel-Pak X0 with this new orientation showed improved results with only two failures in 100 trials. After about ten pick and place cycles the die would

115

be slightly shifted out of alignment and manual replacement of the die was required. This is a problem for our robotic system, but Micralyne Inc. will have strict alignment guidelines and more advanced robotics to prevent this from occurring. The misalignment was a result of the die slightly shifting during the shearing motion, and after 5-10 cycles the cumulative shift significantly offsets the die, such than the center of the die moved into the area of contact. If a different die were moved each time rather than the same die, this shifting would not be an issue.

Following the success of Gel-Pak X0 testing, more end effectors were prepared for testing Gel-Pak X4 with robotics. Preliminary tests had limited success, with the die successfully being removed from, or placed on, the Gel-Pak approximately 10-20% of the time. The first source of failure considered was a loose connection within the system, including the screws connecting the end effector to the linear actuator and those connecting the horizontal linear actuator to the Gel-Pak. Although both connections were slightly loose, tightening them did not increase the success rate. The second issue considered was the alignment of the adhesive with respect to the die. If the contacting surfaces are not parallel, only a small portion of the adhesive may make contact much like the problem encountered during adhesion testing of flat-flat surface contacts [140]. The end effector was manually adjusted such that alignment was as close as possible to parallel but again this did not improve the success of the testing. The final issue was the applied preload. There is no load cell in the apparatus so the preload is judged visually. If the linear stage begins to raise itself up when pushing against the die and Gel-Pak, the preload is too high. Multiple preloads were tested and, for a third time, the success of the system was not improved. Thus it was concluded that with the current model and strength of the adhesive, it is not practical to use the robotic system with Gel-Pak X4. For

removing die from surfaces of that adhesive strength, additional measures are needed such as pins pushing on the die from below to begin to break contact similar to what is currently done for tape drum die removal.

5.9.1 *Manual Adhesion Trials*

Although the end effectors were not able to robotically move the die from Gel-Pak X4, manual manipulation proved to be effective. Accurate placement by hand meant that the adhesive was able to remove the die purely through normal force, and, as the adhesive degraded, applying a slight torque was enough to remove the die. Using these manual techniques the die was successfully picked up, and replaced on the Gel-Pak 298 times before needing replacement. There were numerous failures however, and the pick or place motion often needed to be repeated to be successful. This is easy for an operator to do, but difficult for the robotics, as it would require a sensor to detect when the die was successfully moved. In addition, there was four occasions when the die slipped and fell in an uncontrolled motion. These slips were caused when one of the parallel strips adhered to the edge of the die and the other did not, causing one edge of the die to not maintain contact and ultimately ejecting the die into the air. Three of these failures occurred during the last 75 pick and place motions and thus replacing the end effector sooner could prevent this.

5.9.2 *Application to Real Die*

This study was the first part of a series of steps in a project to implement a robotic system into the pick and place of MEMS die. Thus the system is not yet prepared for use with real MEMS die. Although no real die were used for pick and place, the adhesive was tested on real die to evaluate the adhesion ability. As seen in Figure 57, the adhesive is able to support the entire MEMS device while only contacting its edge.

117
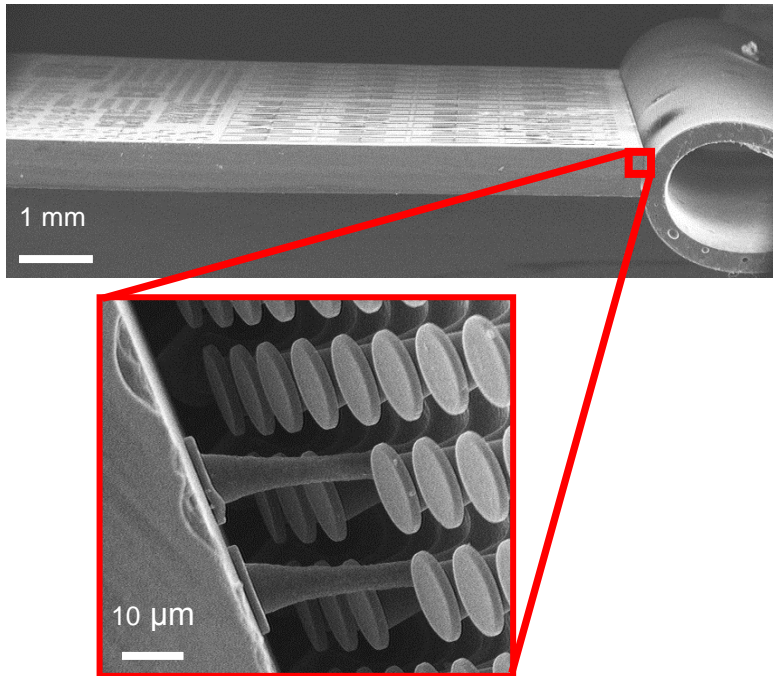
Figure 57: A MEMS die being held with the adhesive only by its edge. A zoomed in section shows the extended fibers in contact, one of which is maintaining adhesion around a small particle.

There are a number of important observations to be made from Figure 57. Of most interest is that the adhesive is able to support the die only on one edge, which suggests that a future pick and place technique may only need to contact the edge of the die, reducing the risk of contamination or damage to the top surface. Next, inspecting the contact interface reveals that only a small fraction of the fibers are in contact at this particular location, suggesting the adhesive is strong enough to support the die with a much smaller contact area than what appears. The fibers in contact are extended approximately 100%, showing the robustness of these particular fibers. In addition, one fiber is maintaining contact despite conforming to a small particle. It is likely that the slight off-axis load is assisting the fiber to maintain contact, as the majority of stress is on the opposite side of the fiber away from the particle. These results show the future

118

potential of the adhesive, but the current technology will need to contact the top surface of the die.

MEMS die will have a number of bonding pads around the perimeter on the top surface, and it is these that the gecko adhesive will most likely adhere to. Micralyne Inc. uses a variety of bond pad sizes, but they typically measure 200 µm x 200 µm. The issue with these bonding pads is that their edges often have sharp topography at the edge. This 10 µm wide edge will likely prevent any fibers from making contact if they overlap this topography. This is an excellent reason to reduce the size of the fibers. Although more of the smaller fibers will contact the edges, less contact area will be lost to those fibers, decreasing the reduction of adhesion from bond pad edges. This effect can be seen in Figure 58.
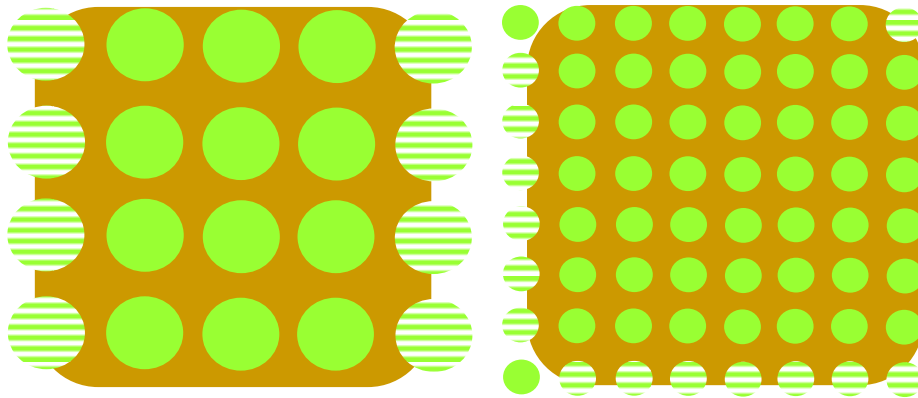
Figure 58: A idealized visualization of the effect of bond pad topography on adhesion to MEMS die. The circles represent the contact points of single adhesive fibers and the background shapes represent bond pads. The striped circles represent fibers which would not contribute adhesion because of the sharp bond pad topography. The larger fibers (left) are more susceptible to changes in topography compared to smaller fibers (right).

For real die, a balance is needed between reducing the fiber size to improve contact over bond pads, while retaining a minimum fiber size that will not be affected by

manufacturing defects. Using current manufacturing techniques, this ideal size is likely between 16 and 24 μm.

5.10 Summary

A pick and place procedure has been developed for the manipulation of small MEMS die. Gecko adhesive running in two parallel strips along the upper edge of the die was enough to successfully remove it from Gel-Pak X0 and Gel-Pak X4 manually. A robotic system was only successful in reliable pick and place from Gel-Pak X0. To remove a die, the preloaded gecko adhesive has enough adhesion strength to overcome the underlying Gel-Pak tackiness. If more assistance is required, an operator can apply a torque to the tool to begin peeling the underside. To place a die, the tool needs to reapply the die to the Gel-Pak or equally tacky surface, and then apply a shearing motion to reduce the gecko adhesive's normal adhesion strength. An operator can use a twisting motion to apply this shear should it be easier. For a lateral shear, it is important to shear parallel to the orientation of the two strips of gecko adhesive to prevent the edge of the die from damaging the adhesive. Using these techniques the manipulation of MEMS die is possible and practical.

5.11 Future Work

With preliminary success in the feasibility of the pick and place apparatus, the next step is to ensure the MEMS devices will not be adversely affected by contact with the adhesive. In the future, a static dissipating material will permanently replace standard ST-1060 as the adhesive material. Currently the best candidate is the ST-1060 (antistatic version) carbon black composite used in this study. The composite has proven to be dissipative enough to prevent charging during the SEM operation, but the resistivity needs to be more quantitatively characterized and improved mixing techniques are

needed to better disperse the nanoparticles. The resistivity will need to be calculated on the structured adhesive, rather than the unstructured base material to account for any possible geometry effects from the microstructures.

The new adhesive material will need to be tested for any evidence of fouling a surface identical to the die bonding pads after repeated contact cycles. Each die should only contact the adhesive one or two times, and thus no fouling after tens or hundreds of contact cycles should assure that the adhesive will not leave any residue behind. The bonding pad material can then be wire bonded at the adhesive contact site, and the wires can be tested for any reduction in strength.

Beyond the adhesive material itself, the end effector will need to be grounded to dissipate charge as discussed in Section 5.2. A conducting material or grounding technique will need to be tested with the gecko adhesive to ensure it does not adversely affect the pick and place system. This decision can be made by Micralyne Inc., as they will need to integrate it with their current robotic pick and place apparatus.

Finally the adhesive will need to be tested with real, working die. If a die can be moved safely and effectively without adversely affecting its performance, the project is successful and Micralyne Inc. can begin integrating the adhesive into their manufacturing process should they choose to adopt it.

The system can also be enhanced by replacing the normal adhesive with a directional adhesive. Directionality can reduce the strain on the adhesive by requiring less shearing during release, potentially extending its operational life. It can also make the system more robust and controllable if the adhesive can more easily be activated and deactivated. There are numerous methods for producing anisotropic adhesives [100-103], and the

simplest to integrate with our existing system and fabrication methods may be to create anisotropic cap geometry. The linear stages can easily be programmed to shear in one direction to engage the adhesives, and the opposite direction to release the die. It is recommended to test the pick and place system with an anisotropic adhesive when one as reliable and effective as the current adhesive becomes available.

6   CONCLUSION

In this study an established gecko adhesive fabrication method was optimized, and the adhesive was applied to the pick and place of MEMS die. Both manual and robotic actuation was attempted with a number of different techniques and designs. New fabrication methods and strategies were developed and adhesion testing techniques were improved. The following conclusions can be drawn:

- During UV exposure in the cleanroom, contact between the photomask and substrate is paramount for achieving fine features. The specialized screw apparatus combined with bulldog clips is effective for improving contact and achieving sharp features on slightly warped PMMA substrates.

- The development stage of fabrication is most important for determining the cap overhang. Using a combination of the development depth characterization curves and visual inspection is best for achieving the desired cap overhang.

- During replica molding, using a squeegee fills the micromolds not by forcing material into them, but by collapsing and expanding the microstructures, which forms a vacuum that draws the prepolymer into the mold.

- For highly viscous polymers, the lamination method can effectively fill the mold while creating a smooth, even backing layer. This facilitates applying the adhesive to other objects and surfaces.

- To create anti-static adhesives, carbon black nanoparticles can be added to the prepolymer with a ratio of at least 12% carbon black by weight. The viscous composite must be laminated into the mold.

- Finite element modeling shows that the hourglass shape of the fibers directs stresses towards the center of the cap, rather than the more vulnerable cap edges,

123

resulting in increased adhesion strength compared to a purely cylindrical fiber stalk.

- Large, handheld tweezers are too bulky to transport small die effectively, and a smaller, lighter, simpler design is better.

- A small shearing motion is normally adequate to disengage the adhesive, and is an excellent method of controlling adhesion with these isotropic adhesives.

- The simplest design is best, and relying on normal adhesive strength is superior to incorporating springs, wedges, and/or attaching to the edge of the MEMS die for the pick and place operations used in this study.

- Under normal operating conditions, the end effectors should be effective for up to, or exceeding 200 attachment/detachment cycles. Manual manipulation can be done for Gel-Pak X0 or Gel-Pak X4, while robotic manipulation is effective for Gel-Pak X0 with 98% reliability.

- Further improvements are needed to improve reliability on tackier Gel-Paks. Techniques such as using anisotropic adhesives may be needed.

This study has demonstrated the potential for using these gecko inspired adhesives in a commercial manufacturing setting.

7   BIBLIOGRAPHY

[1] Mühlbauer Group. 2012; Available at: http://www.muehlbauer.de/. Accessed 11/21, 2012.

[2] Virtual Industries, Inc. 2010; Available at: http://www.virtual-ii.com/. Accessed 11/21, 2012.

[3] Royce Instruments. 2012; Available at: http://www.royceinstruments.com/. Accessed 11/21, 2012.

[4] Gel-Pak(R). 2006; Available at: www.gelpak.com. Accessed 9/14, 2012.

[5] Kaeslin H. Digital integrated circuit design: from VLSI architectures to CMOS fabrication: Cambridge University Press; 2008.

[6] Sarah K. Meeting Today's Die Sorting Challenges. 2012; Available at: http://www.us-tech.com/RelId/979000/ISvars/default/Meeting_Today's_Die_Sorting_Challenges.htm Accessed 9/14, 2012.

[7] Carlson A. 2011 Shear-enhanced adhesiveless transfer printing for use in deterministic materials assembly *Appl Phys Lett* **98** 264104-3.

[8] Wu J, et al. 2011 Mechanics of reversible adhesion *Soft Matter* **7** 8657-8662.

[9] Menguc Y, et al. 2012 Gecko-Inspired Controllable Adhesive Structures Applied to Micromanipulation *Adv Funct Mater* **22** 1246-1254.

[10] Yang SY, et al. 2012 Elastomer Surfaces with Directionally Dependent Adhesion Strength and Their Use in Transfer Printing with Continuous Roll-to-Roll Applications *Adv Mater* **24** 2117-2122.

[11] Heepe L, et al. 2010 Suction component in adhesion of mushroom-shaped microstructure *J R Soc Interface* **8** 585-589.

[12] Autumn K, et al. 2002 Evidence for van der Waals adhesion in gecko setae *Proc Natl Acad Sci* **99** 12252-12256.

[13] Autumn K, Peattie AM. 2002 Mechanisms of Adhesion in Geckos *ICB* **42** 1081-1090.

[14] Autumn K, et al. 2000 Adhesive force of a single gecko foot-hair *Nature* **405** 681-685.

[15] Israelachvili J.N. Intermolecular and surface forces: revised third edition: Academic press; 2011.

[16] Arzt E, et al. 2003 From micro to nano contacts in biological attachment devices *Proc Natl Acad Sci* **100** 10603-10606.

[17] Gao H, et al. 2005 Mechanics of hierarchical adhesion structures of geckos *Mech Mater* **37** 275-285.

[18] Williams E, Peterson J. 1982 Convergent and alternative designs in the digital adhesive pads of scincid lizards *Science* **215** 1509.

[19] Artz E, et al. 2003 From micro to nano contacts in biological attachment devices *Proc Natl Acad Sci* **100** 10603-10606.

[20] Johnson KL, et al. 1971 Surface Energy and the Contact of Elastic Solids *Proc R Soc Lond A Math Phys Sci* **324** 301-313.

[21] Autumn K, et al. 2006 Effective elastic modulus of isolated gecko setal arrays *J Exp Biol* **209** 3558-3568.

[22] Hui C-, et al. 2005 How Compliance Compensates for Surface Roughness in Fibrillar Adhesion *The Journal of Adhesion* **81** 699-721.

[23] Persson BNJ, Gorb S. 2003 The effect of surface roughness on the adhesion of elastic plates with application to biological systems *J Chem Phys* **119** 11437-11444.

[24] Autumn K, et al. 2006 Frictional adhesion: a new angle on gecko attachment *J Exp Biol* **209** 3569-3579.

[25] Hsu PY, et al. 2011 Direct evidence of phospholipids in gecko footprints and spatula–substrate contact interface detected using surface-sensitive spectroscopy *J R Soc Interface* **9** 657-664.

[26] Denny MW. 1981 A Quantitative Model for the Adhesive Locomotion of the Terrestrial Slug, Ariolimax Columbianus *J Exp Biol* **91** 195-217.

[27] Hanna G, et al. 1991 Adhesion and Detachment of the Toe Pads of Tree Frogs *J Exp Biol* **155** 103-125.

[28] Hansen WR, Autumn K. 2005 Evidence for self-cleaning in gecko setae *Proc Natl Acad Sci* **102** 385-389.

[29] Yao H, Gao H. 2006 Mechanics of robust and releasable adhesion in biology: Bottom–up designed hierarchical structures of gecko *J Mech Phys Solids* **54** 1120-1146.

[30] Russell AP. 1975 A contribution to the functional analysis of the foot of the Tokay, Gekko gecko (Reptilia: Gekkonidae) *J Zool* **176** 437-176.

[31] Tian Y, et al. 2006 Adhesion and Friction in Gecko Toe Attachment and Detachment *Proc Natl Acad Sci* **103** 19320-19325.

[32] Yao H, Gao H. 2007 Mechanical principles of robust and releasable adhesion of gecko *J Adhes Sci Technol* **21** 1185-1212.

[33] Schargott M, et al. 2006 Spring model of biological attachment pads *J Theor Biol* **243** 48-53.

[34] Autumn K. Properties, Principles, and Parameters of the Gecko Adhesive System. In: Smith AM, Callow JA, editors. Biological Adhesives: Springer Berlin Heidelberg; 2006. p. 225-256.

[35] Sameoto D, Menon C. 2010 Recent advances in the fabrication and adhesion testing of biomimetic dry adhesives *Smart Mater Struct* **19** 103001.

[36] Kroner E.K. 2011 Adhesion measurements on patterned elastomeric surfaces.

[37] Yurdumakan B, et al. 2005 Synthetic gecko foot-hairs from multiwalled carbon nanotubes *Chem Commun* 3799-3801.

[38] Zhao Y, et al. 2006 Interfacial energy and strength of multiwalled-carbon-nanotube-based dry adhesive *J Vac Sci Technol B* **24** 331-335.

[39] del Campo A, Artz E. 2007 Design Parameters and Current Fabrication Approaches for Developing Bioinspired Dry Adhesives *Macromol Biosci* **7** 118-127.

[40] Eun Y, et al. 2011 Integrated Carbon Nanotube Array as Dry Adhesive for High-Temperature Silicon Processing *Adv Mater* **23** 4285-4289.

[41] NITTO DENKO CORPORATION. 2012; Available at: www.nitto.com. Accessed 11/19, 2012.

[42] Dai L editor. Carbon Nanotechnology: Recent Developments in Chemistry, Physics, Materials Science and Device Applications. 1st ed. Amsterdam: Elsevier Science; 2006.

[43] Tong T, et al. 2004 Multiwalled Carbon Nanotube/Nanofiber Arrays as Conductive and Dry Adhesive Interface Materials *ASME Conf Proc* **2004** 7-12.

[44] Qu L, Dai L. 2007 Gecko-foot-mimetic aligned single-walled carbon nanotube dry adhesives with unique electrical and thermal properties *Adv Mater* **19** 3844.

[45] Sethi S, et al. 2008 Gecko-inspired carbon nanotube-based self-cleaning adhesives *Nano Letters* **8** 822.

[46] Qu L, et al. 2008 Carbon Nanotube Arrays with Strong Shear Binding-On and Easy Normal Lifting-Off *Science* **322** 238-242.

[47] Jeong HE, Suh KY. 2009 Nanohairs and nanotubes: efficient structural elements for gecko-inspired artificial dry adhesives *Nano Today* **4** 335.

[48] Wirth CT, et al. 2008 Surface properties of vertically aligned carbon nanotube arrays *Diam.Relat.Mater.* **17** 1518-1524.

[49] Maeno Y, Nakayama Y. 2009 Geckolike high shear strength by carbon nanotube fiber adhesives *Appl Phys Lett* **94** 012103.

[50] Ge L, et al. 2007 Carbon nanotube-based synthetic gecko tapes *Proc Natl Acad Sci* **104** 10792-10795.

[51] Ko H, et al. 2010 Flexible Carbon-Nanofiber Connectors with Anisotropic Adhesion Properties *Small* **6** 22-26.

[52] Hu S, et al. 2012 Strong Adhesion and Friction Coupling in Hierarchical Carbon Nanotube Arrays for Dry Adhesive Applications *ACS Appl Mater Interfaces* **4** 1972-1980.

[53] Maeno Y, Nakayama Y. 2012 Experimental Investigation of Adhesive Behavior in Carbon Nanotube Based Gecko Tape *J Adhesion* **88** 243-252.

[54] Zhou M, et al. 2012 Anisotropic interfacial friction of inclined multiwall carbon nanotube array surface *Carbon* **50** 5372-5379.

[55] Ghatak A, et al. 2004 Peeling from a biomimetically patterned thin elastic film *Proc R Soc Lond A Math Phys Sci* **460** 2725-2735.

[56] Glassmaker NJ, et al. 2005 Adhesion enhancement in a biomimetic fibrillar interface *Acta Biomaterialia* **1** 367-375.

[57] Chung JY, Chaudhury MK. 2005 Roles of discontinuities in bio-inspired adhesive pads *J R Soc Interface* **2** 55-61.

[58] Geim AK, et al. 2003 Microfabricated adhesive mimicking gecko foot-hair *Nat Mater* **2** 461-463.

[59] Nabesawa H, et al. 2008 Polymer surface morphology control by reactive ion etching for microfluidic devices *Sensor Actuat B-Chem* **132** 637-643.

[60] Sameoto D, et al. 2008 Micromask Generation for Polymer Morphology Control: Nanohair Fabrication for Synthetic Dry Adhesives *Adv Sci Technol* **54** 439-444.

[61] Menon, C, et al. 2008 Abigaille-I: Towards the development of a spider-inspired climbing robot for space use. Biomedical Robotics and Biomechatronics, 2008. BioRob 2008. 2nd IEEE RAS & EMBS International Conference

[62] Xia Y, Whitesides GM. 1998 Soft lithography *Annu Rev Mater Sci* **28** 153-184.

[63] Sitti M, Fearing RS. 2003 Synthetic gecko foot-hair micro/nano-structures as dry adhesives *J Adhes Sci Technol* **17** 1055.

[64] Peressadko A, Gorb SN. 2004 When Less is More: Experimental Evidence for Tenacity Enhancement by Division of Contact Area *J Adhes* **80** 247-261.

[65] Glassmaker NJ, et al. 2004 Design of biomimetic fibrillar interfaces: 1. Making contact *J R Soc Interface* **1** 23.

[66] Crosby AJ, et al. 2005 Controlling Polymer Adhesion with "Pancakes" *Langmuir* **21** 11738-11743.

[67] Thomas T, Crosby AJ. 2006 Controlling Adhesion with Surface Hole Patterns *The Journal of Adhesion* **82** 311-329.

[68] Aksak B, et al. 2007 Adhesion of Biologically Inspired Vertical and Angled Polymer Microfiber Arrays *Langmuir* **23** 3322-3332.

[69] Cheung E, Sitti M. 2008 Adhesion of Biologically Inspired Oil-Coated Polymer Micropillars *J Adhes Sci Technol* **22** 569-589.

[70] Cheung E, Sitti M. 2009 Adhesion of Biologically Inspired Polymer Microfibers on Soft Surfaces *Langmuir* **25** 6613-6616.

[71] Cheung E, Sitti M. 2011 Enhancing Adhesion of Biologically Inspired Polymer Microfibers with a Viscous Oil Coating *J Adhesion* **87** 547-557.

[72] Cho WK, Choi IS. 2008 Fabrication of Hairy Polymeric Films Inspired by Geckos: Wetting and High Adhesion Properties *Adv Funct Mater* **18** 1089-1096.

[73] Davies J, et al. 2008 A practical approach to the development of a synthetic gecko tape *Int J Adhes Adhes* **29** 380.

[74] del Campo A, et al. 2007 Contact shape controls adhesion of bioinspired fibrillar surfaces *Langmuir* **23** 10235.

[75] del Campo A, et al. 2007 Patterned Surfaces with Pillars with Controlled 3D Tip Geometry Mimicking Bioattachment Devices *Adv Mater* **19** 1973-1977.

129

[76] Greiner C, et al. 2009 Hierarchical Gecko-Like Adhesives *Adv Mater* **21** 479-482.

[77] Greiner C, et al. 2007 Adhesion of Bioinspired Micropatterned Surfaces: Effects of Pillar Radius, Aspect Ratio, and Preload *Langmuir* **23** 3495-3502.

[78] Jeong HE, et al. 2009 A nontransferring dry adhesive with hierarchical polymer nanohairs *Proc Natl Acad Sci* **106** 5639-5644.

[79] Kim S, Sitti M. 2006 Biologically inspired polymer microfibers with spatulate tips as repeatable fibrillar adhesives *Appl Phys Lett* **89** 261911.

[80] Kim T, et al. 2009 Shape-Tunable Polymer Nanofibrillar Structures by Oblique Electron Beam Irradiation *Langmuir* **25** 8879-8882.

[81] Kustandi TS, et al. 2007 Fabrication of a gecko-like hierarchical fibril array using a bonded porous alumina template *J Micromech Microengineering* **17** N75.

[82] Lamblet M, et al. 2007 Adhesion Enhancement through Micropatterning at Polydimethylsiloxane-Acrylic Adhesive Interfaces *Langmuir* **23** 6966-6974.

[83] Lee H, et al. 2007 A reversible wet/dry adhesive inspired by mussels and geckos *Nature* **448** 338-341.

[84] Pokroy B, et al. 2009 Fabrication of Bioinspired Actuated Nanostructures with Arbitrary Geometry and Stiffness *Adv Mater* **21** 463-469.

[85] Reddy S, et al. 2007 Bioinspired Surfaces with Switchable Adhesion *Adv Mater* **19** 3833-3837.

[86] Yoon H, et al. 2009 Adhesion hysteresis of Janus nanopillars fabricated by nanomolding and oblique metal deposition *Nano Today* **4** 385-392.

[87] Parness A, et al. 2009 A microfabricated wedge-shaped adhesive array displaying gecko-like dynamic adhesion, directionality and long lifetime *J R Soc Interface* **6** 1223.

[88] Glass P, et al. 2009 Enhanced Reversible Adhesion of Dopamine Methacrylamide-Coated Elastomer Microfibrillar Structures under Wet Conditions *Langmuir* **25** 6607-6612.

[89] Tamelier J, et al. 2012 Vertical Anisotropic Microfibers for a Gecko-Inspired Adhesive *Langmuir* **28** 8746-8752.

[90] Jin K, et al. 2012 Design and Fabrication of Gecko-Inspired Adhesives *Langmuir* **28** 5737-5742.

[91] Aksak, B, et al. 2008 Gecko inspired micro-fibrillar adhesives for wall climbing robots on micro/nanoscale rough surfaces. 2008 IEEE International Conference on Robotics and Automation.

[92] Murphy MP, et al. 2007 Adhesion and anisotropic friction enhancements of angled heterogeneous micro-fiber arrays with spherical and spatula tips *J Adhes Sci Technol* **21** 1281.

[93] Murphy M P et a. 2009 Gecko-inspired directional and controllable adhesion *Small* **5** 170.

[94] Kim S, et al. 2009 Reversible dry micro-fibrillar adhesives with thermally controllable adhesion *Soft Matter* **5** 3689-3693.

[95] Shen L, et al. 2008 Strongly enhanced static friction using a film-terminated fibrillar interface *Soft Matter* **4** 618-625.

[96] Vajpayee S, et al. 2009 Effect of Rate on Adhesion and Static Friction of a Film-Terminated Fibrillar Interface *Langmuir* **25** 2765-2771.

[97] Murphy MP, et al. 2009 Enhanced Adhesion by Gecko-Inspired Hierarchical Fibrillar Adhesives *ACS Appl Mater Interfaces* **1** 849-855.

[98] Li Y, et al. 2010 Enhanced Compliant Adhesive Design and Fabrication with Dual-Level Hierarchical Structure *J Bionic Eng* **7** 228-234.

[99] Lee H, Bhushan B. 2012 Fabrication and characterization of hierarchical nanostructured smart adhesion surfaces *J Colloid Interface Sci* **372** 231-238.

[100] Sameoto D, Menon C. 2009 Direct molding of dry adhesives with anisotropic peel strength *J Micromech Microeng* **19** 115026.

[101] Kwak MK, et al. 2011 Anisotropic Adhesion Properties of Triangular-Tip-Shaped Micropillars *Small* **7** 1-5.

[102] Murphy MP, et al. 2007 Adhesion and Anisotropic Friction Enhancements of Angled Heterogeneous Micro-Fiber Arrays with Spherical and Spatula Tips *J Adhes Sci Technol* **21** 1281-1296.

[103] Lee Jea. 2008 Directional adhesion of gecko-inspired angled microfiber arrays *Appl Phys Lett* **93** 191910.

[104] Jung G, et al. 2005 Vapor-Phase Self-Assembled Monolayer for Improved Mold Release in Nanoimprint Lithography *Langmuir* **21** 1158-1161.

[105] Keil, M, et al. 2004 Process development and characterization of antisticking layers on nickel-based stamps designed for nanoimprint lithography. ; November 2004; AVS.

[106] Kim B, et al. 2012 Controlling Mold Releasing Propensity: The Role of Surface Energy and a Multiple Chain Transfer Agent *ACS Appl Mater Interfaces* **4** 3465-3470.

[107] Maboudian R, Carraro C. 2004 Surface chemistry and tribology of MEMS *Annu Rev Phys Chem* **55** 35-54.

[108] Kim Sea. 2008 Fabrication of bio-inspired elastomer nanofiber arrays with spatulate tips using notching effect *IEEE Nano 2008* 780.

[109] Sameoto D, Menon C. 2010 Deep UV patterning of acrylic masters for molding biomimetic dry adhesives *J Micromech Microeng* **20** 115037.

[110] ST-1060 Technical Data Sheet. 2011; Available at: http://www.bjbenterprises.com/pdf/ST-1060.pdf. Accessed 11/14, 2012.

[111] Bartlett MD, et al. 2012 Looking Beyond Fibrillar Features to Scale Gecko-Like Adhesion *Adv Mater* .

[112] Sameoto D, Menon C. 2009 A low-cost, high-yield fabrication method for producing optimized biomimetic dry adhesives *J Micromech Microeng* **19** 115002.

[113] Jeong HE, et al. 2008 High aspect-ratio polymer nanostructures by tailored capillarity and adhesive force *Colloids Surf Physicochem Eng Aspects* **313–314** 359-364.

[114] TC-5045 Technical Data Sheet. 2011; Available at: http://www.bjbenterprises.com/pdf/TC-5045.pdf. Accessed 11/05, 2012.

[115] Hamaker H. 1937 The London—van der Waals attraction between spherical particles *physica* **4** 1058-1072.

[116] Hertz H. Miscellaneous papers. : Macmillan; 1896.

[117] A. D. Roberts. The extrusion of liquids between highly elastic solidsUniversity of Cambridge (United Kingdom); 1968.

[118] K. Kendall. The stiffness of surfaces in static and sliding contactUniversity of Cambridge (United Kingdom); 1970.

[119] Maugis D. 1985 Subcritical crack growth, surface energy, fracture toughness, stick-slip and embrittlement *J Mater Sci* **20** 3041-3073.

[120] Bradley R. 1932 LXXIX. The cohesive force between solid surfaces and the surface energy of solids *Philos Mag* **13** 853-862.

[121] Tabor D. 1977 Surface forces and surface interactions *J Colloid Interface Sci* **58** 2-13.

[122] Johnson K, Greenwood J. 1997 An adhesion map for the contact of elastic spheres *J Colloid Interface Sci* **192** 326-333.

[123] Spolenak R, et al. 2005 Effects of contact shape on the scaling of biological attachments *R Soc Lond Proc Ser A Math Phys Eng Sci* **461** 305-319.

[124] Derjaguin B, et al. 1975 Effect of contact deformations on the adhesion of particles *J Colloid Interface Sci* **53** 314-326.

[125] Zhao YP, et al. 2003 Mechanics of adhesion in MEMS - a review *J Adhes Sci Technol* **17** 305-319.

[126] Kendall K. 2002 The adhesion and surface energy of elastic solids *J Phys D* **4** 1186.

[127] Griffith A. 1920 The phenomena of flow and rupture in solids *Phil.Trans.Roy.Soc.London A* **221** 1921.

[128] Gorb SN, Varenberg M. 2007 Mushroom-shaped geometry of contact elements in biological adhesive systems *J Adhes Sci Technol* **21** 1175-1183.

[129] Carbone G, et al. 2011 Origin of the superior adhesive performance of mushroom-shaped microstructured surfaces *Soft Matter* **7** 5545-5552.

[130] Gorb S, et al. 2007 Biomimetic mushroom-shaped fibrillar adhesive microstructure *J R Soc Interface* **4** 271-275.

[131] Sameoto D, Ferguson B. 2012 Robust large-area synthetic dry adhesives *J Adhes Sci Technol* 1-17.

[132] Majidi, C, et al. 2004 Clumping and packing of hair arrays manufactured by nanocasting. Proc. ASME IMECECiteseer.

[133] Carbone G, Pierro E. 2012 Sticky Bio-inspired Micropillars: Finding the Best Shape *Small* **8** 1449-1454.

[134] Kim S, et al. 2012 Enhanced adhesion with pedestal-shaped elastomeric stamps for transfer printing *Appl Phys Lett* **100** 171909.

[135] Autumn K, et al. 2008 Gecko adhesion: evolutionary nanotechnology *Phil Trans Math Phys Eng Sci* **366** 1575-1590.

[136] Lee J, et al. 2008 Sliding-induced adhesion of stiff polymer microfibre arrays. I. Macroscale behaviour *J R Soc Interface* **5** 835-844.

[137] Varenberg M, et al. 2006 Advanced testing of adhesion and friction with a microtribometer *Rev Sci Instrum* **77** 066105-066105-3.

[138] Kroner E, et al. 2012 Note: An adhesion measurement setup for bioinspired fibrillar surfaces using flat probes *Rev Sci Instrum* **83** 6101.

[139] Long R, et al. 2008 Modeling the soft backing layer thickness effect on adhesion of elastic microfiber arrays *J Appl Phys* **104** 044301.

[140] Kroner E, et al. 2011 Adhesion of Flat and Structured PDMS Samples to Spherical and Flat Probes: A Comparative Study *J Adhesion* **87** 447-465.

[141] Sameoto D, et al. 2012 Nonangled anisotropic elastomeric dry adhesives with tailorable normal adhesion strength and high directionality *J Adhes Sci Technol* 1-13.

[142] Sitti M, et al. 2009 Dangling chain elastomers as repeatable fibrillar adhesives *ACS Appl Mater Interfaces* **1** 2277-2287.

[143] Kim Sea. 2009 Wet self-cleaning of biologically inspired elastomer mushroom shaped microfibrillar adhesives *Langmuir* **25** 7196.

[144] Northen M T et a. 2008 A gecko-inspired reversible adhesive *Adv Mater* **20** 3905.

[145] Ortiz C, Boyce MC. 2011 Mechanics of Indentation into Micro-and Nanoscale Forests of Tubes, Rods, or Pillars *J Eng Mater Tech* **133** 011014-011011.

[146] Kendall K. 2001 Thin-film peeling-the elastic term *J Phys D* **8** 1449.

[147] Meitl MA, et al. 2006 Transfer printing by kinetic control of adhesion to an elastomeric stamp *Nat Mater* **5** 33-38.

[148] Kim S, et al. 2010 Microstructured elastomeric surfaces with reversible adhesion and examples of their use in deterministic assembly by transfer printing *Proc Natl Acad Sci* **107** 17095-17100.

[149] Cheng H, et al. 2012 An analytical model for shear-enhanced adhesiveless transfer printing *Mech Res Commun* **43** 46-49.

[150] Lee KJ, et al. 2005 Large-Area, Selective Transfer of Microstructured Silicon: A Printing-Based Approach to High-Performance Thin-Film Transistors Supported on Flexible Substrates *Adv Mater* **17** 2332-2336.

[151] Wester BA, et al. 2011 Development and characterization of a packaged mechanically actuated microtweezer system *Sensor Actuat A-Phys* **167** 502-511.

134

[152] Beyeler F, et al. 2007 Monolithically fabricated microgripper with integrated force sensor for manipulating microobjects and biological cells aligned in an ultrasonic field *J MEMS* **16** 7-15.

[153] Bøggild P, et al. 2001 Fabrication and actuation of customized nanotweezers with a 25 nm gap *Nanotechnology* **12** 331.

[154] Chronis N, Lee LP. 2005 Electrothermally activated SU-8 microgripper for single cell manipulation in solution *J MEMS* **14** 857-863.

[155] Cohn, M B, et al. 1998 Microassembly technologies for MEMS. Micromachining and Microfabrication International Society for Optics and Photonics.

[156] Subramaniam V, et al. 2006 Methods and Characterization of Pick and Place Microassembly *ASME Conf Proc* **2006** 199-208.

[157] Dechev N, et al. 2004 Microassembly of 3-D microstructures using a compliant, passive microgripper *J MEMS* **13** 176-189.

[158] Jericho S, et al. 2004 Micro-electro-mechanical systems microtweezers for the manipulation of bacteria and small particles *Rev Sci Instrum* **75** 1280-1282.

[159] Keller, C G and Howe. 1997 Hexsil tweezers for teleoperated micro-assembly. Micro Electro Mechanical Systems, 1997. MEMS'97, Proceedings, IEEE., Tenth Annual International Workshop onIEEE.

[160] Acrylic Sheet Education, Specs & Inspiration | Plaskolite. 2012; Available at: http://www.plaskolite.com/. Accessed 01/29, 2013.

[161] Haiducu Mea. 2008 Deep UV patterning of commercial grade PMMA for low cost, large scale microfluidics *J.Micromech.Microeng.* **18** 115029.

[162] SU-8 2000 Processing Guidelines. 2012; Available at: http://microchem.com/pdf/SU-82000DataSheet2000_5thru2015Ver4.pdf. Accessed 12/16, 2012.

[163] MicroChem. SU-8 Developer Material Safety Data Sheet. 2001; Available at: http://www.cen.iitb.ac.in/cen/usage-policies/msds/su8.pdf. Accessed 01/29, 2013.

[164] Abusomwan U, Sitti M. 2012 Effect of retraction speed on adhesion of elastomer fibrillar structures *Appl Phys Lett* **101** 211907.

[165] Kroner E, et al. 2010 Adhesion Characteristics of PDMS Surfaces During Repeated Pull-Off Force Measurements *Adv Eng Mater* **12** 398-404.

[166] Kim S, et al. 2007 Effect of backing layer thickness on adhesion of single-level elastomer fiber arrays *Appl Phys Lett* **91** 161905.

[167] Díaz Téllez J, et al. 2010 Cleaning properties of dry adhesives *SCIENCE CHINA Technological Services* **53** 2942-2946.

[168] Spuskanyuk AV, et al. 2008 The effect of shape on the adhesion of fibrillar surfaces *Acta Biomaterialia* **4** 1669-1676.

[169] Bschaden, B, et al. 2013 Hyperelastic Simulation for Accurate Prediction of Gecko Inspired Dry Adhesive Deformed Shape and Stress Distribution Prior to Detachment. Adhesion Society Annual Meeting & Expo; March 3-6, 2013; .

[170] UNIVERSAL LASER SYSTEMS VLS3.5 Laser Engraver. 2011; Available at: http://www.ulsinc.com/products/vls350. Accessed 11/15, 2012.

[171] Paretkar D, et al. 2011 Bioinspired pressure actuated adhesive system *Mater Sci Eng , C* **31** 1152-1159.

8   APPENDICIES

8.1   Appendix A: Squeegee Report

Summary

Biomimetic dry adhesive materials show great promise in a wide variety of applications. There are currently no methods for mass production of these adhesives. This research aims to develop the framework for developing a large scale production method of these adhesives. Currently the adhesives are produced by casting polyurethane in silicone rubber molds by spreading the polyurethane over the mold with a spatula. This study focuses on optimizing an autonomous method of manufacturing the adhesives by investigating the parameters that have the greatest effect on casting reliable adhesives.

A custom built apparatus was used to investigate the effect of applied spatula pressure, spatula angle, polyurethane material and number of pulls over the mold on the fill percentage of the mold. Two molds were tested, one with small round fibers, and one with much larger square fibers.

It was found that applied pressure and number of pulls had the greatest effect on the fill percentage with higher pressure and higher number of pulls increasing the fill percentage. Spatula angle and polyurethane did not have a significant effect on fill percentage. Video analysis showed that the small fiber molds collapse under pressure and the vacuum created when pressure is released pulls the polyurethane into the micro-structures. Higher pressure did not have this effect on the larger fibers. The videos also show that a trail of polyurethane behind the spatula is required for any filling to occur.

<u>Introduction and Background</u>

Polyurethane gecko inspired dry adhesives have been under investigation for the past decade. They mimic the gecko's foot by using van der Waals forces and specific geometries of microscale fibers to produce effective adhesion[1] and can potentially be mass produced through the use of silicone rubber molds[2]. These molds have the advantage of not requiring a clean room or vacuum environment for the casting. The molds can be fabricated in large sheets and polyurethane can be cast in bulk quantities. Currently there is no standardized method for casting the adhesives although research has been done in the scaling up of doctor blade and screen printing techniques for applying thin polymer films[3-8]. The doctor blade technique is primarily used for creating a film with a controllable thickness[5]. The thickness of the backing layer for these adhesives is a future concern when the final manufacturing methods are being developed. Once an effective method of filling the mold and producing reliable structures has been found, the research can investigate methods for producing an effective backing layer for the structures. The doctor blade technique is an excellent way to deposit a polymer layer with controllable thickness during a roll to roll process. This research will focus primarily on producing effective structures rather than an effective backing layer. The screen printing methods do not leave a microscale structure from the mesh pattern[3] and can potentially be used to create specific patterns of dry adhesive on the mold. It is known that, during a screen printing process, the squeegee dragging speed and pressure have a significant effect on the properties of the deposited layer[9,12], with higher speed and higher pressure giving better results. The most effective speeds were approximately 50 mm/s.

The current method for filling these molds is to manually apply the polyurethane and spread it over and into the mold with the squeegee. This can cause inconsistencies with

the fibers which affect their adhesion, and is time consuming. It is known that manual squeegee methods for screen printing can produce inconsistent results due to variations in the speed and pressure of the squeegee[11]. This research involves developing a method that can one day be scaled up to produce large quantities of reliable adhesive. The focus is on the manufacturing parameters that most effectively spread a thin film of the liquid polyurethane over the mold and fill the microstructures reliably. The hypothesis is than an effective pressure is required to compress the mold and collapse the fiber structures. This will remove any air from the mold cavities and upon releasing the pressure the structures will regain their shape and the vacuum that is created will pull the polyurethane into the mold. The goal is to find a method that produces the most reliable structure for a particular adhesive. Ideally the method can be used on a large scale for mass production of the adhesives. This may involve roll to roll manufacturing, screen printing or another technique.

Experimental Apparatus

Description

A device was needed to carry out the tests in a controlled manner. In the laboratory,
existing linear stages were modified to carry out the experiments. The device was based
on the preliminary idea as seen in Figure 1. The final design can be seen in Figure 2 and
Figure 3.
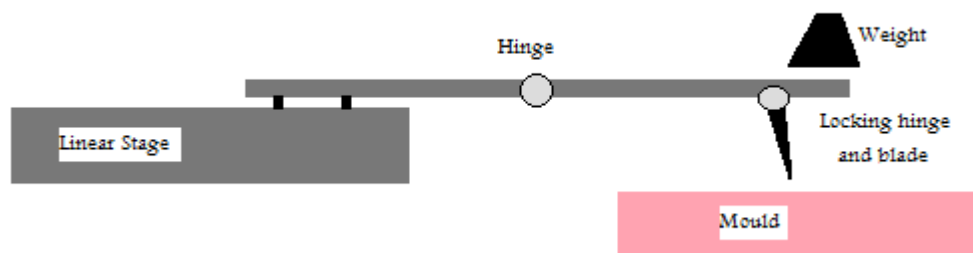
Figure 1: Original experimental apparatus design
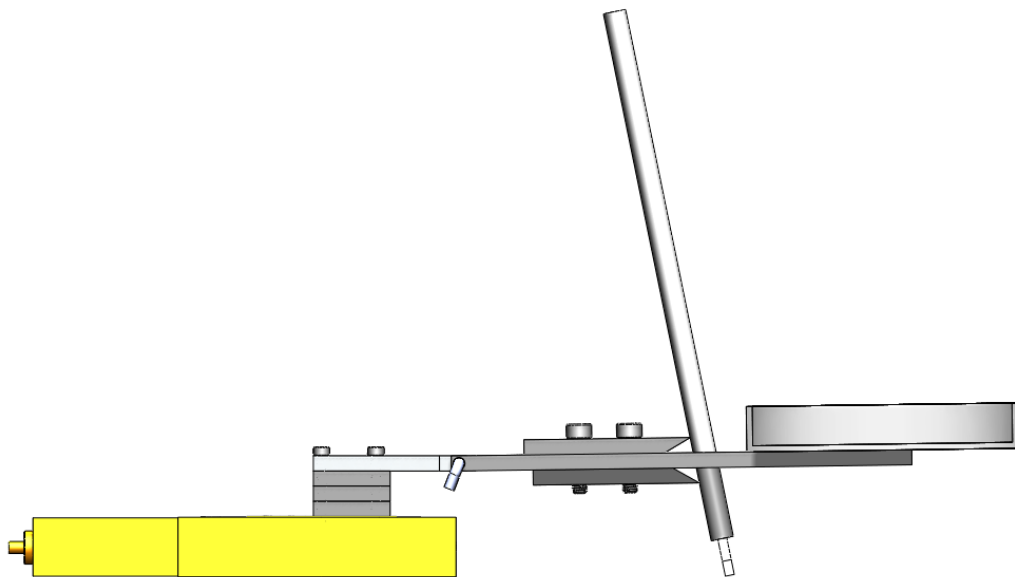
Figure 2: Final apparatus design. Side view
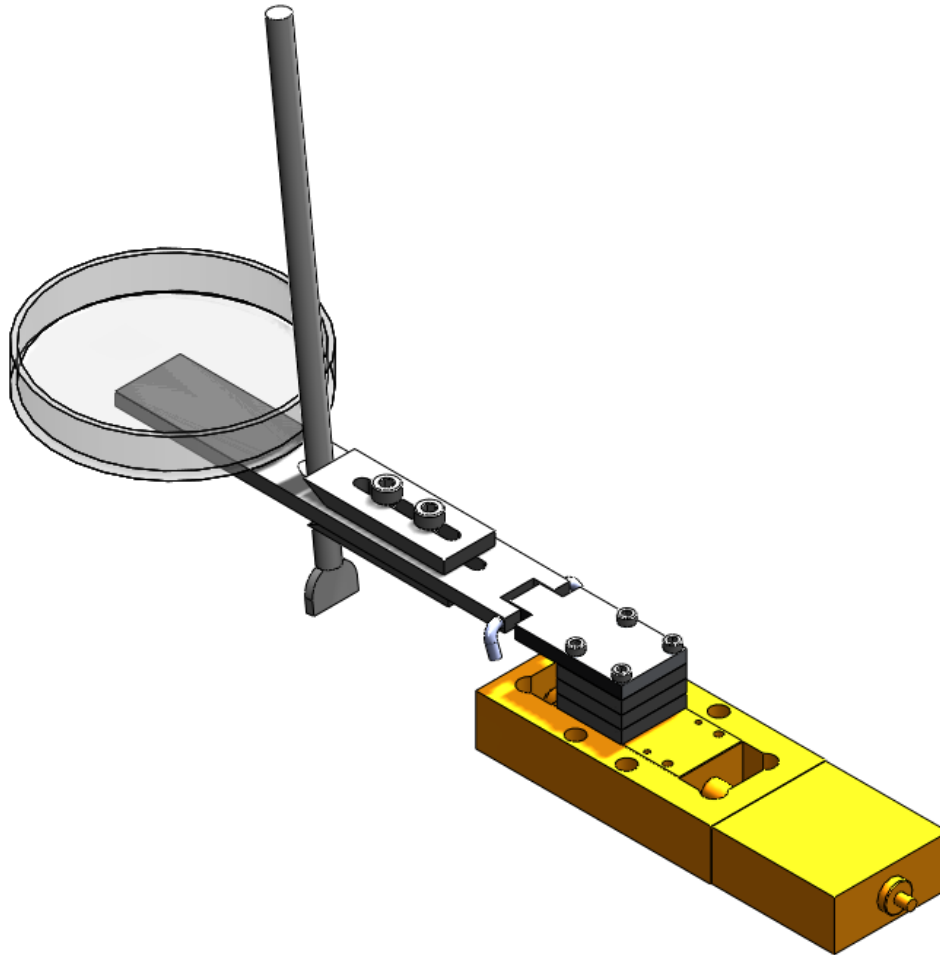
Figure 3: Final apparatus design. Isometric view

Force Application

The device needed to have an adjustable level of pressure being delivered to the mold from the spatula. This was accomplished by using a large Petri dish as a receptacle for holding small weights. To maintain a consistent pressure, a loose hinge was used to connect the linear stage to the weighted end of the apparatus. This ensures a smooth and consistent application of force during the tests.

Spatula Gripper

The spatula is held in place at 3 points as seen in Figure 4.
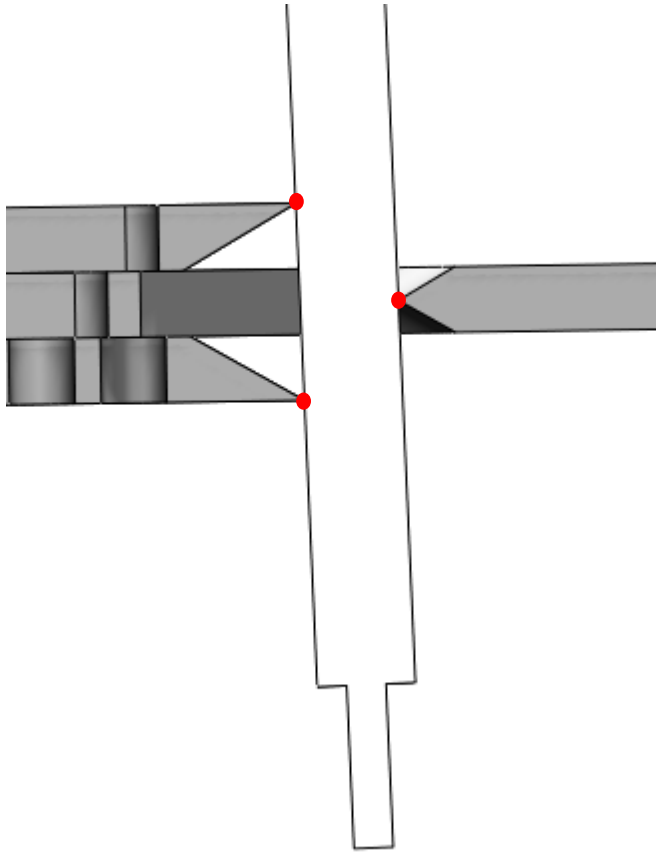
Figure 4: Cross sectional view of spatula gripping mechanism. The three holding points are highlighted.

There are two sliding blocks on the upper and lower side of the central plate. This allows the angle of the spatula to be adjusted within the range of 30° to 150°. This study investigated the effect of the spatula angle at 45° and 90°. The gripper has poor lateral stability and careful vertical alignment was required to ensure the contact point is not angled; an uneven contact edge will apply extra pressure to one edge of the spatula. Different styles of spatula can be used assuming they have similar cylindrical handles or the handles can be modified for this system; however, only one type of spatula was used in this study.

Other Features

Three blocks were designed to boost the height of the connection to the linear stage. These prevent the apparatus from contacting the edge of the linear stage as the hinge moves. These also allow the height to be adjustable for different scenarios in the future. The linear stage has built in programming to control the speed and direction of movement. Custom LABview software was designed to control the linear stage, and, as an alternative, it is possible to control the stage manually through the motion controller box.

Experimental Methods

The main purpose of this experiment is to find an optimized method of manufacturing quality adhesives. To accomplish this, a number of different parameters were investigated. All experiments followed a similar process as shown in Figure 5.
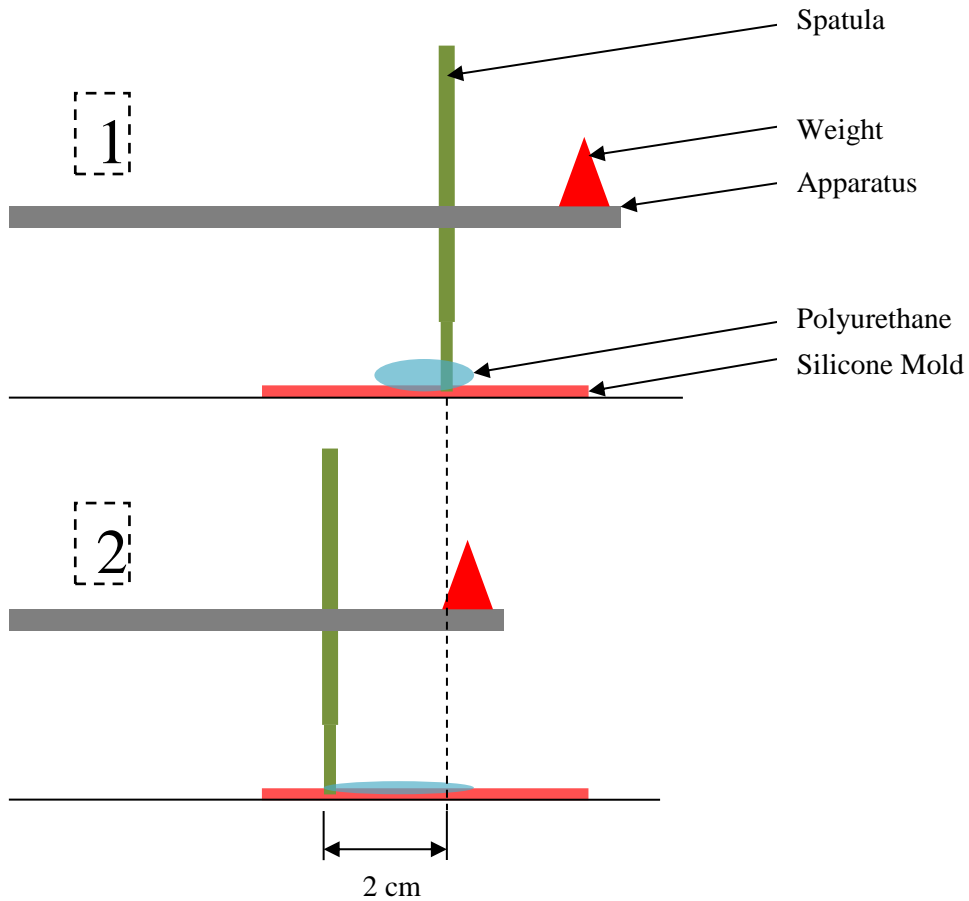
Figure 5: Schematic of testing method. Step 1, add mass to the end of the apparatus, adjust the spatula to desired angle, and apply polyurethane over the mold. Step 2, drag spatula across polyurethane to fill the mold.

First, the apparatus was put into position with the desired weight in the Petri dish and the spatula set to the desired angle. The apparatus was positioned such that the dragging motion would not have it contact the edge of the linear stage. The spatula tip was placed approximately 1 cm from the far edge of the structured mold to ensure a full range of movement from the linear stage. Second, a small volume of prepolymer was poured over the mold so that the spatula tip was just in contact with the far edge of the prepolymer. Third, a command was sent to the linear stage to pull the spatula over the polyurethane, driving it into the mold at the desired speed. For each trial the dragging distance was

8

approximately 2 cm. After each movement, the spatula was either separated from the mold and moved to a new position for the next trial, or the direction was simply reversed for the multi-pull trials (i.e. the spatula is not disturbed, and a command is sent to the linear stage to move 2 cm in the opposite direction).

Each parameter was tested four times on one section of the mold (i.e. four pulls were done side by side).

The Adhesive

The primary tests involved two different large area silicone rubber molds as seen in Figure .
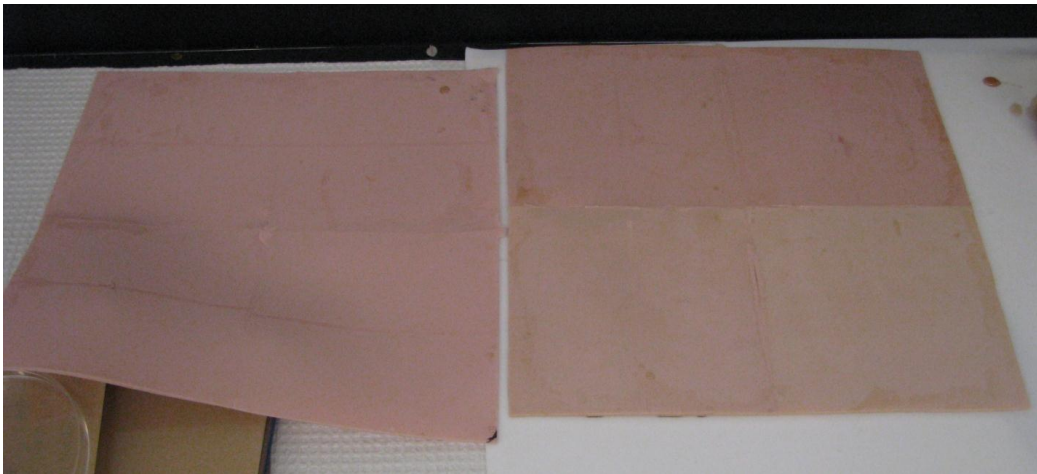
Figure 6: Large area silicone rubber molds used in this study

The first mold consists of large fibers with square caps and the second mold has smaller fibers with circular caps. A scanning electron microscope image of the adhesive produced by each mold is seen in Figure 6 and the dimensions are shown in Table 1.

Table 1: Fiber dimensions produced by each mold

	"A"	Square
Diameter (μm)	12	120
Height (μm)	15	100
Spacing (μm, center to center)	20	150
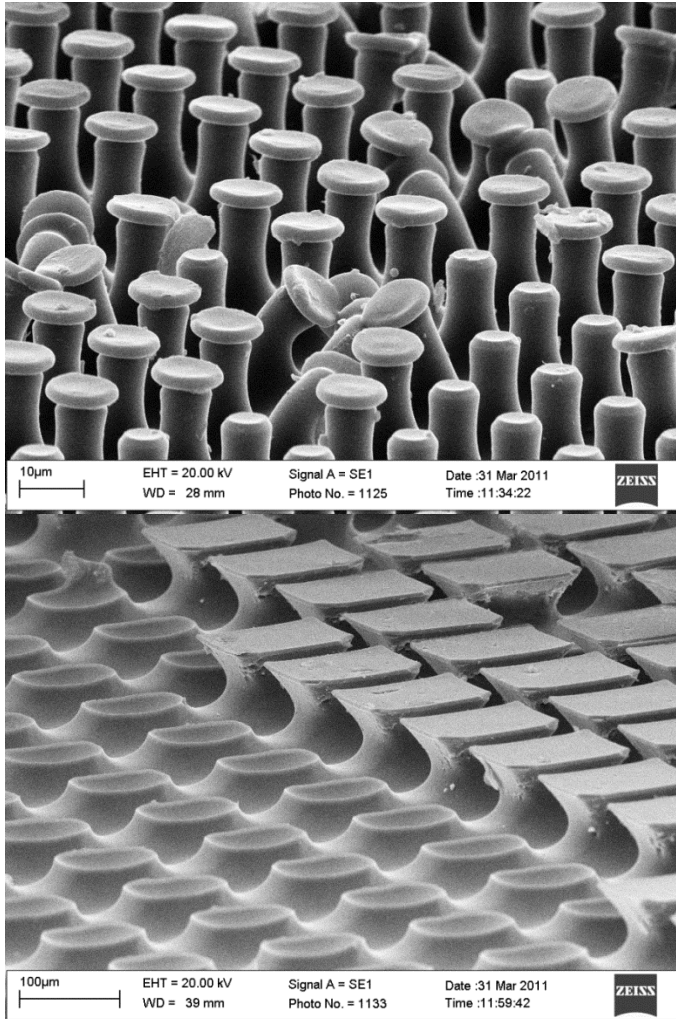
Figure 7: SEM image of "A" adhesive (top) and square adhesive (bottom). There are some missing fibers on the right hand side of the image and some dust contaminants. The image of the square fibers is taken at the edge of the spatula scraping test, so the adhesive is only partially filled.

Evaluation Techniques

Due to time constraints, some parameters were not fully tested. However, the parameters that we felt were most important were investigated in more detail. All parameters were evaluated based on the percentage of the spatula contact area that contained fully filled fibers. This required two methods. For the larger square fibers, the cured adhesive was placed in a beam of light so that only the fully filled fibers would reflect the light as seen in Figure 8. A picture was taken with a DSLR camera on super macro mode and the image was analyzed using custom National Instruments Vision Builder software. The software detects the areas of the image that are a different shade of colour due to the reflected light. The dimensions of the detection area were based on the width of the spatula and length it was dragged across the mold. The software displays the percentage of the area that is highlighted which gives a good approximation for the fill percentage. The data for each parameter test was averaged over the four test locations.
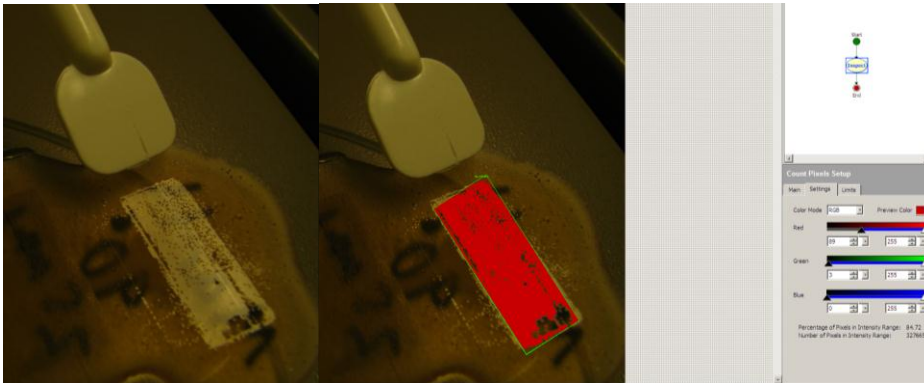
Figure 8: Light reflection highlights the fully filled fibers (left). National Instruments Vision Builder software is used to detect the percentage of filled fibers (right). The software outputs the percentage of the area within the green box that is highlighted red.
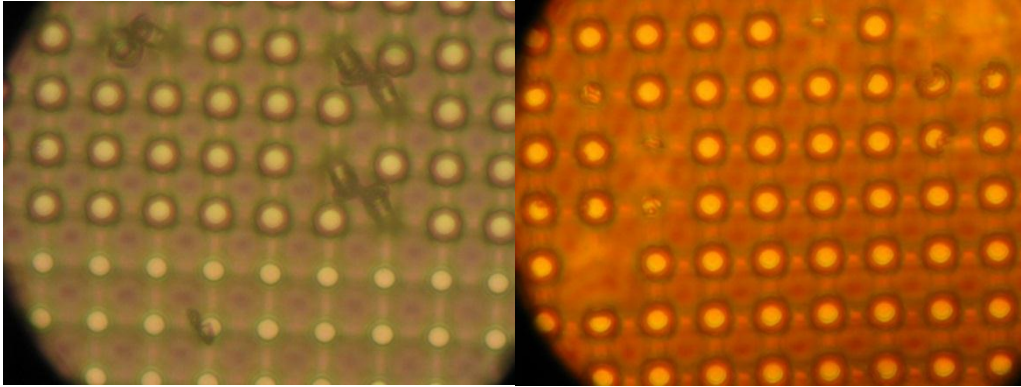
Figure 9: Example of images used to calculate the fill percentage of the small "A" fibers. Collapsed, missing, or damaged fibers reduce the total count.

The smaller, round "A" fibers are too small for the normal camera settings to show any discernible contrast to identify the fibers. The same camera was used in conjunction with an inverted microscope to take images where the individual fibers could easily be seen. Two pictures were taken for each strip of the structured adhesive, which corresponds to eight images for each set of parameters. An example of the images can be seen in Figure 9. Rather than using the imaging software to detect missing caps, the number of missing, collapsed, or deformed fibers in the array were manually counted. The average fill percentage over the eight images was used for each parameter. The width of the strip in relation to the width of the spatula was estimated manually for each strip and used to adjust the calculated fill in percentage.

Results and Discussion

The data for the "A" fibers is summarized in Figure 10 and Figure 11. The data for the square fibers is summarized in Figure 12 and Figure 13.
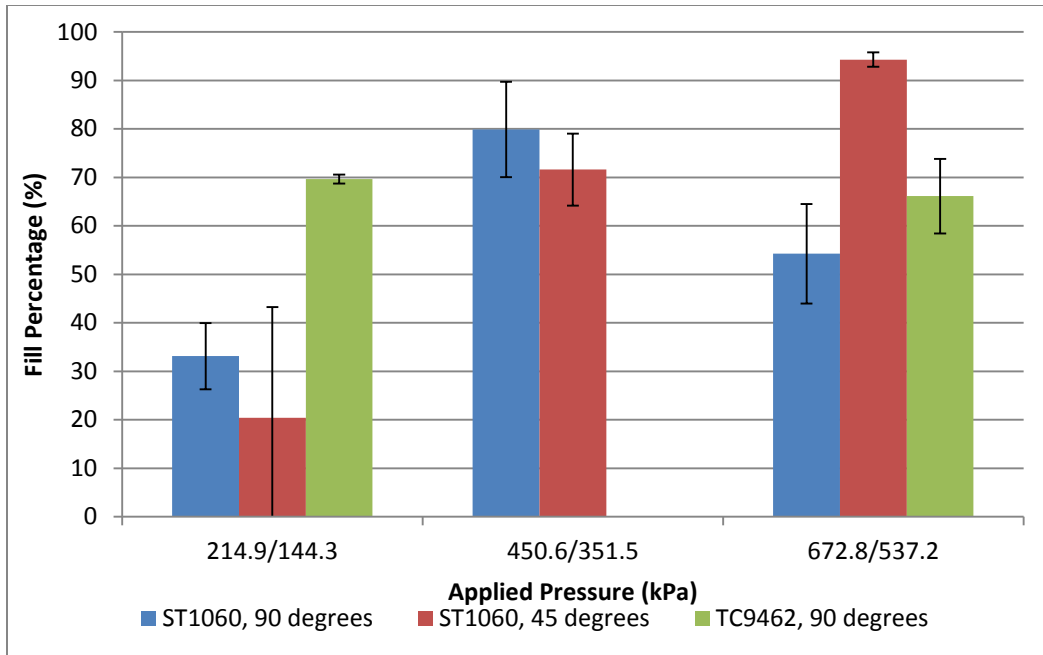
Figure 10: Fill percentage data for "A" fibers. All tests are done with one pull of the spatula. The applied pressure is depicted as x/y where x is the pressure for the 90° trials, and y is the pressure for the 45° trials
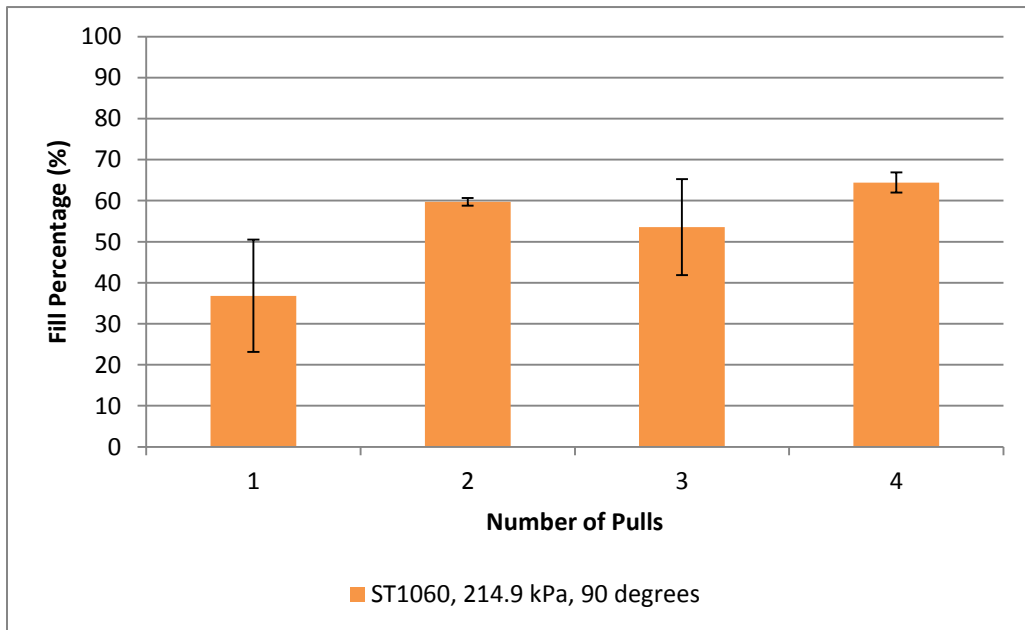
Figure 11: Fill percentage data for the "A" fibers based on number of pulls
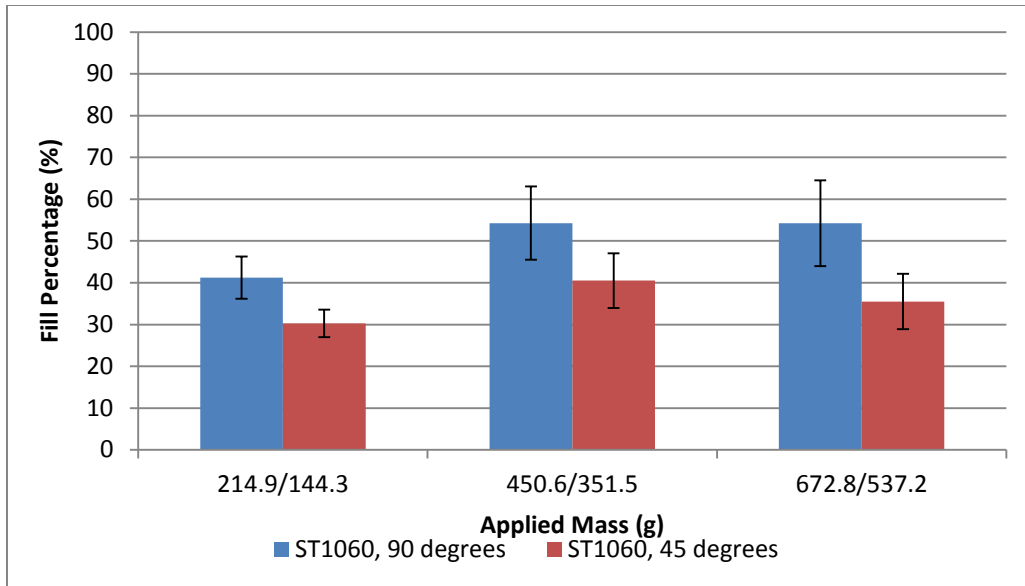
Figure 12: Fill percentage data for the large square fibers based on applied pressure and spatula angle
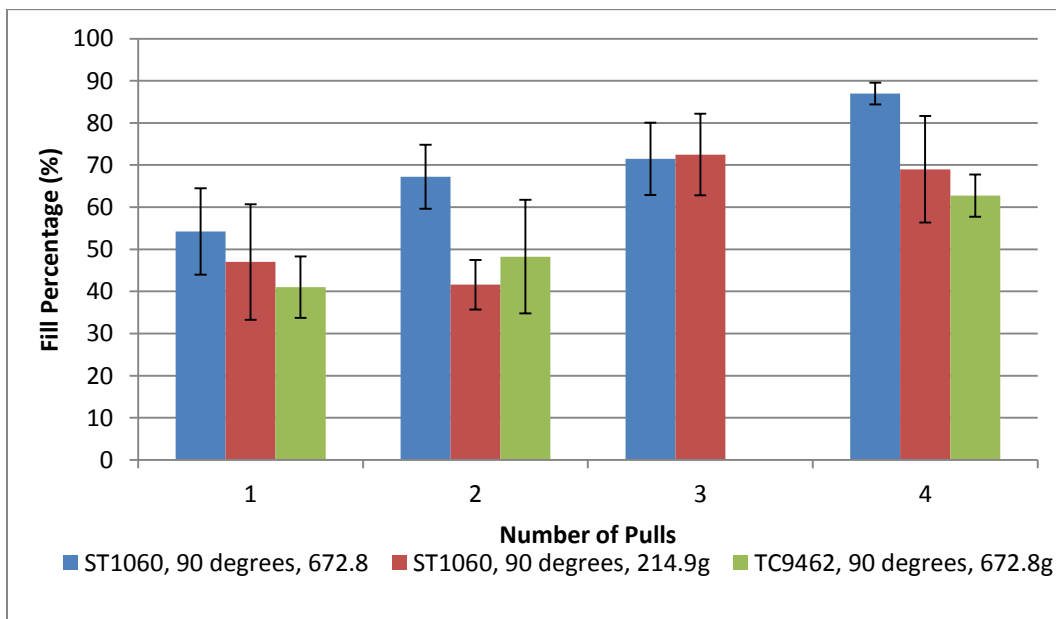
Figure 13: Fill percentage of the large square fibers based on the number of pulls, applied pressure and polyurethane material. A trial for three pulls was not done with TC9462.

The applied pressure was found by first calculating the force exerted on the mold when a

50 g or 100 g mass was placed in the Petri dish on the apparatus. The lowest measure of

pressure was done with no mass in the Petri dish, effectively using the self-weight of the

apparatus. To measure the force, the apparatus was

placed next to a mass balance such that the spatula

was resting on the balance. The mass applied to the

scale was found for each mass placed in the Petri

dish. The moment arm length changes for different

spatula angles, which causes the applied force for the

trials at a spatula angle of 45° to be less than the

trials at 90°. A simple way to correct this in the

future is to adjust the mass in the Petri dish each time

the spatula angle is changed so the applied pressure

for the different spatula angle trials is equal. The

effective contact length
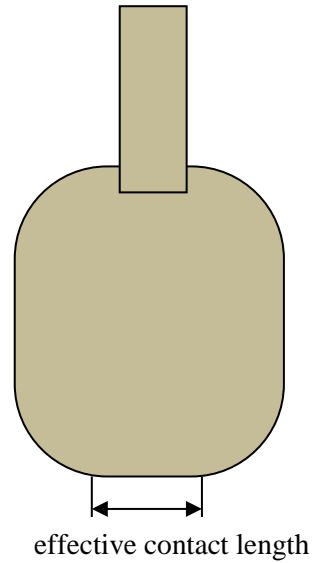
**Figure 14: Effective contact area
is based on the portion of the**

contact area was found by measuring the width of the spatula tip under an inverted

microscope and measuring the length of the spatula tip according to Figure 14. The

spatula width and length was estimated at 0.4 mm and 9.3 mm respectively which gives a

contact area of 3.72 mm^2. The low, medium and high pressures for each angle are

summarized in Table 2.

Table 2: Applied pressures based on spatula angle

Spatula Angle	Low Pressure (kPa)	Medium Pressure (kPa)	High Pressure (kPa)
45	144.3	351.5	537.2
90	214.9	450.6	672.8

Effect of Spatula Pressure

The goal of this research is to characterize the pressure to find an approximate relationship between applied pressure and fill in percentage. As seen in Figure 10 and Figure 12, applying a higher pressure generally increases the fill percentage of the fibers. More testing is needed to investigate and possibly correct the exceptions to this trend. In the trial with ST1060 at a 90° spatula angle, the fill percentage is 79.9 ± 9.8% for the 450.6 kPa trial compared to 54.3 ± 10.3 % for the 672.8 kPa trial. This follows an opposite trend to what is expected. This may be due to experimental variability, different environmental conditions the day of the test, or variability in how the fill in percentage is evaluated. We expect that with repeated trials and more precise experimental and evaluative techniques these outliers would disappear. The TC9462 trial seen in Figure 10 is affected by the applied pressure very little, staying nearly constant from the lowest to highest pressures. This is likely due to the previous explanations; however, the applied pressure may have a lesser effect for this polyurethane. One possible explanation is that TC9462 is able to flow into the mold easily and doesn't require a large spatula pressure. This may be due to TC9462 having a higher wettability with respect to the silicone mold. Another possibility is that we have reached a plateau in the nonlinear relationship of applied pressure to fill percentage. Increasing the pressure further beyond what was tested may not increase the fill percentage and other techniques may be needed to increase it further such as multiple pulls. For the square fibers in Figure 12, the correlation between increased pressure and higher fill percentages is much less when compared to the round fibers of Figure 10Figure . This may be due to the inability of the larger square fibers to fully collapse and form a vacuum to pull polyurethane into the structures in a manner similar to the round fibers.

Effect of Spatula Angle

The angle of the spatula did not have a significant effect on the fill percentage when changing from 45° to 90°. The apparent differences in the data are merely due to the different pressure applied when the spatula angle was adjusted. The data presented in Figure 15 ignores the spatula angle and shows the trend for increasing pressure and, with the exception of the last data point, behaves as expected. The contact area between the spatula and mold changes very little when changing the angle from 90° to 45°. The spatula will develop more of a wedge shape than flat plane contact, but this does not seem to affect the data.
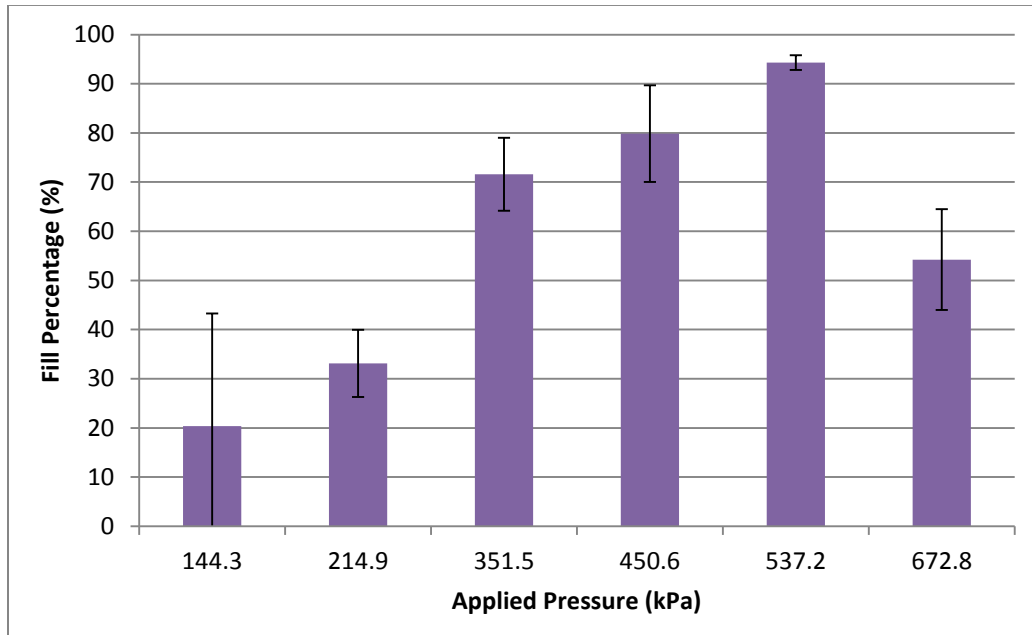

Figure 15: ST1060, "A" fibers. Ignoring different spatula angles and aligning the data in order of pressure, the expected trend can be seen with the exception of the last point

Exception: 45° Pull and Push Test

One test involved pulling the spatula towards the acute angle of the spatula followed by pushing away from the acute angle as visualized in Figure 16. This trial was done with the "A" fibers at 537.2 kPa and the spatula at 45°. This was the only multi-pull trial done with the spatula at 45°. This trial produced an excellent fill in percentage of $93.5 \pm 6.5\%$. The higher fill percentage is likely caused by the mechanism of the second pushing motion. Since the tendency of the wedge shape is to press into the mold, the applied pressure is likely higher than what was measured statically. This may have produced better results by compressing the mold more effectively, which helps to remove trapped air and produce a more effective suction force into the microscale fibers.
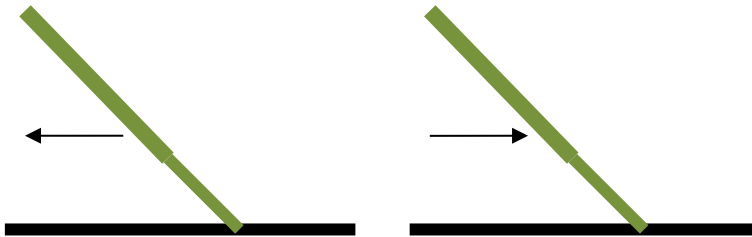
Figure 16: ST1060, 537.2 kPa, first pull (left) is towards acute angle of spatula. Second pull (right) is away from acute angle of spatula.

Effect of Multiple Pulls

Nearly all trials showed an increasing fill percentage as the number of pulls increased within experimental error. This is an expected trend as each additional pull will help to fill in more of the unfilled fibers. There is a small exception for the square fibers at 214.9 kPa. The second and fourth pull does not increase the fill percentage. Each of these pulls is in the reverse direction to the original pull which suggests that the square fibers are affected by the directionality of the pulling mechanism. This may be due to the trapped air bubbles being shifted back into the fibers when the spatula moves in the opposite

18

direction rather than being removed. If the first pull moves a bubble to the edge of the fiber, the second pull may only move the bubble back to the center. If all pulls were in the same direction the bubble would likely be pulled in one direction only till it escapes the microstructure. As long as the pull direction is constant the fill percentage should follow an increasing trend.

Miscellaneous Tests

5 Minute Epoxy

A test was done using Lepage Speed Set Epoxy. This epoxy has similar properties to the polyurethanes with the important difference being a much higher viscosity, approximately 27500 cps [10]. The test was done with a spatula angle of 90°, 672.8 kPa of pressure, and a mold with similar shape and dimensioned fibers to "A". The result was a fill percentage of $74.2 \pm 7.2\%$. This is very similar to the results using ST1060 and TC9462 which suggests than an increase of viscosity to these levels does not affect the fill percentage.

Dragging Speed

One test was done with the square fibers at a 90° spatula angle, 81.5 kPa, and 1 mm/s rather than 2.5 mm/s. The result was a fill in percentage of 37.5 ± 4.0 %. This is very similar to the results with the same conditions at 2.5 mm/s which suggests a speed change of this magnitude does not affect the fill percentage. The majority of manual scraping before this was done at much higher speeds (20+ mm/s) without any issues.

Video Analysis

Using a transparent Sylgard mold and the inverted microscope, the microscale behavior of the mechanical processes during filling the mold were analyzed. It was seen that the

microstructures in the "A" mold are completely compressed and collapsed when the spatula applies pressure. When the pressure is released the structures are reformed, which creates a vacuum that draws in polyurethane, confirming our hypothesis. When observing the larger square fibers, it was evident that the applied pressure does not collapse the fibers completely. Trapped air is simply forced into the structures when pressure is applied rather than being forced out. At higher pressures slightly more air is forced out but trapped air remains in the structures. This confirms the trend seen in Figure 12 where the fill percentage is not strongly affected by the applied pressure. This trend suggests there is a maximum fiber size for which a compressive squeegee will be effective.

Regardless of fiber size, the videos revealed that a trail of polyurethane following directly behind the mold is critical for ensuring complete filling. A lack of this reserve material will result in the fibers not filling.

<u>Scanning Electron Microscope Analysis</u>

Samples of the adhesives were analyzed under the SEM as seen in Figure 17. It can be clearly seen that many of the "A" fibers are incompletely filled with their caps missing. There are also areas where the fibers have collapsed or have adhered to the adjacent fiber. Since there are no locations where the fiber stalk is completely missing this suggests that the spatula pressure is only required to fill in the caps and the stalks can fill through the natural flow of the polyurethane. The larger square fibers seem to fill in very sporadically and a roughness can be seen at the corners of each fiber just below the cap. This may be due to the polyurethane being only partially cured, fiber damage during demolding or damage on the mold. The high pressures used in this study may have damaged the mold itself during the testing. Figure 18 shows a typical fiber failure where a bubble has been trapped in the center of the fiber. During demolding the cap folded on top of itself. A

20

bubble can also be seen in the fiber directly behind the failed cap. This suggests that the

bubbles within the fibers can easily cause the fiber to fail while bubbles deeper in the

adhesive may affect the adhesion, but will not immediately fail a fiber.
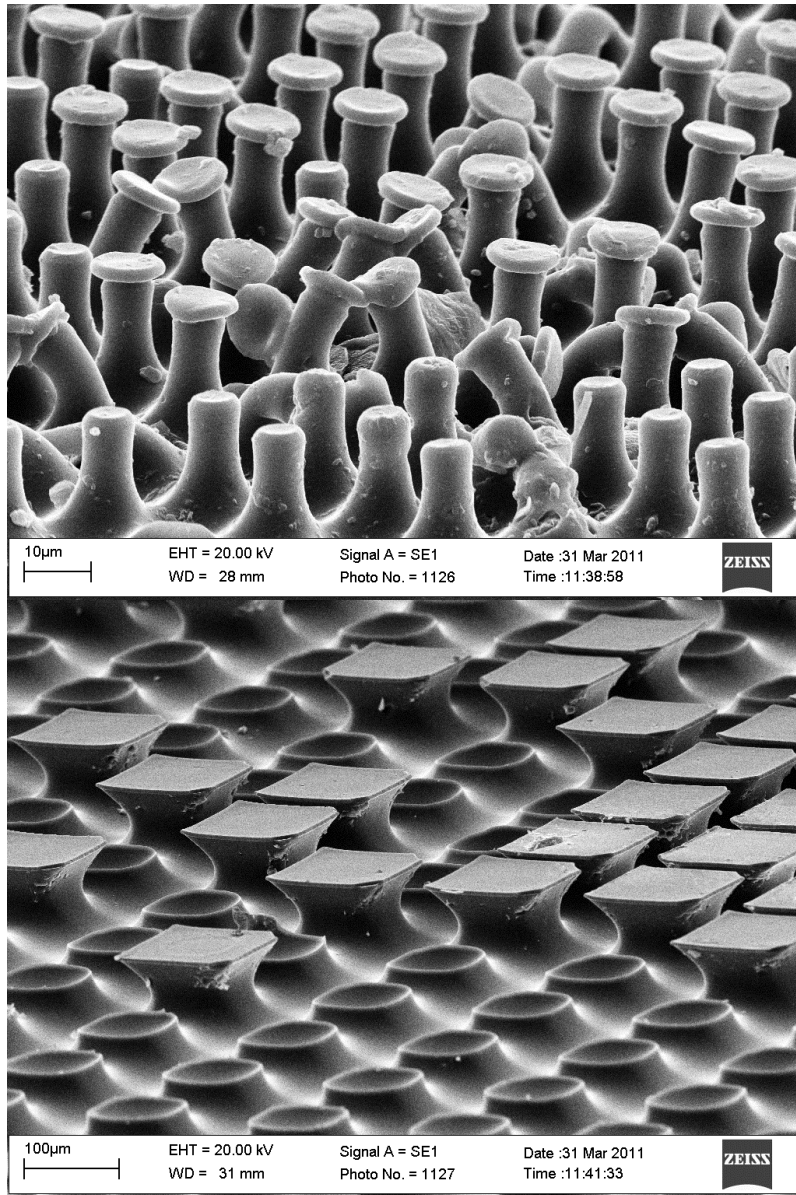

Figure 17: SEM images of the adhesives manufactured in this study. Manufacturing parameters: Adhesive "A", 90° spatula angle, 450.6 kPa, ST1060 (top) and the larger square adhesive, 45° spatula angle, 537.2 kPa, ST1060 (bottom)
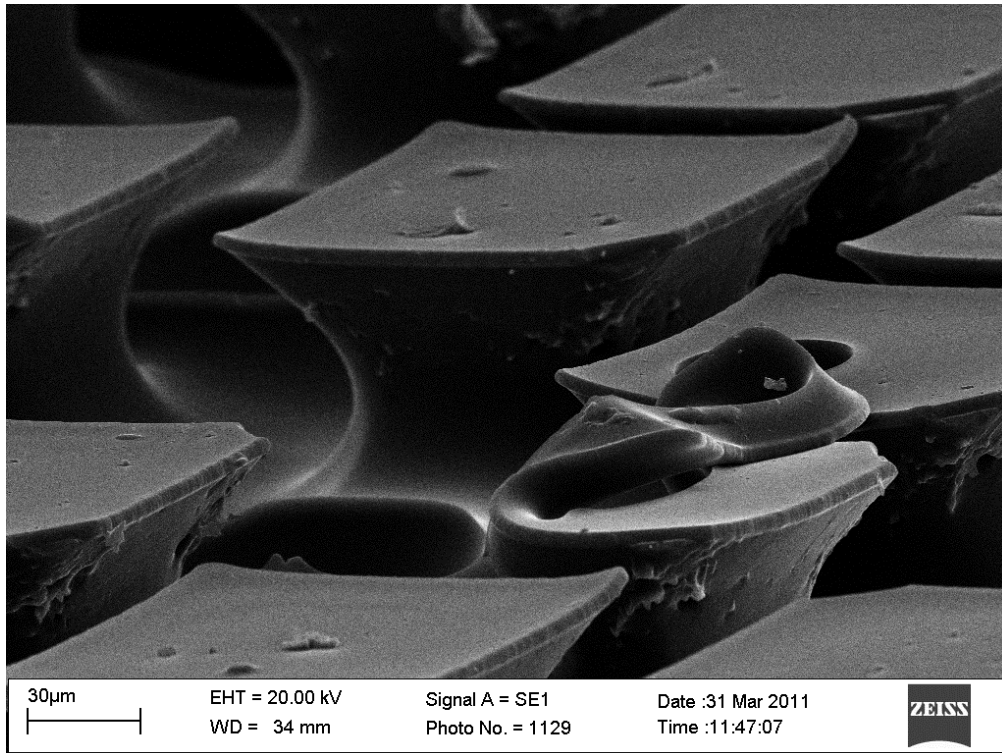
Figure 18: SEM close up image of the larger square fibers. A bubble has caused the collapse of this fiber. A bubble can also be seen in the fiber on the right side of the image.

Sources of Error

The data shows a high variability which may be caused by the following issues:

Limited Number of Trials -Due to time constraints, very few tests were done and some pieces of data were missing. Each set of parameters was tested only one time, with four strips of adhesive formed that one time. Error and outliers could be reduced by increasing the number of trials.

Inaccurate Evaluation Techniques- The methods used for evaluating the fill percentage have a large degree of error. For the square fibers, the exact contact area of the spatula is difficult to determine, and the colour recognition software has a range of colour magnitude that would be appropriate. A more accurate measure of the exact contact area by redesigning the spatula and a more effective way of reflecting light would reduce error.

An alternative method for finding fill percentage may also be desired. For the "A" fibers, each image is a very small area of the entire strip. This causes problems if the viewing area is not an accurate representation of the entire strip. The error could be reduced by increasing the number of sample locations on each strip.

Spatula Roughness- After the spatula is manufactured through injection molding, it is removed from its support frame at each end. The break will often leave a small amount of residue at the tip which is visible as a jagged edge. This causes areas of local high and low pressure which, for some trials, corresponded to visible streak marks on the adhesive strips. The flat edge of the spatula also may not be planar at the microscale, further adding to the uneven pressure distribution. This error can be greatly reduced by planarizing the spatula before testing.

Apparatus Design- The primary source of error in the apparatus design is the poor stability of three point holding mechanism of the spatula in the lateral direction. It allows the spatula to drift slightly which can cause uneven pressure along its length. If the spatula is not perpendicular to the mold, the applied pressure can be much higher at one edge. This issue will often correct itself since the force imbalance will likely push the spatula back to a more perpendicular position. This issue can be fixed by introducing a lateral stabilization clamp.

Future Work

Apparatus re-design

The linear stage used in this study is not designed for this type of testing. It has a very limited range (~20 mm) and limited speed (maximum 2.5 mm/s). Manufacturing of these adhesives on a large scale will require a much longer range and higher speed. Future

testing is unlikely to use such a linear stage; a simple manual pull over a roller will be more realistic. The speed can be controlled by hanging weights or by estimating the speed of manual dragging. Based on the results of this study the speed is not an important factor in fill percentage which means the variability in speed for a manual dragging system will not have a significant effect on the result.

Spatula re-design

The spatula needs to be designed in a way such that a trail of polyurethane will remain as dragging occurs. One possible way to do this is to use a combined spatula and doctor blade as seen in Figure 19Figure. The spatula will provide the pressure to the adhesive which compresses the mold and initially fills the fibers while the doctor blade distributes an even coating behind the newly filled fibers. This method will ensure there is always a stream of adhesive following the spatula. The apparatus will need to be designed in a way such that the doctor blade mechanism has a reservoir of polyurethane.
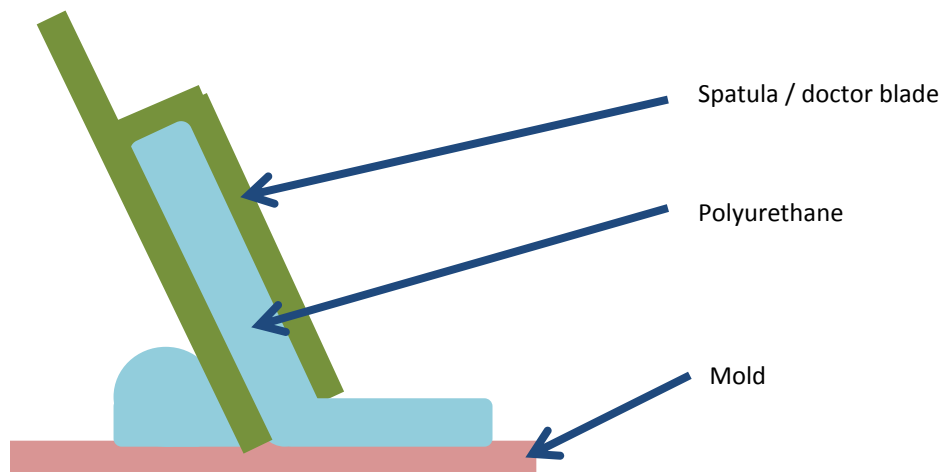

Figure 19: Spatula redesign 1. A combination squeegee and doctor blade.

An alternative to the combination spatula and doctor blade is to simply carve a hole in the current spatula similar to Figure 20. The goal is to allow the deposited layer of polyurethane to flow through the newly created hole. This will require the bottom lip of the spatula to be thin enough to allow the flow of polyurethane overtop of it, while being rigid enough to supply the pressure needed to compress the mold.

An additional challenge with redesigning the spatula is the redesign of the spatula holding mechanism. The mechanism needs to distribute the force evenly along the length of the contact edge. This may include a spring mechanism or strict tolerances for stability. Alternative spatula materials may also be useful in creating a more even pressure distribution. A softer squeegee will deform under higher pressure which redistributes the force along its length. However, if the squeegee is made from polyurethane it will bond to the polyurethane that is spread over the mold. This

Figure 20: Spatula redesign 2. A thin edge in contact that allows polyurethane to flow through.

will require the squeegee to be replaced after each use which is not feasible. An alternative material or coating over the polyurethane squeegee may be required.

Future Experiments

Further testing is needed to fully optimize the manufacturing process. Once a better testing method and testing apparatus is developed, the effect of different testing parameters can be further characterized. The effect of some parameters was not explored in enough depth. Polyurethane of very high or very low viscosity will be the next priority in addition to the parameters deemed most important such as applied pressure and

number of pulls. Testing the effect of very high viscosities (+250000 cps) will allow the development of a wide variety of dry adhesive materials. Additional testing is also needed at higher speeds that will be more realistic for high volume manufacturing.

<u>Conclusion</u>

We have proven that it is possible to autonomously produce synthetic dry adhesives. There is still much development to be done before up-scaling is possible. The manufacturing parameters that had the greatest effect on fill percentage included the applied pressure and number of pulls. These parameters need to be further characterized to develop a model for manufacturing. It was found that having an adequate supply of polyurethane following the spatula during dragging is critical to ensure the structures are filled in. To achieve this, the spatula will need to be redesigned. The next generation spatula may either include a doctor blade and reservoir of polyurethane to distribute a thin film behind the spatula during dragging, or a spatula with a transferring hole to allow the polyurethane to flow through. The linear stage used in this study will not be used again due to its limited range of motion and speed. To replace it, a manual pulling system will be developed. Future experiments include further characterization of the effect of applied pressure, number of pulls, and very high or very low viscosity.

References

[1] Aksak B, et al. 2007 Adhesion of Biologically Inspired Vertical and Angled Polymer Microfiber Arrays *Langmuir* **23** 3322-3332.

[2] Sameoto D, Menon C. 2009 A low-cost, high-yield fabrication method for producing optimized biomimetic dry adhesives *J Micromech Microeng* **19** 115002.

[3] Shaheen SE, et al. 2001 Fabrication of bulk heterojunction plastic solar cells by screen printing *Applied Physics Letters* **79** 2996-2998.

[4] Krebs FC. 2009 Fabrication and processing of polymer solar cells: A review of printing and coating techniques *Solar Energy Mater Solar Cells* **93** 394-412.

[5] Weitao Jiang et al. 2009 Investigation of ink transfer in a roller-reversal imprint process *J Micromech Microengineering* **19** 015033.

[6] Yang H, Jiang P. 2011 Macroporous photonic crystal-based vapor detectors created by doctor blade coating *Appl Phys Lett* **98** 011104-011104-3.

[7] Krebs FC, et al. 2004 Production of large-area polymer solar cells by industrial silk screen printing, lifetime considerations and lamination with polyethyleneterephthalate *Solar Energy Mater Solar Cells* **83** 293-300.

[8] Aernouts, T, et al. 2004 Polymer solar cells: screen-printing as a novel deposition technique. MRS ProceedingsCambridge Univ Press.

[9] Lepage Speed Set Epoxy Technical Data Sheet. 2010; Available at: http://dashboard.lepageproducts.com//upload/english/general/75f84672-6274-4265-8d5e-998eac6914a8.pdf. Accessed 02/15, 2013.

[10] Manuelli, A, et al. 2002 Applicability of coating techniques for the production of organic field effect transistors. Polymers and Adhesives in Microelectronics and Photonics, 2002. POLYTRONIC 2002. 2nd International IEEE Conference on IEEE.

[11] Tongbi Jiang, et al. 1997 Optimizing stencil printing parameters for organic materials. Electronics Manufacturing Technology Symposium, 1997., Twenty-First IEEE/CPMT International.

[12] Sameoto D, Ferguson B. 2012 Robust large-area synthetic dry adhesives *J Adhes Sci Technol* 1-17.

[13] Yang H, Jiang P. 2010 Large-Scale Colloidal Self-Assembly by Doctor Blade Coating *Langmuir* **26** 13173-13182.

8.2 Appendix B: Adhesion Testing Software Issues

User input withdraw distance

This method was used as opposed to the program automatically detecting when contact is lost due to the complexities of programming such a detection system. To detect when the load cell goes above or below a particular force is simple, but the signal has noise and will drift slightly, so it will rarely hover exactly on or around zero force. In addition, the force passes by zero as the graph moves from the maximum to the minimum as seen in Figure 24. This can cause false positives in the detection of when the indenter is truly out of contact, which can cause errors in data collection. Unfortunately this method introduces another issue. If the withdraw distance is too short, the indenter will remain in contact with the adhesive through multiple tests, invalidating those tests. If the withdraw distance is too large, there is no issue with the data, but the test runtime will be increased. The withdraw distance should be selected to ensure that contact is lost, and the test is still completed in a reasonable amount of time.

Program crash during full data recording

The program is able to record every data point for the duration of the test, but only for short tests. There is a bug in the software that will crash the program after it has taken so much data. The amount of data appears to be random although it normally occurs before an hour of testing time has elapsed. This problem is dangerous because the program does not automatically stop the linear stage. If the user is not present to witness the crash the load cell could be damaged as the indenter impacts the sample. As a result, when taking complete data for adhesion trials, user monitoring is required to correct for any software crashes.

Camera Quality

The experimental setup exists such that the inverted microscope is looking upwards through the sample to where contact is made with the indenter. Often it is difficult to determine which fibers are in contact. With proper lighting, there will be a contrast change for the fibers that are contacting the indenter. However, for some samples it is impossible to get the lighting setup properly to easily distinguish the contact circle. In either case, another problem arises in getting proper focus and lighting settings on the camera. The images are normally distinguishable to the eye, providing an estimate of the area in contact, but it is impractical for the user to inspect every image to count the number of fibers in contact. Ideally image recognition software can count the fibers, but the contrast problems prevented this solution. As a final problem, the camera records very high detail, but low resolution images when taking video. The result is a low quality video of unreasonable size, normally ~750 MB for a 30 second video. Better video compression is needed before videos can be continuously taken during testing.